



**Development and validation of a novel
approach for evaluation of broadband UVA
irradiance and total daily UVA exposures from
OMI satellite data**

A thesis submitted by

Mustapha A.Setar A.Jebar

BSc. (Physics), MSc. (Physics)

For the award of

Doctor of Philosophy

2018

ABSTRACT

It is important to collect and validate data from satellites in order to obtain global information about the solar UVA (320-400 nm) environment. This research reconstructed and validated the broadband UVA irradiances derived from discrete spectral irradiance data retrieved from the Ozone Monitoring Instrument (OMI) satellite from 1 January to 31 December 2009. OMI data at solar noon was compared to ground based spectral irradiance at Toowoomba (27°36' S 151°55' E), Australia at 310, 324 and 380 nm for both cloud free and all sky conditions. There was a strong relationship between the ground based UV spectroradiometer data and satellite based measurements with an R^2 of 0.89 or better in each waveband for cloud free days. Models developed for the sub-tropical site data account for these differences and are essential for any correlation between satellite and ground based measurements. Additionally, this research has developed a model to evaluate the solar noon broadband UVA irradiance from the discrete satellite spectral irradiance at 310, 324 and 380 nm, comparing the UVA irradiance at solar noon on cloud free days to those measured over 12 months with a ground based UVA radiometer. An R^2 of 0.86 was obtained confirming that for cloud free days the broadband UVA can be evaluated from the OMI satellite spectral measurements.

This research also investigated the influence of cloud on the broadband UVA solar noon irradiance evaluated from the solar noon satellite based OMI spectral UV data that were compared to the ground based radiometer irradiance in a twelve year period, from 1 October 2004 to 31 December 2016. The correlation, calculated with the model, between ground based radiometer data and the evaluated OMI broadband UVA irradiance depend on whether or not the solar disc was obscured by the presence of cloud and on the total sky cloud fraction. For conditions when the sun was not obscured by cloud, the evaluated satellite and the ground-based UVA irradiance correlation was best for cloud cover between 0-2 okta ($R^2 = 0.78$) and worst for high cloud cover of >4 and up to 8 okta (R^2 between 0.30 and 0.40). The R^2 value reduced with increasing cloud cover and showed significantly weaker correlation when the sun was obscured. The correlation between the evaluated satellite broadband UVA and ground-based measurements over the twelve years for total cloud cover conditions of 4 okta or less confirmed that the broadband UVA satellite evaluation model using the OMI spectral

data is valid for approximately 71% of the days at the Southern Hemisphere subtropical study site.

This research then developed a method to accurately calculate the total daily broadband UVA exposure from the satellite derived solar noon irradiance on cloud free days. The method utilises cloud free UVA irradiance data, collected daily at high temporal resolution over the period 2005 to 2016, to derive the normalised diurnal UVA exposure and determine a factor relating the solar noon irradiance to the total daily UVA exposure. To demonstrate the versatility of this approach, OMI satellite solar noon UVA irradiance data were employed in calculating the total daily UVA exposures and compared to the respective ground based site measurements. There was a strong correlation between the total daily satellite and ground based broadband UVA exposures ($R^2 = 0.90$). The developed method enables the total daily UVA exposures to be evaluated from satellite solar noon UVA irradiances at sites that do not record short term temporal variations in terrestrial UVA.

Finally, this research investigated and evaluated the influence of cloud on the total daily UVA exposure calculated from the three OMI UV spectral irradiance measures at solar noon. These evaluated satellite total daily UVA exposures were compared to the total daily UVA exposures of a ground based broadband radiometer over the period of October 2004 to December 2014 at the Toowoomba site under all cloud cover conditions including sun obscured and not obscured states. The method was employed to evaluate the influence of cloud on the total daily UVA exposure. When the sun was not obscured by cloud, there was good agreement between satellite and ground based daily UVA exposure with R^2 between 0.80 and 0.84 for the cloud conditions 0 to 2, > 2 to 4, > 4 to 6 and > 6 to 8 okta. For sun obscured by cloud, the R^2 was 0.71, 0.64 and 0.75 respectively for > 2 to 4, > 4 to 6 and > 6 to 8 okta. The method was validated using total daily UVA exposures from ground measurements taken in 2015 and 2016 giving a mean absolute error of 84.2 kJ/m² (10%) and 138.8 kJ/m² (30%) respectively for the cases of sun not obscured cloudy days and sun obscured by cloud cover. Total daily UVA exposures were able to be calculated from the OMI satellite spectral irradiance data for all cloud conditions, including cases when the sun was obscured, demonstrating the potential of the technique to be applied remotely in locations that do not record surface UVA measurements directly.

CERTIFICATION OF THESIS

This thesis is entirely the work of Mustapha A.Setar A.Jebar except where otherwise acknowledged. The work is original and has not previously been submitted for any other award, except where acknowledged.

Student and supervisors signatures of endorsement are held at USQ.

Professor Alfio Parisi

Principal Supervisor

Dr Nathan Downs

Associate Supervisor

Dr Joanna Turner

Associate Supervisor

ACKNOWLEDGMENTS

I gratefully would like to thank my supervisor **Professor Alfio Parisi** for guiding my PhD journey with big efforts, care and patience.

I would like to thank my associate supervisor **Dr Nathan Downs** for his ideas, help and support.

I would like to thank my associate supervisor **Dr Joanna Turner** for her valuable suggestions and efforts.

I would like to acknowledge **the Higher Committee for Education Development in Iraq** for providing the scholarship for this PhD research.

I would like to acknowledge the OMI mission scientists and associated NASA personnel for the production of the data used in this research effort.

I would like to thank the proof reader **Tim Passmore**.

Very big thanks to my mother, who provides everything to make me a successful person.

My love and my wife **Nedher**, thank you so much for your patience and sacrifice.

This thesis is dedicated to my missed and great father **A.Setar A.Jebar** (1955-2011).

TABLE OF CONTENTS

ABSTRACT	i
CERTIFICATION OF THESIS	iii
ACKNOWLEDGMENTS	iv
TABLE OF CONTENTS	v
LIST OF FIGURES	ix
LIST OF TABLES	xiii
LIST OF ABBREVIATIONS	xiv
CHAPTER 1	1
INTRODUCTION	1
1.1 RATIONALE	2
1.1.1 Objectives	3
1.2 HYPOTHESIS	4
1.3 THESIS OUTLINE	4
1.4 OVERVIEW	5
1.5 LITERATURE REVIEW	5
1.5.1 Effects of UV Radiation	5
1.5.2 Effects of UVA Radiation	9
1.5.3 Factors influencing UV irradiance	11
1.5.3.1 Ozone	11
1.5.3.2 Aerosols.....	13
1.5.3.3 Solar Zenith Angle.....	14
1.5.3.4 Surface Albedo.....	14
1.5.3.5 Altitude and Earth’s Orbit	14
1.5.3.6 Clouds	15
1.6 METHODS OF MEASURING UV RADIATION	16
1.6.1 Ground-based instruments	17
1.6.1.1 Spectroradiometers	17
1.6.1.2 Dobson Spectrophotometer	18
1.6.1.3 Brewer Spectrophotometer.....	18
1.6.1.4 Radiometers	19
1.6.2 Satellite-based Instruments	19
1.6.2.1 Total Ozone Mapping Spectrometer (TOMS).....	20
1.6.2.2 Global Ozone Monitoring Experiment (GOME)	20
1.6.2.3 Moderate Resolution Imaging Spectrometer (MODIS).....	21
1.6.2.4 Ozone Monitoring Instrument (OMI)	22

1.7 COMPARISON OF GROUND-BASED TO SATELLITE DATA.....	23
1.7.1 OMI Broadband UV.....	23
1.7.2 GOME and TOMS Ozone	24
1.7.3 Spectral UV.....	25
1.7.4 Nitrogen Dioxide.....	27
1.7.5 TOMS Broadband UV.....	28
1.7.6 GOME UV.....	28
1.8 SIGNIFICANCE OF THE PROJECT.....	28
1.9 CHAPTER SUMMARY	29
CHAPTER 2.....	30
MATERIALS AND METHODS.....	30
2.1 OVERVIEW.....	31
2.2 SPECTRAL AND BROADBAND SURFACE BASED MEASUREMENTS TO VALIDATE OMI UV SATELLITE DATA.....	31
2.2.1 Ground-based measurements	32
2.2.1.1 Spectroradiometer Data.....	32
2.2.1.2 Total Sky Imager	33
2.2.1.3 Biometer data.....	36
2.2.2 Satellite-based Measurements.....	39
2.2.3 Derivation of Satellite Broadband UVA Irradiance	40
2.3 UVA IRRADIANCE OVER A TWELVE-YEAR PERIOD FROM OMI DATA INCLUDING THE INFLUENCE OF CLOUD	41
2.3.1 Ground Based Data	41
2.3.2 Satellite-based Data.....	42
2.4 TOTAL DAILY UVA EXPOSURE EVALUATED FROM OMI SATELLITE SPECTRAL IRRADIANCE FOR CLOUD FREE DAYS	42
2.4.1 Total Daily UVA Exposure	47
2.5 INFLUENCE OF CLOUD ON OMI SATELLITE TOTAL DAILY UVA EXPOSURES OVER AN EXTENDED PERIOD.....	47
2.5.1 Validation.....	48
2.6 CHAPTER SUMMARY	48
CHAPTER 3.....	49
SPECTRAL AND BROADBAND UV MEASUREMENTS	49
3.1 OVERVIEW.....	50
3.2 SPECTRAL AND BROADBAND SURFACE BASED MEASUREMENTS TO VALIDATE OMI UV SATELLITE DATA.....	50
3.2.1 Spectral Data.....	50
3.2.2 Broadband UVA.....	55

3.3 CHAPTER SUMMARY	56
CHAPTER 4	57
INFLUENCE OF CLOUD ON THE SATELLITE AND GROUND BASED UVA MEASUREMENTS	57
4.1 OVERVIEW.....	58
4.2 SPECTRAL UV IRRADIANCES AND THE INFLUENCES OF CLOUD.....	58
4.3 EVALUATED UVA IRRADIANCE OVER A TWELVE-YEAR PERIOD FROM OMI DATA INCLUDING THE INFLUENCE OF CLOUD	63
4.3.1 All Sky Conditions	63
4.3.2 Cloud Data	66
4.3.3 Sun Not Obscured Sky Conditions.....	67
4.3.4 Sun Obscured Sky Conditions	71
4.4 INFLUENCE OF AEROSOLS ON THE UV IRRADIANCE.....	73
4.5 CHAPTER SUMMARY	75
CHAPTER 5	76
EVALUATION OF THE TOTAL DAILY UVA EXPOSURES	76
5.1 OVERVIEW.....	77
5.2 TOTAL DAILY UVA EXPOSURE EVALUATED FROM SOLAR NOON OMI SATELLITE SPECTRAL IRRADIANCE FOR CLOUD FREE DAYS	77
5.3 INFLUENCE OF CLOUD ON OMI SATELLITE TOTAL DAILY UVA EXPOSURES OVER A TWELVE YEAR PERIOD	79
5.3.1 Cloud and Fractions of Maximum Daily Exposure	79
5.3.2 All Sky Conditions	80
5.3.3 Sun Not Obscured Sky Conditions.....	84
5.3.4 Sun Obscured Sky Conditions	87
5.3.5 Model Validation.....	89
5.4 CHAPTER SUMMARY	91
CHAPTER 6	92
CONCLUSION	92
6.1 OVERVIEW.....	93
6.2 SPECTRAL AND BROADBAND SURFACE BASED MEASUREMENTS TO VALIDATE OMI UV SATELLITE DATA.....	93
6.3 UVA IRRADIANCE OVER A TWELVE-YEAR PERIOD FROM OMI DATA INCLUDING THE INFLUENCE OF CLOUD	94
6.4 TOTAL DAILY UVA EXPOSURE EVALUATED FROM SOLAR NOON OMI SATELLITE SPECTRAL IRRADIANCE FOR CLOUD FREE DAYS.	94
6.5 INFLUENCE OF CLOUD ON OMI SATELLITE TOTAL DAILY UVA EXPOSURES OVER A TWELVE YEAR PERIOD	95
6.6 CONCLUSION.....	96

6.7 FUTURE WORKS	97
REFERENCES.....	98
APPENDIX: Published Refereed Papers.....	120

LIST OF FIGURES

Figure 1.1 Electromagnetic spectrum distribution of the solar radiation (Soehnge, Ouhitit & Ananthaswamy 1997).	2
Figure 1.2 Penetration of ultraviolet radiation into the eye (Behar-Cohen et al. 2011).	8
Figure 1.3 Vitamin D action spectrum showing the relative effectiveness of the UV wavelengths for vitamin D production (CIE 2006).	9
Figure 1.4 UV spectral irradiance recorded by a spectroradiometer on a cloud free day at the University of Southern Queensland, Toowoomba, Australia (measured 12.15pm, 10 September 2004).	10
Figure 1.5 UVA penetration into the human skin (Amaro-Ortiz, Yan & D'Orazio 2014).	11
Figure 2.1 Bentham spectroradiometer in the laboratory (top) and on the roof inside the environmentally shaded box (bottom).	33
Figure 2.2 Total Sky Imager instrument with clear sky image (left) and a cloudy sky (right).	35
Figure 2.3 Erythemal UV (right) and UVA (left) Biometers.	38
Figure 2.4 Time series of biometer erythemal UV irradiance for a cloud free day (a) and a cloudy day (b).	38
Figure 2.5 The Giovanni website provides the UV irradiances at solar noon from 1/10/2004 to 31/12/2016. In this study, the spectral irradiance data is collected for the three UV wavelengths (310, 324 and 380 nm) at solar noon. The area of this data is the Toowoomba region, Australia (151.80360, -27.71850, 152.22660, -27.3120).	40
Figure 2.6 The solid line shows the trapezoidal integral of the UV irradiance with the wavelength using the spectral irradiances 310, 324 and 380 nm. This is superimposed on the UV spectrum collected with the Bentham spectroradiometer.	41

Figure 2.7 Seasonal variation in UVA (320-400 nm) exposure recorded at five-minute intervals and measured for cloud free days between February 2005 and December 2016. 43

Figure 2.8 Measured UVA exposure curves, normalised in x and y for each of the 187 cloud free days in the period February 2005 to December 2016 (points). Gaussian model approximations normalised to the peak of the measured exposure data are plotted as blue dashed curves showing the range in possible Gaussian fits to the measured data. 46

Figure 3.1 Time series of spectral irradiance at 310, 324 and 380 nm for cloud free days for the OMI satellite data from 1 January 2009 to 31 December 2009. The total number of days in the 1 January to 31 December period classified as cloud free was 71 (19.5% of the total number of days in the research period). 51

Figure 3.2 Cloud free days OMI and ground based spectroradiometer spectral irradiance comparison for (a) 310 nm, (b) 324 nm, (c) 380 nm (n=71 cloud free days). The error bars correspond to the $\pm 9\%$ error associated with the Bentham spectroradiometer data. The solid line in each graph is the 1:1 line. 53

Figure 3.3 Histograms of the ratio of the satellite to ground-based spectral solar noon UV measurements for each of 310, 324 and 380 nm. The darker bars correspond to the measurements for the 71 cloud free days and the lighter bars correspond to 221 measurements on cloudy days. N is the number of values. For each graph, there are 2 or less values above the value of 6. 55

Figure 3.4 Comparison of the broadband UVA irradiance values evaluated from OMI spectral data and the UVA irradiance from the ground based measurements as derived from Equation 2.1 using the OMI spectral irradiances. The error bars are the $\pm 10\%$ error associated with the ground based data and the solid line is the 1:1 line. 56

Figure 4.1 OMI and Bentham spectral irradiance comparison for (a) 310 nm, (b) 324 nm, (c) 380 nm, for the cloud cover of 0 to 2 okta. 59

Figure 4.2 OMI and Bentham spectral irradiance comparison for (a) 310 nm, (b) 324 nm, (c) 380 nm, for the cloud cover of > 2 to 4 okta. 60

Figure 4.3 OMI and Bentham spectral irradiance comparison for (a) 310 nm, (b) 324 nm, (c) 380 nm, for the cloud cover of > 4 to 6 okta. 61

Figure 4.4 OMI and Bentham spectral irradiance comparison for (a) 310 nm, (b) 324 nm, (c) 380 nm, for the cloud cover of > 6 to 8 okta. 62

Figure 4.5 Time series of solar noontime UVA irradiance evaluated from the 310, 324 and 380 nm satellite data. 65

Figure 4.6 Distribution of the solar noon UV irradiance evaluated from the satellite data. 65

Figure 4.7 Box and whisker plots of the broadband UVA irradiance evaluated from the OMI spectral data from October 2004 to 31 December 2016 for all sky conditions. The line within each box is the median and the box is the data within quartiles one and three. The dashed line of the whiskers represents the range of the data up to ± 5 standard deviations, with two outliers. The dataset for 2004 is shifted to higher irradiance due to only the last three months of the year being available. 66

Figure 4.8 Time series of the cloud conditions from zero to eight okta for October 2004 to December 2016 as measured by the Total Sky Imager. 67

Figure 4.9 Comparison of the evaluated OMI satellite solar noon UVA irradiance with ground-based UVA data for the four categories of cloud cover of (a) 0 to 2, (b) > 2 to 4, (c) > 4 to 6 and (d) > 6 to 8 okta for sun non obscured sky conditions. The error bars are the $\pm 10\%$ error associated with the ground-based data. The dashed line is the fitted trend line. 70

Figure 4.10 Comparison of the evaluated OMI satellite solar noon UVA irradiance with ground-based UVA data. The data are plotted for the three categories of the amount of cloud cover of (a) > 2 to 4, (b) > 4 to 6 and (c) > 6 to 8 okta for sun obscured sky conditions. The error bars are the $\pm 10\%$ error associated with the ground-based data. The dashed line is the fitted trend line. 72

Figure 4.11 (a) The time series of the daily UV aerosol index and (b) the aerosol optical depth for the Toowoomba study site from October 2004 to December 2016. 74

Figure 5.1 Comparison of satellite derived cloud free daily UVA exposure versus surface measured UVA exposure. The error bars represent the variation in surface UVA measurements ($\pm 10\%$). 78

Figure 5.2 Time series of satellite total daily UVA exposures evaluated from the OMI solar noon spectral irradiance values. 82

Figure 5.3 (a) The total daily satellite UVA exposure for all sky conditions. (b) The total daily satellite UVA exposure at the four cloud amount categories (0-2, > 2-4, > 4-6 and > 6-8 okta) for sun not obscured sky conditions. (c) Total daily satellite UVA exposure at the three cloud amount categories (> 2-4, > 4-6, and > 6-8 okta) for sun obscured sky conditions. The horizontal line in each box and whisker is the median, the box is the Q1 and Q3 range and the dashed vertical line is the range of values. . 83

Figure 5.4 Box and whisker plots for each year of satellite total daily UVA exposures data October 2004 to December 2016. 84

Figure 5.5 Comparison of the 2004 to 2014 satellite total daily UVA exposure evaluated from the OMI spectral irradiance evaluated at solar noon with the ground based total daily UVA exposure for the four categories of cloud cover of (a) 0 to 2, (b) > 2 to 4, (c) > 4 to 6 and (d) > 6 to 8 okta for solar disc non-obscured sky conditions. The dashed lines are the regression lines fitted to the data and the error bars correspond to the $\pm 10\%$ error associated with the ground-based data. 87

Figure 5.6 Comparison of the satellite total daily UVA exposure for 2004 to 2014 evaluated from the three OMI spectral irradiance with the ground-based total daily UVA exposure for the three categories of cloud cover of (a) > 2 to 4, (b) > 4 to 6 and > 6 to 8 okta for sun obscured sky conditions. The dashed lines are the regression lines fitted to the data and the error bars represent the $\pm 10\%$ errors with the measured ground based data. 89

Figure 5.7 Validation of the satellite total daily UVA exposure evaluated from the three OMI spectral irradiances with the ground-based total daily UVA exposure for the two categories of (a) sun not obscured cloudy days and (b) sun obscured cloudy days for the 2015 and 2016 data set. The dashed line in each graph is the 1:1 line. ... 90

LIST OF TABLES

Table 1.1 The relationship between skin types and erythematous UV exposure as defined by Fitzpatrick type (Fitzpatrick 1988).....	6
Table 2.1 Example of TSI imager information for cloudy day (sun obscured sky condition) with a cloud fraction of 1.0.	35
Table 2.2 Example of TSI imager information for cloud free day (non-sun obscured sky condition) with a cloud fraction of 0.094.	36
Table 2.3 Number of cloud free days from February 2005 to December 2016 used in deriving the UVA exposure integral for each day under cloud free conditions. The percentages in brackets represent the measured fraction of cloud free days in each month. The final column is the integral of the UVA exposure data that has been normalized in x and y, $\int UVA_{NORM}$	44
Table 3.1 The first quartile (Q1), median and third quartile (Q3) values for cloudy and cloud free days at 310, 324 and 380 nm.	54
Table 4.1 Distribution statistics of the cloud cover at solar noon for the 2004 to 2016 dataset (between 0 to 8 okta). Q1 is the first quartile of the range, Q3 is the third quartile of the range and N is a number of days with data in the respective category.	67
Table 5.1 Number of days in each category of cloud cover between zero and eight okta and the average of the fraction of the maximum daily exposure for all categories. ..	80

LIST OF ABBREVIATIONS

AOD	Aerosol Optical Depth
BCC	Basal Cell Carcinoma
GOME	Global Ozone Monitoring Experiment
MAE	Mean Absolute Error
MED	Minimum Erythema Dose
MODIS	Moderate Resolution Imaging Spectrometer
NMSC	Non-Melanoma Skin Cancer
OMI	Ozone Monitoring Instrument
Q1	First quartile of a range of data
Q3	Third quartile of a range of data
R ²	Coefficient of Determination
rRMSE	Relative Root Mean Square Error
SCC	Squamous Cell Carcinoma
SZA	Solar Zenith Angle
TOMS	Total Ozone Mapping Spectrometer
TSI	Total Sky Imager
UV	Ultraviolet
UVA	Ultraviolet A (320 – 400 nm)
UVB	Ultraviolet B (280 – 320 nm)
UVC	Ultraviolet C (100 – 280 nm)
WMO	World Meteorological Organisation

CHAPTER 1

INTRODUCTION

1.1 RATIONALE

The solar radiation incident on the earth's surface is divided into the three wavebands depending on wavelengths: visible, infrared and ultraviolet (Calbó, Pagès & González 2005). Johann Ritter discovered ultraviolet (UV) radiation in 1801 (Diffey 2002b). UV radiation has significantly higher energy at shorter wavelengths than to solar radiation in the visible waveband (De Miguel et al. 2011). The UV radiation waveband has been divided into three wavelength regions: UVC (100-280 nm), UVB (280-320 nm) and UVA (320-400 nm) (Figure 1.1).

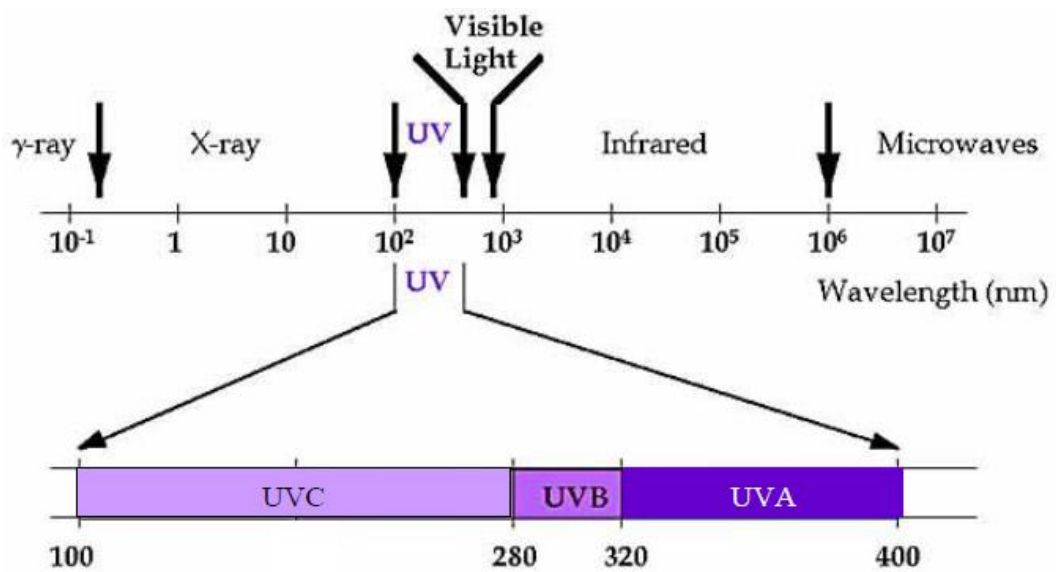


Figure 1.1 Electromagnetic spectrum distribution of the solar radiation (Soehnge, Ouhtit & Ananthaswamy 1997).

UVA has a longer wavelength, less energy and lower biological effectiveness than short wavelength UV. As a comparison, UVA exposures of 25 kJ/m^2 are considered equivalent to UVB exposures of 250 J/m^2 in terms of biological effectiveness (Miller et al. 1998). However, regular exposure to small amounts of UVA, leads to significant damage and cutaneous alterations in the human epidermis (skin) (Lavker et al. 1995).

Since 2004, the satellite borne Ozone Monitoring Instrument (OMI) has been providing UV data complementing the Total Ozone Mapping Spectrometer (TOMS) which provided data from 1978 to 2010 (Ialongo et al. 2011). The sunburning (erythema) UV data that are taken from the OMI has previously been compared and

Chapter 1 Introduction

validated to ground based data (Mateos et al. 2013; Fioletov, Kerr & Wardle 1997). However, no such comparison has been undertaken for the UVA radiation wavelengths. This project proposes to develop a method to evaluate the broadband UVA solar noon irradiances from the OMI satellite data and present a method to evaluate the total daily UVA exposures for comparison with calibrated ground-based measurements. UVA is still a health concern and must be accounted for in research that investigates the relationship of UVA to disease/damage to the body. Correlating the ground based to satellite derived solar noon UVA irradiance and total daily UVA exposures data will allow for improved UVA measurements and data coverage for future research.

1.1.1 Objectives

The solar noon spectral irradiance at several specific wavelengths are determined by the OMI and TOMS instruments. The OMI instrument provides the discreet spectral irradiance at 305, 310, 324 and 380 nm, with no provision of the broadband UVA irradiance from 320 to 400 nm. The overall objective of this research is to reconstruct and validate the broadband solar noon UVA irradiance and the total daily UVA exposures derived from current Ozone Monitoring Instrument (OMI) data. To achieve this aim, the research has the following specific objectives:

- 1- Comparison and validation of the spectral UVA data from the OMI satellite against ground based spectroradiometer data located at the sub-tropical site in Toowoomba, Australia.
- 2- Development of a method (mathematical model) to reconstruct the solar noon broadband UVA irradiance from the OMI data (310, 324 and 380 nm) at a sub-tropical site.
- 3- Evaluation and validation of the reconstructed satellite UVA irradiance to the ground based data on cloud free days from an independent radiometer over a period of one year (2009).

Chapter 1 Introduction

- 4- Comparison of the evaluated OMI solar noon irradiance over a 12 year period with ground based data including the influence of cloud.
- 5- Development and validation of a method for the evaluation of total daily UVA exposures from the OMI satellite data.
- 6- Comparison of the OMI reconstructed total daily UVA exposure on cloud free days with the ground-based measurements over the years from 2004 to 2016.
- 7- Investigation and analysis of the influence of cloud conditions on the UVA exposures from the OMI satellite data and comparison with the measurements of the ground based instrument.

1.2 HYPOTHESIS

The OMI discrete spectral UV irradiance can be used as a proxy for broadband surface UVA irradiance and total daily UVA exposure.

1.3 THESIS OUTLINE

1. Chapter 1- provides an overview of the effects of UV radiation, factors that influence the UV environment, UV measurement methods and previous studies about the comparison between satellite and ground based UV measurements.
2. Chapter 2 - presents the methods and equipment used in this project.
3. Chapter 3 - details the validation of solar noon UVA satellite data using ground based spectral UV data and the evaluation of the solar noon broadband irradiance for cloud free days over a year.
4. Chapter 4 – compares the solar noon satellite derived UVA irradiance and surface measurements including the influence of clouds and aerosols over a 12 year period.
5. Chapter 5 – presents the method developed for evaluation of the total daily UVA exposures. The method is applied to cloud free days over a 12 year period. The total daily UVA exposures are then evaluated for

all sky conditions. This employs a 10 year data set to extend the method for cloudy days and the use of a 2 year data set for validation.

6. Chapter 6 – provides conclusions and suggestions for future research.

1.4 OVERVIEW

Both the UVB (280-320 nm) and UVA (320-400 nm) wavebands have significant influences for human health and the earth's ecosystems. CIE (1987) has used the wavelengths region as UVA (315-400 nm). However, Photobiologists use the wavelength region as UVA (320-400 nm) (Diffey 2002b). Therefore, in this research, it is appropriate to use UVA (320-400 nm). Solar UV irradiance on a global scale need to be collected on a time repetitive basis. This is required for the monitoring of the UV climatology that influences the biological system on the earth. It is essential to provide awareness of the importance of the global coverage of UV irradiance using satellite-based measurements as the basis of atmospheric factors. It is important to compare and validate the global satellite data against ground-based instrumentation. This chapter will discuss the effects of UV radiation and factors influencing UV radiation. Then, the methods and instrumentation for measuring UV radiation will be reviewed in this chapter. The chapter will also address the comparisons between ground-based and satellite measurements.

1.5 LITERATURE REVIEW

1.5.1 Effects of UV Radiation

The earth's surface is exposed to a significant quantity of solar UV radiation (8-9%) (Frederick et al. 1989). Of this radiation, UVA radiation makes up 6.3% and a majority of this is transmitted to the earth's surface without absorption (although it is prone to scattering and attenuation by aerosols, water droplets and ice crystals in tropospheric cloud layers and undergoes natural fluctuations in magnitude depending on total cloud fraction and cloud optical depth). UV radiation is an important factor in the harm done to a number of biological systems on the earth (Hollosy 2002).

Chapter 1 Introduction

Solar UV radiation has two effects on human health. UV radiation has serious biological ramifications, including skin diseases (Rass & Reichrath 2008). Both the UVB and the UVA wavebands have a damaging influence on human health (Caldwell 1998). One common method of defining the influence of solar radiation on human skin is to weight the UV spectrum with the erythemal action spectrum (CIE 1988; CIE 1998). This spectrum is strongly weighted in the UVB and is often used as a proxy for biological damage. The World Health Organisation together with the World Meteorological Organisation (WMO) and international collaborators have adopted the erythemally weighted UV to define the UV index, an internationally accepted standard used to inform the public of potential sun exposure risk (WHO 2002).

Human skin diseases are a clear consequence of UV radiation exposure effects (Natarajan et al. 2014; D'Orazio et al. 2013; De Grujil 1999). Human skin produces a coloured protein (melanin) that works as a natural sunscreen to filter UV radiation in the human skin (Jablonski & Chaplin 2012). However, this protein does not stop the harmful effects of UV radiation completely, especially those due to long term UV exposure (Honigsmann 2002). In addition, skin colour or skin type determines the quantity of melanin in the skin. Table 1.1 describes the effects of erythemal UV radiation according to the skin type. Sunburn of the skin (erythema) is a consequence of too much weighted UV irradiance (CIE 2014). Therefore, the effects of UV radiation exposure such as sunburn or erythemal effects are disparate depending on the skin type (Diffey 1991).

Table 1.1 *The relationship between skin types and erythemal UV exposure as defined by Fitzgerald type (Fitzpatrick 1988).*

Skin category	Erythemal UV effects	Description
1	Very severe burns and pain with no tan	Persons who have very fair skin, green or blue eyes and freckles
2	Severe burns and pain and light tan	Persons who have fair skin, blue and brown eyes and blond hair

Chapter 1 Introduction

3	Moderate burns and clear tan	Persons who have white skin
4	Sometimes burns and very clear tan	Persons who have white and brown skin and black, brown and hazel eyes
5	Very rare burns and clear tan	Persons who have brown skin
6	No burns and very clear tan	Persons who have black skin

Skin cancer resulting from UV radiation is a common disease around the world, that occurs for millions of people each year (Narayanan, Saladi & Fox 2010). Two main types of skin cancer have been identified: non-melanoma (NMSC) and melanoma skin cancer. Non-melanoma skin cancer (NMSC) is divided into basal cell carcinoma (BCC) and squamous cell carcinoma (SCC) (Rass & Reichrath 2008; Reichrath & Nurnberg 2008; Neidecker et al. 2009; Wright et al. 2012). NMSC is more common than melanoma skin cancer, but melanoma has a higher mortality rate (Narayanan, Saladi & Fox 2010). Due to Australia's latitude, it has high level of UV radiation during the year (Gies 2003; Gies et al. 2004). Worldwide, Australia has the second highest rates of incidence of skin cancer (Australian Institute of Health and Welfare, 2017; Doran et al. 2015). The incidence rates of skin cancer are increasing and are greater than those of any other types of cancer. The high incidence rates of skin cancer have a significant direct and indirect economic impact. For example, in New South Wales in 2010, the cost of 150,000 skin cancer cases was \$536,000,000 (Doran et al. 2015).

The eye, like skin, is affected by UV radiation especially with respect to repeated UV exposure. Consequently, eye problems increase with increasing UV radiation exposure (Stammes & Stammes 2008). Eye damage is related to the UV wavelength (or UV intensity). When the eye is exposed to short wavelength UV radiation (in terms of UVC), the eye damage occurs immediately. Repeated longer wavelength UV radiation (UVB and UVA) also leads to eye problems (Ambach & Blumthaler 1993). Figure 1.2 shows the transmission of UV radiation into the eye. UV eye disease often occurs with basal cell carcinoma (BCC) and squamous cell carcinoma (SCC). Even though, ocular

Chapter 1 Introduction

melanoma is rare in relation to UV exposure, it may occur for population groups with white skin and blue eyes (Gallagher & Lee 2006). Eye or eyelid skin problems caused by UV exposure include blistering, exfoliation, cataracts, Photo keratitis and blurred vision (Stamnes & Stamnes, 2008).

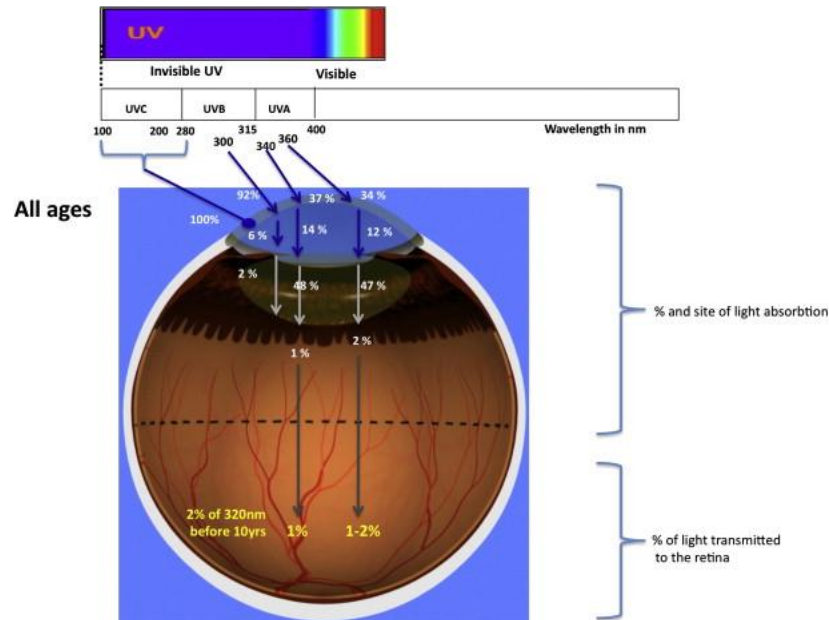


Figure 1.2 Penetration of ultraviolet radiation into the eye (Behar-Cohen et al. 2011).

In contrast, UV radiation exposure can have positive consequences on human health (Juzeniene et al. 2011). It is considered as a main source of vitamin D, which is important for calcium equilibrium in the human body (Webb & Holick 1988; CIE 2006). Vitamin D deficiency has also been linked to breast and ovarian cancer (Grant 2007). The human body's need for vitamin D is variable and depends on environment and genetic makeup (Webb & Engelsen 2006). The effectiveness of the UV for vitamin D production depends on wavelength (Figure 1.3) and the exposure time. The UVB wavelengths are predominantly the ones responsible for vitamin D production (Norman 1998; CIE 2006).

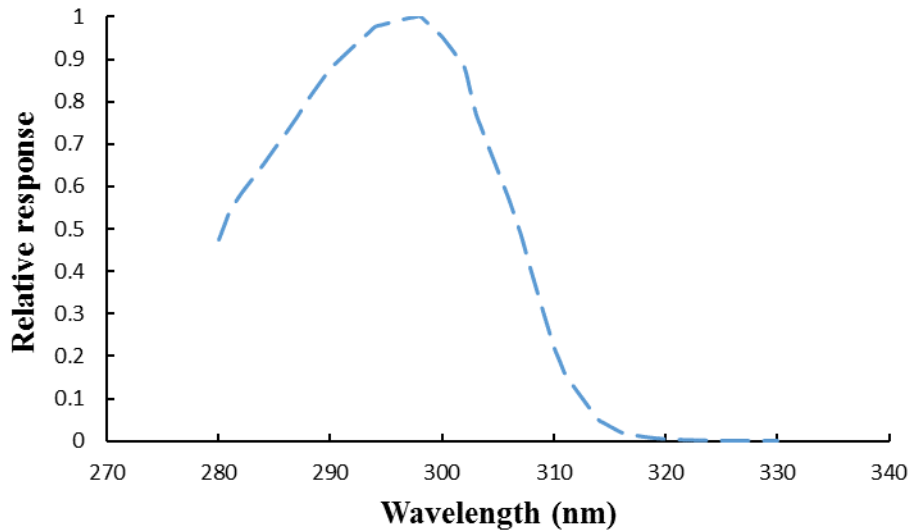


Figure 1.3 Vitamin D action spectrum showing the relative effectiveness of the UV wavelengths for vitamin D production (CIE 2006).

In addition to UV radiation effects on human health, UV radiation affects other systems at the earth's surface. Solar UV radiation causes a negative influence on aquatic ecosystems and species (Häder et al. 2007). It has indirect effects on plants through an increase or a decrease in the capability of the plants to fight insects and pathogens. UVB is also responsible for direct effects on plants such as changes in the genetic activities that create variations in the forms and functions of plants (Caldwell et al. 1998). Moreover, solar ultraviolet radiation, especially UVB radiation, degrades the quality of materials such as wood, paper, biopolymers and plastics (polymers), decreasing the outdoor service life of these materials (Andrady et al. 1998).

1.5.2 Effects of UVA Radiation

UVA radiation has the lowest energy and the longest wavelength of the UV radiation wavebands. Importantly, UVA radiation is not attenuated by atmospheric ozone and is much more abundant on the Earth's surface than UVB radiation (Figure 1.4). UVA solar radiation at the Earth's surface makes up more than 90% of the available ultraviolet and experiences less relative atmospheric attenuation at high solar zenith angles (SZA, see section 1.5.3.3) than UVB (Diffey 2002a; Frederick et al. 1989). It is well established that UVA can have harmful effects on human health (Kozmin et al. 2005; Moyal & Fourtanier 2002; Krutmann 2000). Through unknown internal

interactions, DNA absorbs UVA photons and this UVA absorption leads to DNA damage. This can contribute to carcinogenesis and aging (Ravanat & Douki & Cadet 2001). UVA radiation contributes to skin stress due to photo oxidation processes in the DNA (Vile et al. 1994). Furthermore, because of its longer wavelength UVA can penetrate deeper into biological systems, allowing damage to occur in greater depths (Stamnes and Stamnes 2008; Amaro-Ortiz, Yan & D'Orazio 2014) (Figure 1.5).

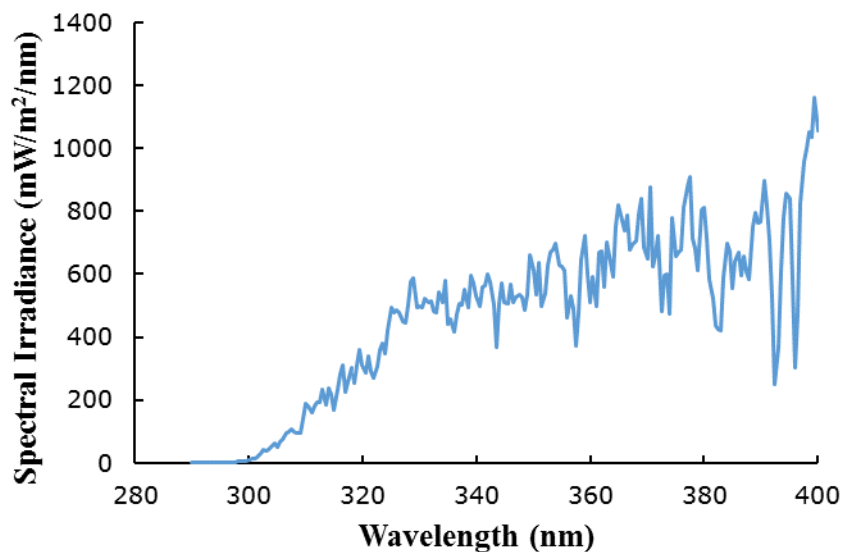


Figure 1.4 UV spectral irradiance recorded by a spectroradiometer on a cloud free day at the University of Southern Queensland, Toowoomba, Australia (measured 12.15pm, 10 September 2004).

Although the energy of UVA radiation absorbed by DNA is significantly lower than absorption of UVB radiation (Freeman et al. 1987), preferential absorption and atmospheric scattering influences the diurnal variation in the ambient UVA and UVB solar radiation, with the two wavebands displaying significant differences in distribution from the measured peak irradiance at solar noon (Diffey 2002b). There is more UVA irradiance due to atmospheric transmission processes.

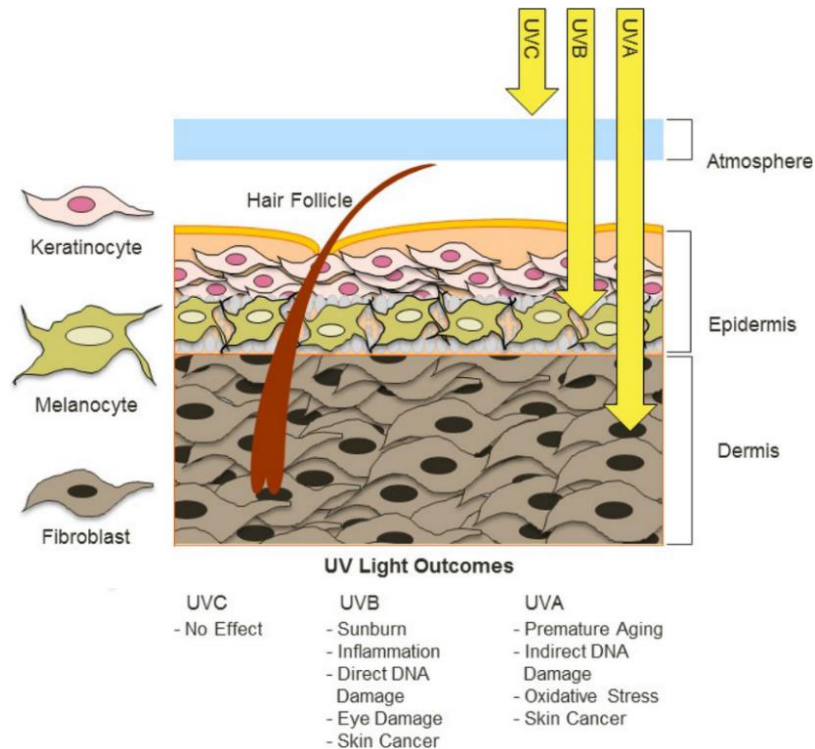


Figure 1.5 UVA penetration into the human skin (Amaro-Ortiz, Yan & D'Orazio 2014).

1.5.3 Factors influencing UV irradiance

Solar UV radiation is subject to many factors, which determine and influence the irradiance that reaches the Earth's surface (Parisi, Sabburg & Kimlin 2004; Cadet et al. 2017). Because of these factors, UV radiation is prone to scattering, absorption and attenuation during its path through the atmosphere to the Earth's surface. All the short wavelength radiation (UVC and part of the UVB) is absorbed by the atmosphere. Longer wavelength radiation will scatter according to Rayleigh or Mie scattering depending on the size of the atmospheric particles, aerosols and cloud particles (Madronich & Flocke 1999).

1.5.3.1 Ozone

The atmospheric layer of the stratosphere (altitude 15-35 km) is one of the atmospheric layers that contains the trace gas called ozone. Ozone is a triatomic oxygen molecule formed by single oxygen atoms and diatomic oxygen. The physical thickness of the layer of ozone is measured depending on the number of ozone molecules per cm² at

Chapter 1 Introduction

standard pressure. The quantity of 2.69×10^{16} molecules cm^{-2} represents one Dobson unit.

The influence on UV radiation can be calculated by a formula at standard temperature and pressure conditions depending on the total ozone column (Calbó, Pagès & González 2005).

$$\frac{D'}{D} = \left(\frac{TOZ'}{TOZ} \right)^{-RAF} \quad (1.1)$$

where D' and D are UV radiation exposure at two different conditions. TOZ' and TOZ are total ozone column at two different conditions and RAF is a radiation amplification factor. Ozone significantly affects the amount of UV radiation reaching the Earth's surface. UVC radiation is absorbed completely, and UVB radiation is absorbed or attenuated during passage through the ozone layer (Fountoulakis et al. 2014). Therefore, any changes in the concentration of atmospheric ozone will affect the terrestrial UV radiation (Bais et al. 2015; McKenzie et al. 2011). There have been changes in stratospheric ozone such as ozone depletion in mid and high latitudes because of increased CFC chemicals during the last part of the 20th century (Sivasakthivel and Reddy 2011; Bais et al. 2011). The Australian population suffers from high levels of UV radiation exposure because of Australia's position in the Southern Hemisphere, which experiences less ozone than the Northern Hemisphere at comparative latitudes (Gies et al. 2013). UVA irradiance has low absorption by ozone and therefore is less influenced by this factor.

Over the last decades, a number of researchers have addressed ozone measurements from satellite-based instruments (Thompson et al. 2003; Fishman and Brackett 1997). For example, Fishman et al. (2003) have studied global distribution of ozone from TOMS measurements to determine tropospheric ozone pollution in some regions of India, USA, China and Africa. This study has concluded that satellite measurements provide a great deal of information about ozone pollution in these regions.

1.5.3.2 Aerosols

There are a variety of types of particles existing in the atmosphere due to natural and anthropogenic factors including dust, soot, sulphate haze and sea-salt aerosols (Wenny et al. 1998). Aerosols have a significant impact on the UV levels in the atmosphere because of their optical properties (absorption and scattering). Since the beginning of the industrial revolution, absorption and scattering of UV radiation by aerosols has reduced the amount of UV radiation that reaches the earth's surface from 5% to 18% (Mckenzie et al. 2008). The degree of absorption or scattering are identified through the aerosol optical depth (AOD) [$AOD = AOD_{absorption} + AOD_{scattering}$] which varies according to using the Angstrom formula (Kerr 2005):

$$AOD(\lambda) = \beta\lambda^{-\alpha} \quad (1.2)$$

where β is the Turbidity coefficient, α is the Angstrom coefficient and λ is wavelength. Additionally, aerosols are considered a main factor in heating the atmosphere and changing its energy distribution processes because they intercept UV and other wavelengths in the atmosphere before it arrives at the Earth's surface, which may suppress the formation of clouds (Feng, Ramanathan & Kotamarthi 2013). Thus, many studies have been researching the influence of aerosols.

Some of the aerosol studies have relied on the satellite-based measurements to study the detection of aerosols absorption and scattering (Hsu et al. 1999; Herman et al. 2013). For example, Torres et al. (1998) have discussed a theoretical method to derive aerosol properties using backscattered UV radiation from satellite (version 7 TOMS instrument) data. In addition, this study has estimated aerosol optical depth using a model error sensitivity at two UV wavelengths (340 nm and 380 nm). Veefkind et al. (2000) have used different satellite-based instruments (GOME and ATSR-2) to compute and determine the distribution of the aerosol optical depth in the UV waveband. Furthermore, this study has addressed a comparison between GOME and ATSR-2 satellites and ground-based measurements. The region of this study was north-western Europe for a perfectly cloud free day (25th July 1995).

Chapter 1 Introduction

1.5.3.3 Solar Zenith Angle

The Solar Zenith Angle (SZA) is the angle of the line of sight to the sun with respect to the zenith. Two factors determine the SZA which influence the amount of UV radiation that reaches the earth's surface: geographical location and changes with time of day and day of the year. An increase of the SZA leads to a decrease in the intensity of UV radiation that falls on the earth's surface. First of all, the proportion of the incident direct radiation decreases with the cosine of SZA [$UV_D \cos(\text{SZA})$] (Schwander, Koepke & Ruggaber 1997) where UV_D is the direct UV radiation. Secondly, the passage of solar radiation through the atmosphere (path length (μ) = slant/vertical) is greater at larger SZA. Thus, the absorption and scattering of UV radiation increases with increasing SZA (Kerr 2005).

1.5.3.4 Surface Albedo

UV radiation reflects from ground surfaces and any other surfaces in the environment. The amount of UV radiation that is absorbed or reflected when it reaches the earth's surface depends on the various surfaces properties (Turner and Parisi 2009). The ground cover reflectivity of UV radiation, expressed as a ratio of the reflected light to the incident light, is represented by the unit less quantity called albedo. Albedo is described from 0 (no reflection) to 1 (total reflection) (Feister & Grewe 1995). There is a positive relationship between surface UV irradiance and surface albedo due to direct reflection and increased atmospheric backscatter toward the terrestrial surface. Ice and snow can reflect UV radiation more than visible radiation (Bais et al. 2015). Consequently, snow condition such as thickness and snow age affect the estimation of UV irradiance by satellites (Simic 2011).

1.5.3.5 Altitude and Earth's Orbit

High altitudes have less thickness of the atmosphere for UV radiation to traverse and as a result the altitude of different locations affects surface UV irradiance. High altitudes usually correspond to zero, or low-pollution atmospheric areas, which in turn leads to high amounts of UV radiation (Piazena 1996). The altitude effect (AE) on the surface UV radiation is calculated as a following percentage (Blumthaler, Ambach & Ellinger 1997):

$$\text{Altitude Effect (AE)} = \left[\frac{U_{HA}}{U_{LA}} - 1 \right] \times \frac{\Delta A}{1000} \times 100\% \quad (1.3)$$

where U_{HA} is the UV radiation at high altitude, U_{LA} is the UV radiation at low altitude and ΔA is the altitude difference .

Solar UV radiation is also affected by the annual change in distance between the earth and the sun due to the earth's elliptical orbit around the sun. The annual earth's orbit reduces the distance to the sun in the Southern Hemisphere summer by about 1.7%. This percentage is sufficient to increase the UV radiation intensity to about 7% in the Southern Hemisphere summer (Parisi & Kimlin 1997).

1.5.3.6 Clouds

Of all the atmospheric factors influencing satellite based monitoring of surface UV irradiance. Cloud is perhaps the most significant influencing factor (Calbó, González & Pagès 2001; Sabburg and Parisi 2006). The physical influences of atmospheric scattering, refraction and reflection are enhanced by the presence of cloud (Anton & Loyola, 2011; Parisi et al. 2008). Water and ice particles that make up clouds scatter solar radiation contributing to the diffuse UV irradiance that reaches the earth's surface (Kazantzidis, Eleftheratos & Zerefos 2011). In recent years, studies have assessed the radiative contribution of clouds to the global surface irradiance because of the potential climatological importance of energy budgets to global warming. As a result, it has been found that clouds either attenuate or enhance the amount of UV radiation that reaches the earth's surface (Calbó, Pagès & González 2005; Sabburg & Wong 2000). However, in general, the influence of clouds is more explicit in the longer wavelength visible spectrum than for UV radiation, due to the predominance of longer wavelength visible radiation in the direct solar spectrum and following scattering according to Rayleigh's criterion. Therefore, in contrast to visible radiation, the level of diffuse UV radiation can still be high, even though the sky may be covered completely and optically dim (Herman et al. 2013). The attenuating impact of clouds on the solar UV at a certain wavelength can be accounted for by using a cloud modification factor (CMF) (Simic et al. 2011), defined here as:

$$\text{CMF} = \frac{E(\lambda)_w}{E(\lambda)_k}, \quad (1.4)$$

where $E(\lambda)_w$ is the UV irradiance under cloud cover and $E(\lambda)_k$ is the UV irradiance expected for cloud-free conditions. It is difficult to quantify the effects of clouds accurately because of the spatial and temporal inhomogeneity of clouds (Bais et al. 2015). Cloud conditions (cover, type, spatial and temporal distribution) play an important role in determining the UV irradiance, measured either by surface or satellite based instruments (Sabburg & Parisi 2006; Udelhofen et al. 1999).

Some studies have obtained information about the cloud conditions using satellite-based measurements. An and Wang (2015) have provided different fields of cloud observations from the satellite-based instrument of the Moderate Resolution Imaging Spectrometer (MODIS) and surface instruments such as the Total Sky Imager (TSI). In this study, the MODIS instrument has a higher annual mean cloud fraction than ground-based measurements, because MODIS has a specially developed cloud detector which is called MODIS-aqua (afternoon overpass).

Fontana et al. (2013) have described cloud fraction data taken from Tera and Aqua MODIS instruments for the period from 2000 to 2012 over Switzerland. In this study, a comparison has been conducted between MODIS satellite data and four ground based stations' data in meteorological Synop station, Switzerland. This comparison has provided valuable information on how climate is varied by cloud cover. Thus, cloud cover detection using satellite based measurements plays an important role to determine and understand the radiative effects on the earth's surface (Stubenrauch et al. 2013; Frey et al. 2008; King et al. 2003).

1.6 METHODS OF MEASURING UV RADIATION

For most of the studies that address the interaction between UV radiation and receiving surfaces, UV radiation is considered in terms of radiometric quantities (irradiance, radiant exposure and quantities that are spectrally weighted). Irradiance is the incident radiant broadband UV radiation and the units are W/m^2 (McCluney 2014). $\text{W/m}^2/\text{nm}$

Chapter 1 Introduction

are the units of spectral irradiance for a single wavelength that is measured by spectroradiometers. Radiant exposure is the energy received by a surface area and the units are J/m^2 (Diffey 2002b). The weighted UV irradiance is the spectral distribution of the irradiance that has been weighted at each wavelength with the wavelength dependent biological effectiveness for a particular biological process, for example, the erythema action spectrum is a weighting for erythema.

1.6.1 Ground-based instruments

Historically, it has been difficult to achieve accurate spectral UV measurements using ground-based instruments. These difficulties arise because UV radiation is subject to a series of absorption and scattering processes, due to aerosols, clouds, ozone and albedo during its path through the atmosphere, making the resulting UV distribution complex. Furthermore, there are real difficulties in maintaining measuring instruments in accordance with long-term stability and calibration standards (Sharma et al. 2011; Kerr et al. 2002). Prior to discovery of the Ozone hole (late 1980s), accurate measurement of UV radiation was not available (McKenzie et al. 2011). By the mid-1990s, there was a noticeable improvement in the accuracy of UV radiation measurements, especially with spectroradiometers (Bais et al. 2015).

1.6.1.1 Spectroradiometers

Spectroradiometers are ground-based instruments that measure the spectrum of UV radiation (UVA and UVB) at 1 nm or better spectral resolution. There are many factors that affect the accuracy of spectroradiometers, for instance, calibration standards, instruments drift and wavelength misalignment (Kerr et al. 2002). However, while other spectrometers may produce higher uncertainty measurements, spectroradiometers have a high accuracy in measuring the quantity of UV radiation (Bais et al. 2015). In addition, recent spectroradiometer developments, such as dual-prism spectrographs, mean spectral measurements have become much faster than other methods. As a result, it is possible to examine changes due to atmospheric factors, such as clouds, which can change over small temporal scales. Moreover, by supplementing these instruments with diffusers, significant improvements have been made to corrections of the cosine error (a measure of the instrument response relative to the cosine response from 0-90° in SZA) (Grobner, Blumthaler & Ambach 1996).

Chapter 1 Introduction

1.6.1.2 Dobson Spectrophotometer

The Dobson Spectrophotometer is a ground-based instrument designed to measure total ozone. This instrument contains two monochromatic prisms which use a differential absorption technique (for two particular wavelengths pairs: 305.5 nm, 325.4 nm and 317.6 nm, 339.8 nm) in the UV region where ozone absorbs strongly for the first pair, but not the second (Kohler 1999). The accuracy of calculations of total ozone, by a Dobson Spectrophotometer depends on spatial circumstances such as instrument location and the nature of the sky, for example whether it is clear or cloudy. In addition, calibration levels play a key role in determining the accuracy of the Dobson instrument (Van Roozendaal et al. 1998). Basher (1982) concludes that if a Dobson instrument is subjected to a high calibration level, the error of its measurements may be around 2-3%.

1.6.1.3 Brewer Spectrophotometer

The Brewer instrument was designed to measure total ozone quantity (Balis et al. 2007). This instrument has two monochromatic prisms, which have differential absorption for five wavelengths (306.3 nm, 310.1 nm, 313.5 nm, 316.7 nm and 320.1 nm) (Gao et al. 2001; Van Roozndeaal et al. 1998). Total ozone values as measured by Dobson and Brewer instruments are calculated by the general relation (Vanicek, 2006):

$$TODS = \frac{(F_0 - F - \beta mp/p_0)}{\alpha \mu} \quad (1.5)$$

where TODS is the total ozone values by the direct sun absorption, F, F_0 are linear combinations of ground spectral irradiance, α, β are linear combinations of ozone absorption and Rayleigh scattering, μ, m are relative optical air masses of ozone and the atmosphere and p, p_0 are observed and air pressure at mean sea level.

The Brewer instrument measures the spectral UV irradiance at a resolution of ~ 0.5 nm (Fioletov et al. 2002). As for the Dobson instrument, one of the factors affecting the Brewer instrument accuracy is calibration. The Brewer instrument is more sensitive

Chapter 1 Introduction

than the Dobson under good calibration conditions, so it can measure at lower sun angles (Van Roozendaal et al. 1998).

1.6.1.4 Radiometers

Solar UV radiometers use a conventional technique to convert UV radiation as electromagnetic radiation to electric signals (Paulescu et al. 2013). There are two types of radiometer instruments: broadband filter radiometers and narrowband multi filter radiometers. The wavelength coverage of broadband radiometers is more than 10 nm (wide wavelength range) while the coverage of narrowband radiometers encompasses from 2 to 10 nm (Kerr et al. 2002). The main purpose of using radiometers is to measure erythemal effective irradiance or a particular waveband (Smith, White & Ryan 1993). There are many factors that affect the performance of radiometers such as the level of calibration, stability (for example, no changes in internal temperature as per manufacture specifications) and weather fluctuations (temperature and humidity). With standard conditions, radiometers can measure the irradiance in less than a second while spectroradiometers require several minutes to complete a measurement over a desired spectral range (Di Sarra, Disterhoft & DeLuisi 2002).

1.6.2 Satellite-based Instruments

Surface-based UV radiometers are used to measure the UVA and UVB irradiance but do not provide sufficient coverage to monitor the majority of the earth's surface, especially over the oceans (Kalliskota et al. 2000). Interest in terrestrial (and marine) UV radiation reaching the earth's surface over the past few decades has created increasing demand for satellite-based instrumentation. Approaches that depend on satellite data are suitable alternatives to surface-based instrumentation because satellites have the capability to determine important parameters over a wide area and provide reasonable estimates of the UV irradiance where local surface instrumentation is not available (Soulen & Frederick 1999; Paulescu et al. 2012).

Satellite based instrumentation has been employed for the provision of global coverage on a time repetitive basis of the atmospheric ozone, aerosols, UVA and UVB at specific wavelengths. There are several satellite instruments that monitor UV radiation that continue to provide a growing body of data enabling remote investigation

Chapter 1 Introduction

of local UV climatology in the mid- to long-term. These have provided high spatial and temporal resolution datasets from the late 20th century to the present day, and include: Total Ozone Mapping Spectrometer (TOMS), Global Ozone Monitoring Experiment (GOME), Moderate Resolution Imaging Spectrometer (MODIS) and Ozone Monitoring Instrument (OMI) satellite platforms (Bais et al. 2015).

1.6.2.1 Total Ozone Mapping Spectrometer (TOMS)

Since the 1970s TOMS instruments have been one of the National Aeronautics and Space Administration (NASA)'s second generation systems designed to perform ozone measurements (Kalliskota et al. 2000; Veefkind et al. 2006). TOMS have significantly contributed to determining atmospheric chemistry, atmospheric dynamics and ozone Pollution. Their measurements work within 1 nm wide bands in the UV irradiance channels (313 nm, 318 nm, 331 nm, 340 nm, 360 nm and 380 nm). Ozone absorbs 313 and 318 nm strongly while the other wavelengths have minimal absorption (Herman et al. 1997). Therefore, the TOMS is ideal for ozone measurements, as the wavelengths can be used to determine total column ozone.

In addition, the TOMS UV algorithm retrieves information about the spectral UV irradiance from the ground level. The spatial resolution of the TOMS retrievals is about $100 \text{ km} \times 100 \text{ km}$ area. Solar noon is the only time that TOMS provides the spectral UV irradiance measurements (Xu et al. 2010). Furthermore, TOMS uses a spectral method, called the residual method for estimating clouds and aerosols during the retrieval of spectral UV irradiances (Herman et al. 1999).

1.6.2.2 Global Ozone Monitoring Experiment (GOME)

The Global Ozone Monitoring Experiment appeared as satellite instruments in 1995 when it was launched on the ERS-2 (second European Remote Sensing) satellite. The main purpose of using the GOME instrument is to provide ozone distribution measurements and other trace gases such as NO_2 , BrO_2 , ClO_2 , SO_2 and H_2CO . Furthermore, GOME instruments measure aerosol optical depth and cloud fraction parameters (Callies et al. 2000).

In addition, the GOME instruments have high spectral resolution (0.2-0.4 nm) which are designed to measure the UV and visible region of solar radiation (240-790 nm)

Chapter 1 Introduction

(Veefkind et al. 2006; Weber et al. 1998; Kujanpää & Kalakoski 2015). The UV and visible radiation enter the GOME instrument through the input optics and undergo a series of processes that are a key feature of these instruments, through a double monochromatator that contains a prism and four gratings as dispersing elements for four channels (Burrows et al. 1999).

The GOME instruments have the capability to determine the polarization of the solar radiation using sensitive broadband detectors (Bramsted et al. 2003). However, the GOME ERS-2 (GOME-1) version has a limited data rate because of the environmental and spatial problems, and the instrument structure. There is another modified version of the GOME instrument (Munro et al. 2016), called GOME-2. The GOME-2 instrument was launched on the larger satellite (METOP) on the ARIANE-5 spacecraft that has a different environment, calibration method and orbit. GOME-2 has new features such as $40 \text{ km} \times 40 \text{ km}$ spatial resolution, enhanced calibration features and a modern polarisation system (Callies et al. 2000).

1.6.2.3 Moderate Resolution Imaging Spectrometer (MODIS)

MODIS entered service in 1999 on board the Earth Observing System (EOS) Terra satellite and in May 2002, MODIS also, launched on the Aqua satellite (Segura et al. 2015). Data for this instrument is taken from reflected solar irradiance and depends on 36 spectral bands. The range of these different spectral bands is between $0.415 \mu\text{m}$ and $14.235 \mu\text{m}$ and are used to measure global aerosols. The MODIS algorithm retrieves information about aerosols by using a 500 m resolution radiance in six bands between 550 m to 2100 m . The information between these ranges provides a stable and accurate product. The MODIS algorithm uses α_λ (spectral reflectance as a function of $l_\lambda, SZA, S_{0,\lambda}$), where,

$$\alpha_\lambda = l_\lambda \frac{\pi}{S_{0,\lambda} \cos(SZA)} \quad (1.6)$$

l_λ is a spectral radiance, SZA is solar zenith angle and $S_{0,\lambda}$ is solar irradiance. The most important condition in obtaining accurate aerosol retrieval is that MODIS must have sufficient stability and sensitivity (Levy et al. 2009).

In addition, MODIS has cloud algorithms that provide cloud detection and all the cloud properties such as thermodynamic phase, temperature, pressure, water path and optical thickness (Segura et al. 2015; Platnick et al. 2003; Kaufman et al. 2005). MODIS Terra and Aqua detect the cloud fraction at two different times (Terra at 10:30 am and Aqua at 1:30 pm). Three hours between Terra and Aqua detection provide a good characterisation of the cloud in the daytime (Ackerman et al. 2008).

1.6.2.4 Ozone Monitoring Instrument (OMI)

OMI is a generation of spectrometers placed in orbit by NASA on 14 July 2004. OMI observes the top layers of the atmosphere and covers the UV band and visible irradiance (270-500 nm) with high spatial resolution ($13 \times 24 \text{ km}^2$ at nadir) and spectral resolution of 0.5 nm. OMI was developed to provide data on the ozone column, clouds, surface UV and gases (NO_2 , SO_2 , HCHO, BRO, OCID). Thus, the purpose of using OMI is to monitor long-term changes of UV levels (Bernhard et al. 2015; Pitkanen et al. 2015; Torres et al. 2007; Veeffkind et al. 2006; Ialongo et al. 2010; Jégou et al. 2011; Zempila et al. 2018). The OMI UV algorithm is a derivative from the TOMS UV based algorithm as developed previously by NASA. This algorithm evaluates the surface irradiance under cloudless conditions (E_{clear}). E_{clear} is then multiplied by the factor C_T (which is equal to the derived cloud divided by the non-absorbing aerosol transmittance factor) to estimate the irradiance in the presence of cloud (E_{cloud}) (Ialongo et al. 2010; Tanskanen et al. 2006) where

$$E_{\text{cloud}} = E_{\text{clear}} \cdot C_T \quad (1.7)$$

However, OMI does not cover the boundary layer of the atmosphere which means that absorption by aerosols is not accounted for by the OMI algorithm. Consequently, the OMI algorithm typically overestimates the surface UV irradiance.

1.7 COMPARISON OF GROUND-BASED TO SATELLITE DATA

1.7.1 OMI Broadband UV

Mateos et al, (2013) have estimated the differences in daily terrestrial erythemal irradiance. This was achieved by comparing the OMI measurements to six Spanish, three Argentinean, two Italian, two Israeli, and one Australian ground stations. The results have shown an overestimation of the satellite values where all these results were compared at low surface albedo conditions. This overestimation significantly depends on cloud condition, ozone and aerosols. Buntoung and Webb (2010) have compared the results of erythemal UV dose measurements between OMI and broadband instruments (at four urban sites in Thailand). OMI measurements show overestimation under clear sky conditions of UV irradiance by 10-40% for urban sites. The researchers have concluded that this overestimation comes from the impact of aerosol absorption that is not taken into account in the OMI algorithm.

Pitkanen et al. (2015) have addressed a comparison to validate OMI satellite UV data using ground-based data (Brewer spectrophotometer and Solar Light 501 radiometer) for two sites at Jokioinen and Sodankyla, Finland. The data of this study represents just the summer seasons of 2005 to 2011. This comparison shows +21% of bias for the satellite data compared to ground based data. This overestimation has been explained by the cloudiness and overcast conditions of the summer seasons.

Bernhard et al. (2015) have compared OMI and ground-based erythemal daily UV data at 13 stations located in Arctic and Scandinavian sites. Measurements of this study were over the years from September 2004 and December 2012. In this comparison, OMI data overestimate ground-based data by up to 11% during the year, when the surface albedo is accounted for in the OMI algorithm and the ground-based data are taken from unpolluted, low-latitude and snow-free areas. However, this study has noted the increase of the OMI overestimation by up to 14% at noon in November each year. This difference was because, the OMI algorithm does not take the local noon solar zenith angle (SZA) into consideration.

Tanskanen et al. (2007) have conducted a comparison between the Ozone Monitoring Instrument data and ground based measurements to validate daily erythemal UV doses. The regions of the study have low levels of aerosols and snow free surfaces. In this

Chapter 1 Introduction

study, OMI overestimation compared to the ground based data is up to 10% where the erythemal doses reach 80%. These results are attributed to the OMI algorithm which does not consider the surface albedo, aerosols or trace gas absorption.

Ialongo, Casale & Siani (2008) have compared the differences of erythemal dose rates (EDRs) and erythemal daily doses (EDD) between OMI and ground-based instruments (Brewer and broadband radiometer) that are located in Rome. The results show OMI overestimation of UV measurements compared to the Brewer and radiometer measurements. The researchers have shown that this overestimation could be because of the nature or the structure of OMI that is not suitable to measure the effects of tropospheric aerosols on UV measurements. In summary, most of the studies show the OMI satellite data provides an overestimation compared to the ground based data because of some factors. These factors such as aerosols and SZA influence UV irradiance measurements by satellite.

1.7.2 GOME and TOMS Ozone

Anton et al. (2011) have measured simultaneous total ozone column (TOC) data that are taken from the GOME-2 and Infrared Atmospheric Sounding Interferometer (IASI) satellites and five calibrated ground based Brewer instruments located on the Iberian Peninsula in Spain. This study showed GOME-2 provides slight underestimation of the Brewer ozone data by 1.6%. In contrast, IASI has clear overestimation of Brewer by 4.4%. These differences are attributed to the differences between the vertical sensitivity of IASI and GOME-2. However, in general, the performance of GOME-2 and IASI present an excellent agreement of ozone data with ground-based instruments especially in cloud-free conditions.

Viatte et al. (2011) have studied ozone total column data by using a comparison between Fourier Transform Infrared (FTIR) and Brewer instruments with OMI, GOME, and Infrared Atmospheric Sounding Interferometer (IASI). This comparison has been conducted in Tenerife from March to June 2009. All the comparisons between satellites and surface instruments provided an excellent agreement of 0.94. This correlation is attributed to the high quality of Brewer and FTIR instruments needed to validate total ozone column with OMI and GOME data.

Bramstedt et al. (2003) have provided a study, which included a comparison between GOME and TOMS satellite instrument data and surface station data (Dobson instrument). Datasets of this study included the measurements from 1996 to 2000. The total ozone has been calculated in this study by applying the TOMS algorithm to GOME spectra. This comparison shows a reasonable agreement between the satellites and surface data. The operational measurements of the GOME instrument show a seasonal variation because of air mass factors that cause derivation difficulties in the GOME algorithm. TOMS satellite measurements have shown a high agreement with Dobson data with about 2% uncertainty. Thus, TOMS and GOME satellites ozone measurements provide an excellent agreement with the ground based measurements, which may be attributed to the high sensitivity of the TOMS and GOME instruments.

1.7.3 Spectral UV

Cachorro et al. (2010) have addressed the comparison between satellites (TOMS and OMI) and Brewer instruments located at a station in the south of Spain. The measurements were taken from 2004 to 2008 for three wavelengths: two wavelengths within the UVB range (305, 310 nm) and one within the UVA range (324 nm). In this case, Brewer measurements overestimate satellite data from 10-15% for all UV wavelengths and about 13% for the erythemal UV. Many factors contributed to this difference including cloud conditions, aerosols, ozone and solar elevation.

Kazadzis et al. (2009) have presented a comparison of the UV measurements of OMI and ground based instruments that are located in urban areas (Thessaloniki, Greece). This study has included the data from 2004 to 2007. The results show large OMI overestimation in the UVB, where 305 nm reaches 30% for all sky conditions (clear and cloudy), and less overestimation in the UVA with 324 nm and 380 nm reaching 20% and 16% respectively. These differences were because the OMI algorithm does not consider aerosol absorption.

Buchard et al. (2008) have compared OMI data and ground based instruments (two spectroradiometers and one radiometer) that were located in Villeneuve d'Ascq France. Their measurements were limited to two wavelengths (324.1 and 380.1 nm). The greatest differences of measurements occurred when the level of UV irradiance was low. Here, OMI presents overestimation of 22%, on average, above spectroradiometer

Chapter 1 Introduction

measurements and 34%, on average, above radiometer measurements. The impact of aerosol optical thickness clearly causes the disparity between OMI and ground-based instruments.

Kazantziadis et al. (2006) have compared the spectral UV irradiance that are measured by four European stations (Finland, Netherlands, Italy, Greece) to TOMS satellite data. The result of this study showed that TOMS overestimates UVB at 305 nm, and 310 nm by almost 12% and 18% respectively, while TOMS overestimates UVA (342 nm) by 13%. This variation in the percentages is due to ozone and aerosols having lower absorption for longer wavelengths.

Sharma et al. (2011) focused on a comparison of OMI satellite data and ground based UV radiation measurements in four different sites of Nepal: Kathmandu, Pokhara, Biratuagar, and Lukla in 2010. Their comparison was taken over two seasons of the year (before the monsoon and during the monsoon). The OMI satellite data overestimated the ground based data by different percentages in each season. Before the monsoon, the overestimation was clearly bigger than that during the monsoon for all sites. This study attributed the reason for the overestimation to the OMI algorithm, which has no aerosol corrections, and to the different atmospheric conditions in these two seasons. In addition, this study shows a good correlation between satellite and surface ozone column measurements that reach 91%.

Fioletov et al. (2004) have addressed the UV index climatology by a comparison between the TOMS satellite instrument and Brewer spectrophotometer measurements located at 28 sites in the United States and Canada. The measurements were taken for snow-cover and snow-free conditions. In the snow-covered conditions, the results show a large TOMS underestimation reaching 60% lower than Brewer measurements. However, UV index measurements show that, TOMS has an overestimation that reaches 30%. This big difference between TOMS and Brewer estimations for two different snow conditions was attributed in this study to the aerosol absorption that is not considered in the TOMS algorithm. For some sites of this study, that were located in clean environments, the correlation between TOMS and Brewer data reaches nearly one.

Chapter 1 Introduction

Meloni et al. (2005) have examined the series of erythemal doses by a comparison between Brewer and versions 7 and 8 of TOMS data. The Brewer instrument was installed at the marine site of Lampedusa. This examination has been conducted in the period 1998-2003. The bias between the Brewer and version 7 TOMS for heavy aerosol conditions, reaches +25%, but this percentage dropped to around 8% for cloud free sky conditions. The main reason for these differences is that, TOMS does not detect the aerosol fraction near the surface. The differences between version 8 TOMS and Brewer data were from 3.4 to 8.4% for cloud free sky conditions. In this case, the comparison was independent of the aerosol optical depth and the satellite estimations are improved by an aerosol absorption correction. These studies show variation of agreement between the satellite and ground based spectral UV measurements. This variation may be attributed to factors such as influence of aerosols and ozone.

1.7.4 Nitrogen Dioxide

Kramer et al. (2008) have compared the measurements of vertical column densities (VCDs) of NO_2 between OMI and the ground-based instrument (C-MAX-DOAS) located at the University of Leicester (UK) for the period of data collection from December 2005 to March 2006. The results showed good agreement between ground-based and satellite instruments for cloudless conditions. However, without the tropospheric layer measurements, there is a strong bias in the OMI measurements in comparison with C-MAX-DOAS. This bias is due to the pollution in the urban area is affecting the ground based measurements. In this study, OMI underestimated the measurements of C-MAX-DOAS in the near-surface layers.

Petritoli et al. (2004) have provided a quantitative comparison of the tropospheric nitrogen dioxide between the GOME satellite instrument and in situ chemiluminescent ground-based instruments located in the Po basin (north Italy). The period of the study is over 2000 and 2001. Even though the study was conducted in high-pollution areas, and has high level of fog and clouds, the comparison between the GOME tropospheric column data and ground based concentrations was a reasonable correlation in a monthly distribution.

1.7.5 TOMS Broadband UV

Kerr et al. (2002) compared UV measurements of Brewer instruments, which are located in different Canadian areas and UV measurements of TOMS. They showed differences ranging from 3-11%. This study attributed differences to many predictable factors that could affect the results, such as: SZA, clouds, angular response error, calibration errors, local microclimate and aerosols. McKenzie et al. (2001) have focused on the differences of UV dose measurements between satellite (TOMS) and ground-based instruments in the southern (Lauder, New Zealand) and Northern hemispheres (Garmisch-Partenkirchen, Germany; Thessaloniki, Greece and Toronto, Canada). This study found that the measurements of ground based instruments were less than the satellite values in most of the sites while, in some unpolluted sites, there is satisfactory agreement between satellite and ground based measurements. The differences were attributed to the effects of ozone, aerosols, and cloud conditions.

1.7.6 GOME UV

Arola et al. (2002) have assessed the UV measurements of satellite (GOME) and from Brewer ground based instruments located in Finland, Germany, Belgium, Netherlands and Norway. The results showed significant differences between the values of UV daily doses of satellite and ground-based data. The differences could reach 30-60%. This deviation of the results has been attributed to many factors such as snow, and the GOME cloud algorithm. This study has concluded that there would still be a strong demand for ground-based instruments in coming years. However, the uncertainties in satellite based instrumentation can be overcome by careful calibration to surface measurements. This proposed project will extend previous research by considering comparisons in the UVA waveband.

1.8 SIGNIFICANCE OF THE PROJECT

Excessive solar UV radiation increases the risk of skin cancer and solar UV related eye diseases. The UVB and UVA radiation have damaging effects for both humans and the Earth's ecosystems (Caldwell et al., 1998). One method of defining the effect on human skin is the erythemal UV, which is defined as the UV spectrum weighted

Chapter 1 Introduction

with the erythemal action spectrum (CIE 1988). This is weighted heavily in the UVB waveband compared to the UVA. However, the UVA waveband has also been shown to be damaging to human skin (Agar et al. 2004).

Satellite based instrumentation has been employed for the provision of global coverage on a time repetitive basis of the atmospheric ozone, aerosols, erythemal UV and the irradiance at specific wavelengths. It is important for this time repetitive, global data to be validated against ground based instrumentation if accurate estimates for the terrestrial irradiance and exposure are to be made using remotely sensed measurements. Various studies have done this for the OMI erythemal UV, however no longitudinal research has been undertaken to reconstruct and validate the broadband UVA irradiance and exposure derived from the OMI data over a series of years.

1.9 CHAPTER SUMMARY

This chapter addressed the rationale for this project and provided a literature review about UV radiation, and its effects, the factors influencing the UV irradiance, methods of measuring UV radiation and comparisons of ground-based to satellite data. The following chapter provides details on the instruments used in this research and the methods developed for evaluation and validation of the UVA irradiance and total daily UVA exposure derived from the satellite data, and their comparison with the ground based measurements.

CHAPTER 2

MATERIALS AND METHODS

2.1 OVERVIEW

This chapter provides details of the equipment and methods used in this research. Three instruments that record the spectral and broadband irradiance and the cloud conditions from ground-based measurements are discussed in this chapter. In addition, this chapter addresses the collection methods of the satellite based data.

Spectral irradiances from OMI for 2009 have been compared with a ground based spectral spectroradiometer data. This research has developed a method to evaluate and validate the broadband UVA solar noon irradiances derived from OMI satellite spectral data. In addition, the broadband UVA solar noon irradiance derived from the OMI satellite spectral UV irradiance over 12 years including the influence of cloud have been calculated. As a part of this research, a new method has been developed for the accurate calculation of total daily UVA exposure integrals under cloud-free conditions. Furthermore, this method was used to calculate the total daily UVA exposure from the broadband UVA irradiance to provide a comparison between total daily UVA satellite exposure data and total daily UVA ground-based exposure data over a 10 year period. This technique was also applied to remotely sensed data collected in 2015 and 2016 using the respective relationships between the ground-based and satellite total daily UVA exposure for each cloud category. Results were compared to integrated surface measurements to test the validity of the method.

2.2 SPECTRAL AND BROADBAND SURFACE BASED MEASUREMENTS TO VALIDATE OMIUV SATELLITE DATA

This research is located at the Southern Hemisphere sub-tropical site of Toowoomba (27°36' S 151°55' E), in Queensland Australia. Toowoomba is a rural inland city, which is located about 120 km west of Brisbane (Queensland's capital city) at an elevation of 691 m above sea level with a population of approximately 135, 000. It has a relatively unpolluted atmosphere with low aerosols concentrations. The UVA radiation data for this research were collected by a UV double grating spectroradiometer and a UVA Biometer and were compared to the satellite data from the OMI instrument. Ground based cloud data was collected using an all sky camera located at the same site and aerosol data from a satellite platform. The first part of the

research involves the study of 12 months of data from 1 January 2009 to 31 December 2009 at solar noon times. The solar noon times were determined using the Toowoomba solar noon calendar (Sundial calendar) for each day (Internetworks, 2018). In this part of the research, the 2009 year data have been used because the number of days when the equipment was operational is greater than the other years and the 2009 year was drier with less cloud than the average of other years in Toowoomba. The other parts of the research have employed data collected from October 2004 to the end of 2016.

2.2.1 Ground-based measurements

2.2.1.1 Spectroradiometer Data

The calibrated spectroradiometer is a double monochromator scanning system (model DTM 300, Bentham Instruments. UK) (Figure 2.1) and was used to record ground-based spectral solar UV irradiance. This instrument is installed on an unshaded roof top site at the University of Southern Queensland in Toowoomba. Parisi and Downs (2004) have described the structure, installation, calibration and operation of the Bentham spectroradiometer in detail. The instrument is housed in an environmentally sealed box with the temperature maintained at $24 \pm 1^\circ \text{C}$. The input optics are provided by a Teflon diffuser (model D6, Bentham Instruments. UK) that is connected via a fibre optic cable to the first monochromator. The global UV spectra are recorded automatically from 5:00 am to 7:00 pm at 10 minutes intervals between 280 nm and 400 nm, in 0.5 nm increments, where each scan takes approximately 3 minute to complete. The calibration of the spectroradiometer is traceable to the UK National Physical Laboratory standard and the error of the spectroradiometer data is estimated to be $\pm 9\%$.

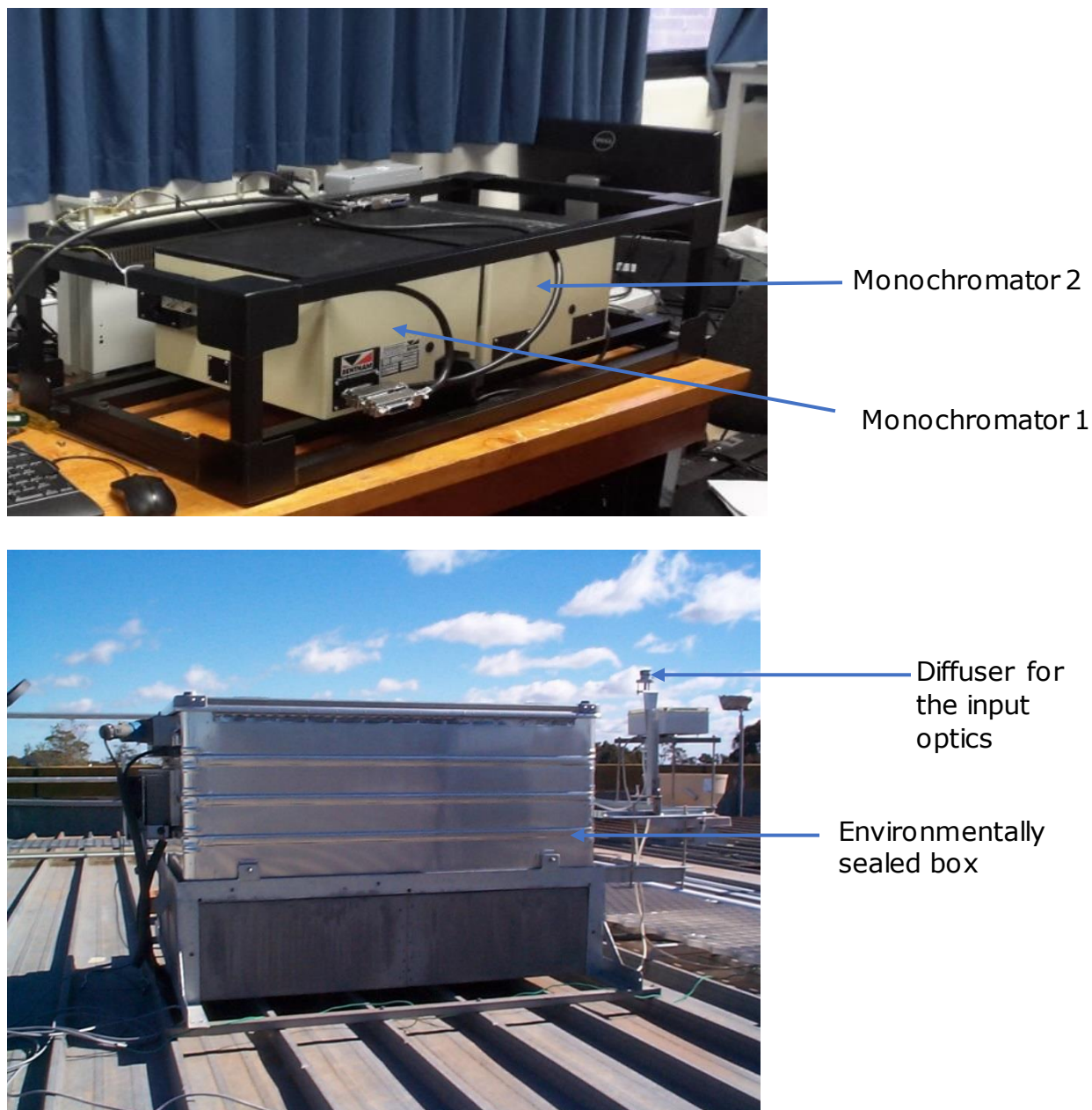


Figure 2.1 Bentham spectroradiometer in the laboratory (top) and on the roof inside the environmentally shaded box (bottom).

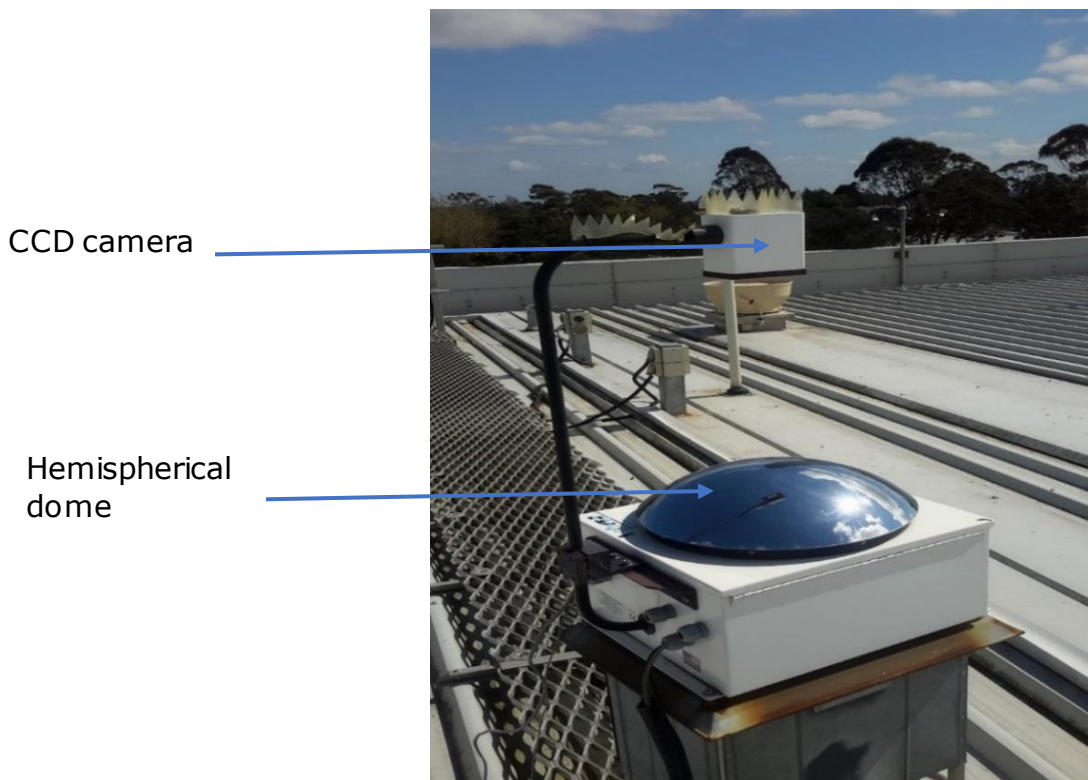
2.2.1.2 Total Sky Imager

To identify the cloud conditions during the intervals of the spectroradiometer scan, this research used a Total Sky Imager (model TSI440 Yankee Environmental Systems, PA, USA) (Figure 2.2). This instrument is based on a CCD colour camera recording images of the sky over a 160° field of view (Sabburg & Long 2004). The operation of the TSI-440 is based on a hemispherical dome, which rotates on a horizontal plane. This dome

Chapter 2 Materials and methods

has a black shadow band for blocking the sun, and a solar-ephemeris to calculate the position of the sun, enabling the dome to rotate during the day to block the sun. The hemispherical dome reflects an image of the sky into the CCD camera, which is suspended above and over the centre of the dome by a thin arm. An image-processing program running on a PC workstation captures images by TCP/IP, processes the images to determine the pixels that are either cloud or no cloud, determines if the solar disc is obscured, or not obscured, and saves the images to JPEG files (Parisi & Downs 2004; Calbó & Sabburg 2008; Long et al. 2006; Yankee Environmental Systems 2006), and the image properties to a text file (Table 2.1 and Table 2.2). The data line entries in these two tables of 'tsi.image.sunny' and 'tsi.image.fraction.opaque' provide the required information on whether the solar disc is obscured or not obscured and fraction of the sky that is covered in cloud.

The Total Sky Imager is programmed to collect and process sky images at the start of each spectroradiometer scan. In the example in Table 2.1, the sun is obscured with a cloud fraction of 1 for the 1 January 2009 for a solar altitude of 85.3°. Similarly, in Table 2.2, the sun is not obscured with a cloud fraction of 0.094 for 16 February 2009 for a sun altitude of 74.7°.



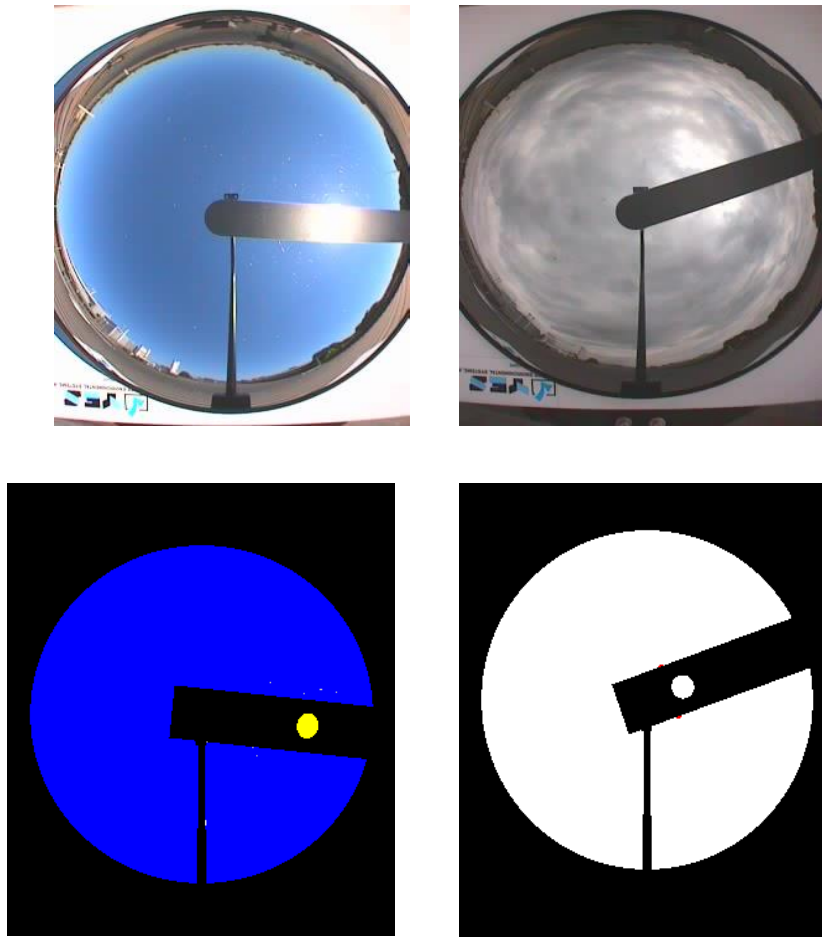


Figure 2.2 Total Sky Imager instrument with clear sky image (left) and a cloudy sky (right).

Table 2.1 Example of TSI imager information for cloudy day (sun obscured sky condition) with a cloud fraction of 1.0.

```
#Thu Jan 01 12:00:04 GMT+10:00 2009
tsi.image.region.horizon.count.thin=0
tsi.image.region.zenith.count.total=14434
tsi.image.count.below.horizon=20839
tsi.image.sunny=false
tsi.image.region.zenith.count.thin=0
tsi.image.solar.azimuth=348.12609506612904
tsi.image.solar.altitude=85.30368008834192
tsi.image.count.box=22194
tsi.image.time=1 January 2009 2\;00\;00
tsi.image.fraction.thin=0.0
tsi.image.count.sky=42514
tsi.image.version=1.1.2
```

```
tsi.image.region.zenith.count.opaque=14434
tsi.image.region.horizon.count.opaque=6673
tsi.image.region.sun.count.thin=0
tsi.image.count.below.proczen=8963
tsi.image.count.mask=6749
tsi.image.region.sun.count.opaque=2805
tsi.image.region.horizon.count.total=6673
tsi.image.count.unknown=117
tsi.image.fraction.opaque=1.0
tsi.image.region.sun.count.total=2922
```

Table 2.2 Example of TSI imager information for cloud free day (non-sun obscured sky condition) with a cloud fraction of 0.094.

```
#Mon Feb 16 12:00:04 GMT+10:00 2009
tsi.image.region.horizon.count.thin=43
tsi.image.region.zenith.count.total=14812
tsi.image.count.below.horizon=20839
tsi.image.sunny=true
tsi.image.region.zenith.count.thin=118
tsi.image.solar.azimuth=5.93113441623094
tsi.image.solar.altitude=74.65763090014225
tsi.image.count.box=22194
tsi.image.time=16 February 2009 2\;00\;00
tsi.image.fraction.thin=0.009195618006521382
tsi.image.count.sky=42629
tsi.image.version=1.1.2
tsi.image.region.zenith.count.opaque=1234
tsi.image.region.horizon.count.opaque=1486
tsi.image.region.sun.count.thin=77
tsi.image.count.below.proczen=8973
tsi.image.count.mask=6724
tsi.image.region.sun.count.opaque=337
tsi.image.region.horizon.count.total=6687
tsi.image.count.unknown=17
tsi.image.fraction.opaque=0.09399704426564076
tsi.image.region.sun.count.total=2543
```

2.2.1.3 Biometer data

The Biometer (model 501, Solar Light Inc, PA, USA) (Figure 2.3) measures the erythemally weighted broadband UV radiation within 280-400 nm and the UVA

Chapter 2 Materials and methods

Biometer (model 501A, Solar Light Inc, PA, USA) measures the broadband irradiance UVA from 320 to 400 nm. The instruments have filters and detectors to record the erythemal UV and the UVA irradiance in five minute daily intervals with a data logger and are temperature stabilised at 25⁰C (Parisi, Sabburg & Kimlin 2004). The erythemal Biometer records the erythemal exposure in units of minimum erythemal dose (MED) for the past five minutes. The UVA instrument records the exposure over the past five minutes in units of J/cm².

In this research the TSI-440 instrument has some missing data for some days during the period of the study (10 October 2004 to 31 December 2016) due to a failure of the instrument on these days. Consequently, the broadband erythemal Biometer data were used to determine if the sky was clear on those particular days. If the data collected in this way formed part of a bell-shaped curve at noon, and met the mathematical criterion according to “The change in magnitude with time test” of Long & Ackerman (2000) it was taken as a cloud free sky. Days which did not fit the criterion of Long and Ackerman were not counted as cloud free (Figure2.4 a). Thus, if the curve was not smooth at solar noon, it was taken as cloudy (Figure2.4 b).

To classify the perfectly cloud-free days, two criteria were implemented. The first criterion: if the difference in successive measurements recorded in each five-minute recording interval of the Biometer exceeded 10% variance of the preceding measurement, the day was excluded from the study dataset, as presumably a measured difference of greater than 10% from the previous measurement would be due to the presence of cloud. Secondly, the distribution of each selected day was examined visually, and excluded if any noticeable discontinuity in the UVA irradiance curve was detected.



Figure 2.3 Erythemal UV (right) and UVA (left) Biometers.

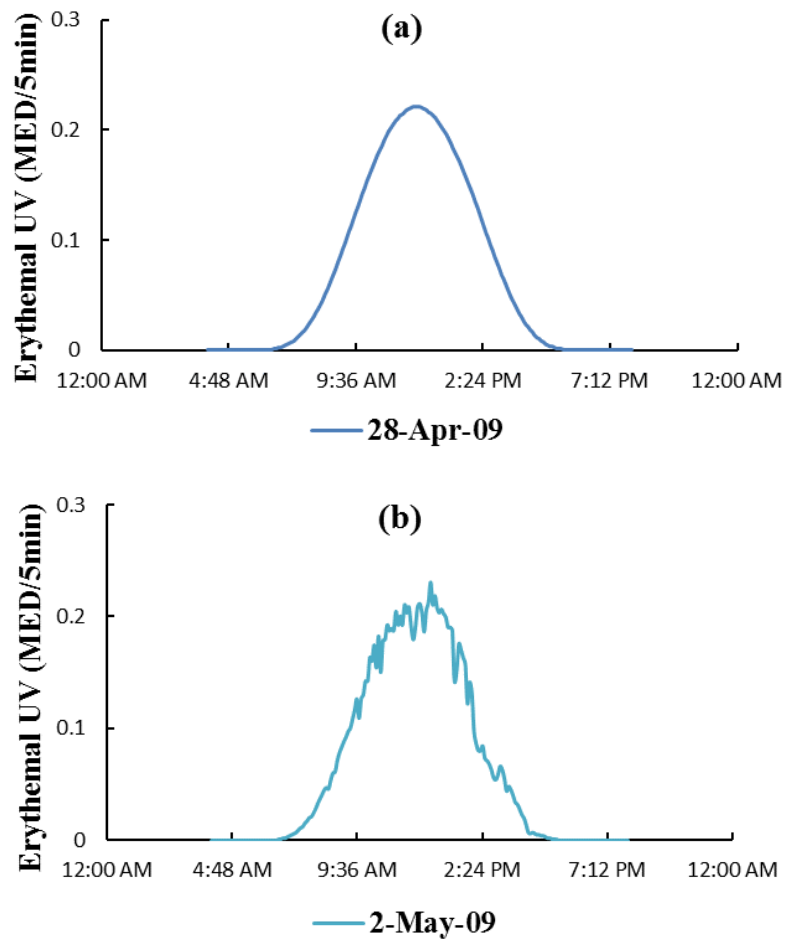


Figure 2.4 Time series of biometer erythemal UV irradiance for a cloud free day (a) and a cloudy day (b).

2.2.2 Satellite-based Measurements

OMI satellite data was retrieved from the Giovanni website which is provided by NASA (<http://giovanni.gsfc.nasa.gov/giovanni/>) (Figure 2.5). The Giovanni website provides the OMI spectral UV irradiance at solar noon from October 2004 until the current day. In this study, the OMI spectral irradiance data was collected for the three UV wavelengths of 310 nm, 324 nm and 380 nm. These wavelengths were selected because the last two are in the UVA waveband and the first one is required to interpolate, to provide information from 320 to 323 nm.

The satellite data were collected from the first day that OMI data was available 1 October 2004, up to 31 December 2016 and provides the OMI satellite solar noontime derived spectral irradiance at a spatial resolution of 1°. The region selected was to provide area averaged data over this region. The data produced is as a CSV file. In order to make a comparison between satellite data (OMI) and ground based Bentham spectroradiometer data, cloud free days were selected by using information from the TSI images when the amount of cloud was determined to be from 0 to 2 okta (all the sky conditions). As explained previously, erythemally effective Biometer data were used for the days with missing data from the TSI to determine if there were any cloud free days.

Chapter 2 Materials and methods

The screenshot shows the GIOVANNI website interface. At the top, there are navigation links for Data Discovery, DAACs, Community, and Science Disciplines. The main header includes the GIOVANNI logo and the tagline 'The Bridge Between Data and Science v 4.26'. Below the header, there is a navigation bar with links for Release Notes, Browser Compatibility, Known Issues, and Log out (murf). A yellow banner at the top of the main content area reads 'Advisory on Web browsers installed on older operating system versions ... [1 of 2 messages] Read More'. The main content area is divided into several sections: 'Select Plot' with radio buttons for Maps, Comparisons, Vertical, Time Series (Area-Averaged), and Miscellaneous; 'Select Date Range (UTC)' with a date range from 2004-10-01 to 2016-12-31; 'Select Region (Bounding Box or Shape)' with a bounding box of 151.8036,-27.7185,152.2266,-27.312; 'Select Variables' with a list of variables including Irradiance 310 nm, 324 nm, and 380 nm; and a table of matching variables. The table has columns for Variable, Units, Source, Temp. Res., Spat. Res., Begin Date, and End Date. The bottom of the page features a footer with NASA logos, contact information for Long Pham and M. Hegde, and logos for NC, OPeNDAP, and CMR. A 'Plot Data' button is highlighted in green.

Variable	Units	Source	Temp. Res.	Spat. Res.	Begin Date	End Date
<input checked="" type="checkbox"/> Irradiance 310 nm (Local Noon) (OMIUVBd v003)	mW/m ² /nm	OMI	Daily	1°	2004-10-01	2018-06-23
<input checked="" type="checkbox"/> Irradiance 324 nm (Local Noon) (OMIUVBd v003)	mW/m ² /nm	OMI	Daily	1°	2004-10-01	2018-06-23
<input checked="" type="checkbox"/> Irradiance 380 nm (Local Noon) (OMIUVBd v003)	mW/m ² /nm	OMI	Daily	1°	2004-10-01	2018-06-23

Figure 2.5 The Giovanni website provides the UV irradiances at solar noon from 1/10/2004 to 31/12/2016. In this study, the spectral irradiance data is collected for the three UV wavelengths (310, 324 and 380 nm) at solar noon. The area of this data is the Toowoomba region, Australia (151.8036° , -27.7185° , 152.2266° , -27.312°).

2.2.3 Derivation of Satellite Broadband UVA Irradiance

The spectral irradiance at 310, 324 and 380 nm at local solar noon during 2009 were firstly compared to the corresponding ground based spectral irradiance on cloud free days. This research compared the solar noon broadband UVA irradiance evaluated from the satellite spectral data with the broadband UVA irradiance measured with the ground based UVA Biometer. The satellite UVA irradiance were evaluated from the satellite spectral irradiance at 310, 324 and 380 nm for cloud free days. The trapezoidal rule was applied to interpolate between 310, 324 and 380 nm, with the spectral irradiance at 380 nm extended out to 400 nm (Anav et al. 2004; Igoe & Parisi 2014) to develop a model for the evaluation of the broadband UVA (W/m^2) from 320 to 400 nm (A Jebar et al. 2017) as follows:

$$E_{UVA} = 0.57 S_{310} + 31.429 S_{324} + 48 S_{380} \quad \text{W/m}^2 \quad (2.1)$$

where S_{310} , S_{324} and S_{380} are the spectral UV irradiance ($\text{W/m}^2/\text{nm}$) at the respective wavelengths from the satellite data. This formula approximates the irradiance limits for summation from 320 to 400 nm to provide the broadband UVA irradiance. Figure 2.6 shows that, for the wavelength range to 400 nm, the value at 380 to 400 nm has been applied in equation 2.1.

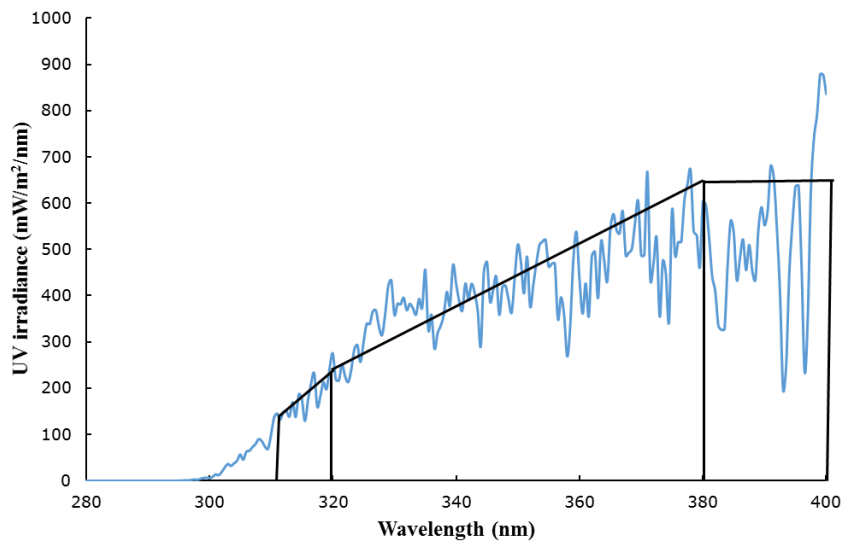


Figure 2.6 The solid line shows the trapezoidal integral of the UV irradiance with the wavelength using the spectral irradiances 310, 324 and 380 nm. This is superimposed on the UV spectrum collected with the Bentham spectroradiometer.

2.3 UVA IRRADIANCE OVER A TWELVE-YEAR PERIOD FROM OMI DATA INCLUDING THE INFLUENCE OF CLOUD

2.3.1 Ground Based Data

In this research, 1,920 days of data were used in the comparison between the Biometer UVA irradiance measured at solar noon and the OMI UVA broadband data at solar noon evaluated using equation 2.1. The average calibration factor of the UVA Biometer to the UVA irradiance derived from the scanning spectroradiometer was 1.007 for the 12 year period of this study. The data spans the period from 1 October 2004 to 31 December 2016. The total number of days depends on when both the Total Sky Imager and the UVA Biometer were concurrently collecting data at solar noon

along with OMI satellite data being available. A total of 115 days (5.9%) were excluded from the analysis due to surface instrument malfunction. The available data set was split into the four cloud categories at solar noon of 0 to 2, > 2 to 4, > 4 to 6 and > 6 to 8 okta based on the TSI image data recorded at solar noon. These four cloud cover categories were each further sub-divided into the days when the sun's disc at solar noon was and was not obscured by optically thick cloud. The statistics used in all the comparison were the relative root mean square error (rRMSE), mean absolute error (MAE) and coefficient of determination (R^2). The MAE is used to provide overall differences and the rRMSE is used for comparison of linear relationships.

2.3.2 Satellite-based Data

To calculate the satellite broadband UVA irradiance [W m^{-2}] over the waveband of 320 to 400 nm from the OMI measurements, this study has applied the broadband UVA evaluation model (equation 2.1) for the period 1 October 2004 to 31 December 2016. The evaluated satellite broadband UVA irradiance data were compared with the Biometer broadband solar noon UVA irradiance for the four cloud categories and the cases of sun obscured and sun not obscured.

2.4 TOTAL DAILY UVA EXPOSURE EVALUATED FROM OMI SATELLITE SPECTRAL IRRADIANCE FOR CLOUD FREE DAYS

The total daily radiant UVA exposure, UVA_{TOT} [J/m^2] is the integral of the daily solar UVA irradiance, E_{UVA} [W/m^2] measured from sunrise to sunset. UVA_{TOT} may be determined for the length of a solar day [$t = 0$ to 1] according to Equation 2.2, where the length of the day is normalized:

$$UVA_{TOT} = \int_{t=0}^1 \int_{\lambda=320}^{400} E_{UVA}(\lambda, t) d\lambda dt \quad (2.2)$$

where E_{UVA} under cloud free conditions is dependent on the diurnal variation in air mass and is a function of local solar zenith angle (SZA), E_{UVA} increases from sunrise, reaching a maximum at solar noon, and decreasing steadily to sunset. Because the

radiant UVA exposure is measured between 320 to 400 nm (Diffey 2002b), the diurnal variation of E_{UVA} is largely independent of atmospheric absorption by ozone, a significant regulator of terrestrial UVB irradiance, but ozone provides negligible attenuation in the UVA before 330 nm (Madronich 1998). Thus, the variation of E_{UVA} under cloud free conditions follows a predictable daily distribution, approximating a normal or Gaussian curve (Figure 2.7).

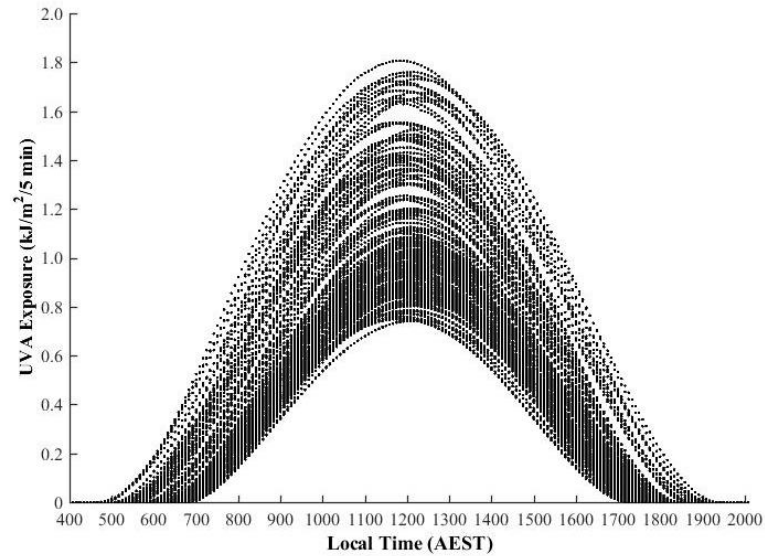


Figure 2.7 Seasonal variation in UVA (320-400 nm) exposure recorded at five-minute intervals and measured for cloud free days between February 2005 and December 2016.

In Figure 2.7, the measured radiant UVA exposure for each five-minute interval is plotted for 186 cloud free days measured in sub-tropical Queensland, Australia for the period February 2005 to December 2016 (12 years). The UVA exposures for each five-minute interval were recorded with the temperature stabilised integrating UVA Biometer (model 501A Solar Light Co. PA, USA). Radiant UVA exposure curves were included in the Figure for all days in the 12 year measurement period that were determined to be cloud free. Cloud free days were those in which no cloud was detected in the daily recording period (from local sunrise to sunset). The exclusion criteria described earlier to exclude days that were not cloud free all day resulted in the removal of 3,771 (95.3%) daily radiant UV exposure curves from the complete 12 year dataset. Variations observed in Figure 2.7 in the measured peak UVA exposure and the length of the daily exposure interval are caused by the seasonal influence in

Chapter 2 Materials and methods

local sun rise and sun set times and peak SZA. The longest days and minimum SZA (maximum UVA_{TOT}) occur in late December, near the summer solstice (Southern Hemisphere) and the perihelion passage of the Earth's annual orbit occurring in early January.

Table 2.3 summarises the total number of cloud free curves included in the current research according to month of the year for all years in the study period. The table shows the seasonal influence of cloud cover for the Toowoomba measurement site, where most cloud free days occur in the austral winter months (June to August) and the least occur in the sub-tropical summer (December to February).

Table 2.3 Number of cloud free days from February 2005 to December 2016 used in deriving the UVA exposure integral for each day under cloud free conditions. The percentages in brackets represent the measured fraction of cloud free days in each month. The final column is the integral of the UVA exposure data that has been normalized in x and y , $\int UVA_{NORM}$.

Month	Cloud-free days	$\int UVA_{NORM}$ (average monthly)
January	2 (0.6%)	0.54
February	4 (1.3%)	0.54
March	8 (2.3%)	0.55
April	5 (1.5%)	0.55
May	20 (5.9%)	0.55
June	26 (7.9%)	0.55
July	44 (12.9%)	0.55
August	41 (12.0%)	0.55
September	17 (5.2%)	0.55
October	16 (4.7%)	0.54
November	2 (0.6%)	0.54
December	2 (0.6%)	0.54

To remove the influence of seasonality in the plotted UVA exposures, each curve in the data-series was normalised with respect to the peak UVA irradiance and with respect to the day length. Each of the 187 cloud-free curves are plotted again in Figure 2.8 after being normalized in x (time of day) and y (measured UVA exposure). The normalization of both axes results in a nominal range and domain [0 to 1] on both axes and was performed according to Equations 2.3 and 2.4, where,

$$t_{NORM}(x) = \frac{hour(x)}{hour_{sunset}(x) - hour_{sunrise}(x)} \quad (2.3)$$

And

$$E_{UVANORM}(x) = \frac{E_{UVA}(x)}{E_{UVA}(x_{max}) - E_{UVA}(x_{min})} \quad (2.4)$$

where, $t_{NORM}(x)$ is the normalised time of day expressed as a fraction of the measured number of hours between sunrise and sunset where the day length ($hours_{SUNSET}(x) - hours_{SUNRISE}(x)$) was determined from the first and last non-zero measurement of E_{UVA} for each of the 187 cloud free days in the 12 year measurement period. Similarly, the normalized exposure is expressed as a fraction by calculation of the quotient of E_{UVA} at each recorded time of day to the daily range in UVA exposure. When corrected for seasonality, the integral of the normalised cloud free exposures represent a unit-less nominal integral occupying a 1 x 1 grid space in x and y . The normalised UVA_{TOT} shows little variation across all 187 UVA curves re-plotted in Figure 2.8.

A Gaussian distribution has been used previously (Diffey 2009) to estimate the total erythemically weighted daily UV exposure. Here, a Gaussian distribution was not implemented to approximate the daily UVA_{TOT} due to noted differences in the exposure distribution with time of day (Diffey 2002b). Specifically, the UVA exposure distribution curve is less sensitive to Rayleigh's criterion for scattering at large SZA and is not sensitive to stratospheric ozone. The result is less tapering of the diurnal UVA distribution at large SZA, making a Gaussian approximation inaccurate for the derivation of the normalized UVA distribution with time of day. A trapezoidal

approximation (Equation 2.5) is used here to derive the normalised UVA exposure integral,

$$\int E_{UVANORM}(x) \approx \frac{0.05}{2} (E_{UVANORM}(0) + E_{UVANORM}(1) + 2 \sum_{i=1}^n E_{UVANORM}(i)) \quad (2.5)$$

where, $E_{UVANORM}(0)$ and $E_{UVANORM}(1)$ represent the starting and terminating normalized exposure and $E_{UVANORM}(i)$ represents the normalised UVA exposure at each step in the numerical integral between the $E_{UVANORM}(0)$ and $E_{UVANORM}(1)$. Normalised integrals averaged for each respective month in the 12 year study period are listed in Table 1.

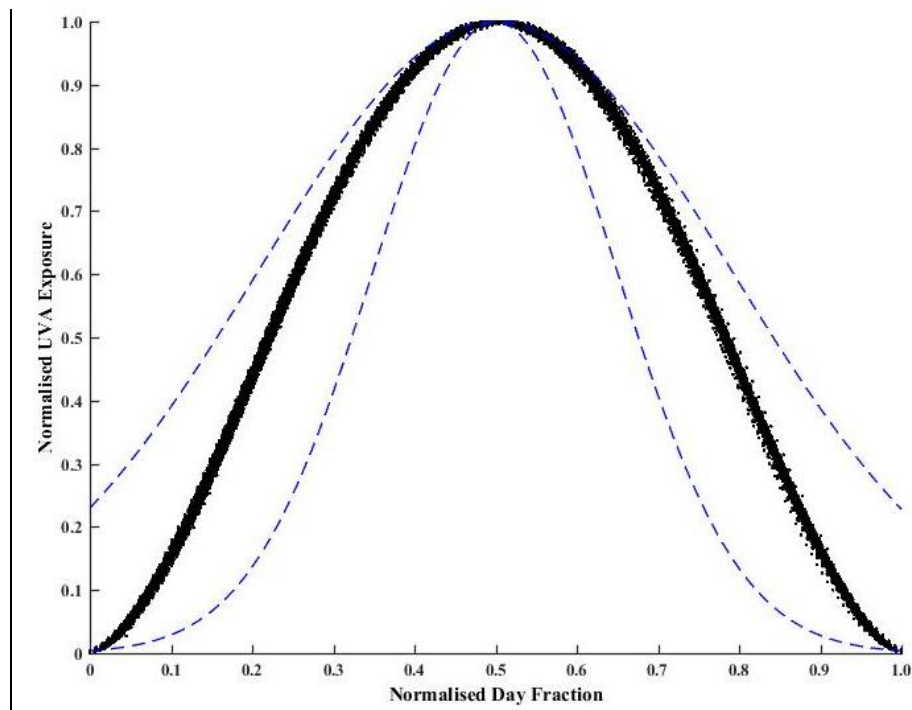


Figure 2.8 Measured UVA exposure curves, normalised in x and y for each of the 187 cloud free days in the period February 2005 to December 2016 (points). Gaussian model approximations normalised to the peak of the measured exposure data are plotted as blue dashed curves showing the range in possible Gaussian fits to the measured data.

2.4.1 Total Daily UVA Exposure

The OMI satellite total daily UVA exposures (UVA_{Day}) have been calculated from the daily solar noon broadband UVA irradiance evaluated from the three OMI spectral irradiance measurements at 310 nm, 324 nm and 380 nm (A Jebar et al., 2017) with the following equation:

$$UVA_{Day} [kJm^{-2}] = \frac{E_{UVA} \times 3600 \times H \times F}{1000}. \quad (2.6)$$

where the daily UVA integral expressed in kJ/m^2 is modeled as the fraction (F) of maximum daily broadband UVA irradiance determined from the OMI satellite (E_{UVA} [$W m^{-2}$]), the constant 3600 is the number of seconds in an hour and H is the number of hours (expressed as a decimal) from sunrise to sunset. F represents the normalised fraction of the day occupied by a bell-shaped UVA cloud free distribution rising at sunrise, peaking at solar noon and falling at sunset (A Jebar et al. 2018b).

2.5 INFLUENCE OF CLOUD ON OMI SATELLITE TOTAL DAILY UVA EXPOSURES OVER AN EXTENDED PERIOD

In this section, the method to determine the total daily UVA exposures from the OMI satellite data has been further developed for cloudy conditions over the 10 years (from the 1 October 2004 to 31 December 2014 period). These data were further categorised into the cases of the solar disc not obscured by cloud and the solar disc obscured by cloud and for each of these two cases, the data were separated into the four cloud categories of 0 to 2, > 2 to 4, > 4 to 6 and > 6 to 8 okta based on available sky image data recorded by the ground based Total Sky Imager (TSI).

The OMI satellite total daily UVA exposures for the ten-year period were derived with the model in Equation 2.6 from the solar noon UVA irradiance calculated from the OMI spectral irradiance measured at 310, 324 and 380 nm for the different cloud categories. There were compared to the ground based total daily UVA exposures measured with the calibrated UVA Biometer at the measurement site. The UVA Biometer provides the five-minute exposures in units of J/cm^2 and these were summed over the day to provide the total daily UVA exposures in kJ/m^2 .

2.5.1 Validation

The technique for the satellite daily UVA exposure estimates developed using remotely sensed data to December 2014 was also applied to remotely sensed data collected in 2015 and 2016 using the respective relationships between the ground-based and satellite total daily UVA exposure for each cloud category for all cloud conditions over these two years. Results were compared to integrated surface measurements to test the validity of the method. For this purpose, surface measurement data from the broadband UVA meter and remote sensed satellite data from 2015 and 2016 was categorised as days with the solar disc not obscured and those with the solar disc obscured.

2.6 CHAPTER SUMMARY

This chapter described the instruments and methods used to obtain the ground based and satellite based data used in this research. The following chapter will present the results of the research on spectral UV data and solar noon UVA data.

CHAPTER 3

SPECTRAL AND BROADBAND UV MEASUREMENTS

3.1 OVERVIEW

This chapter presents and discusses the results of the validation of the OMI UV satellite measurements using ground-based spectral UV data and evaluation of UVA broadband solar noon irradiance, using OMI data from the period of 1 January to 31 December 2009.

3.2 SPECTRAL AND BROADBAND SURFACE BASED MEASUREMENTS TO VALIDATE OMI UV SATELLITE DATA

This research compares the broadband unweighted UVA data derived from the OMI to ground based instruments. This section, will firstly compare the cloud free solar noon spectral irradiance at three wavelengths from OMI with ground based spectral spectroradiometer data. Using the spectral irradiance at these wavelengths a method will be developed to evaluate the broadband UVA solar noon irradiance derived from OMI satellite spectral data for cloud free days and validate this against ground based broadband data obtained from a radiometer at the Toowoomba measurement site (A Jebar et al. 2017).

3.2.1 Spectral Data

The time series of the cloud free spectral irradiance at solar noon during 2009 for the satellite data are shown in Figure 3.1 for the wavelengths of 310, 324 and 380 nm. This figure shows that the signal increases from 310 to 380 nm because the measured UV irradiance increases with wavelength in the UVA spectrum. The total number of days in the 1 January to 31 December period classified as cloud free days was 71 (19.5%) of the total number of days in the period. From 1 January to the end of March of 2009 year, there were no recorded cloud free days.

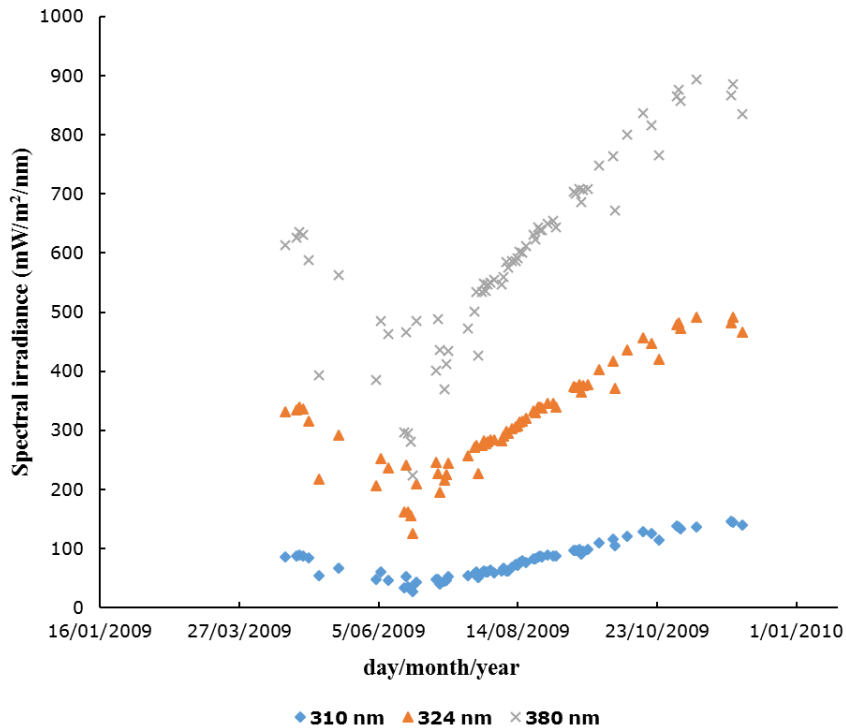


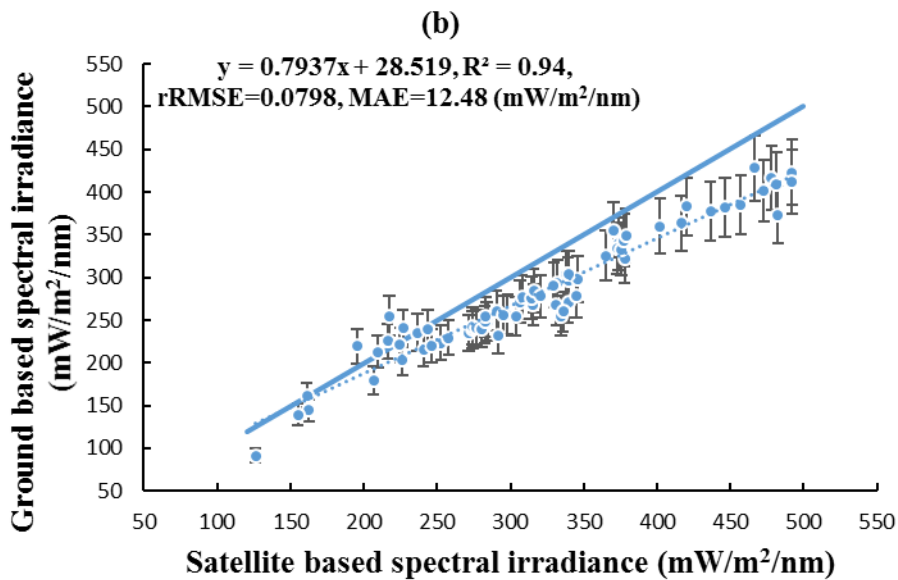
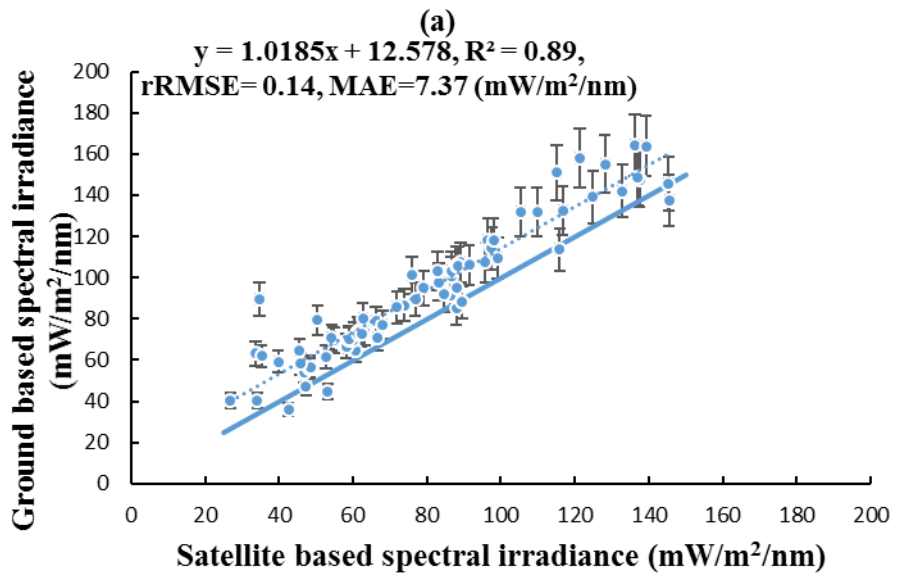
Figure 3.1 Time series of spectral irradiance at 310, 324 and 380 nm for cloud free days for the OMI satellite data from 1 January 2009 to 31 December 2009. The total number of days in the 1 January to 31 December period classified as cloud free was 71 (19.5% of the total number of days in the research period).

The comparison of ground based spectroradiometer data to satellite derived solar noon spectral irradiance on cloud free days is shown in Figure 3.2. The OMI data is a spatial average over a $1^{\circ} \times 1^{\circ}$ grid and the ground based data is at a static point. Additionally, the OMI overpass time is not at solar noon and the data collected at the overpass time is used to calculate the values for solar noon, showing the need to provide calibrations as in this research to ground based data. The error bars correspond to the $\pm 9\%$ error associated with the ground based measurements (Parisi, Sabburg & Kimlin 2004). The average of the aerosol levels from the Giovanni web site on these cloud free days from the MODIS instrument on the Aqua and Tera satellites is 0.04 showing the relatively low aerosol level over the site. The error at 310 nm due to the OMI evaluation of the ozone levels is expected to be minimal as the mean relative difference between OMI and ground based Dobson spectrophotometer ozone data for Brisbane (within 150 km of the site in this research) is within 1% (Balis et al. 2007).

The satellite spectral irradiance comparisons to the ground based measurements show a clear correlation for the wavelengths of 310, 324 and 380 nm. There is a good

Chapter 3 Spectral and broadband UV measurements

comparison between the satellite and ground based spectral irradiance measurements on cloud free days for the three discrete wavelengths with an R^2 of 0.89 and rRMSE of 0.14 or better in each waveband (Figure 3.2). In each graph, the dashed line is the fitted regression line and solid line is the 1:1 line. The R^2 value of 0.89 occurs for 310 nm where the magnitude of the spectral irradiance is the lowest. Sensitivity to ozone variations and instrument noise affect the sensitivity of the instrument at 310 nm, thereby increasing the uncertainty of the comparison at 310 nm.



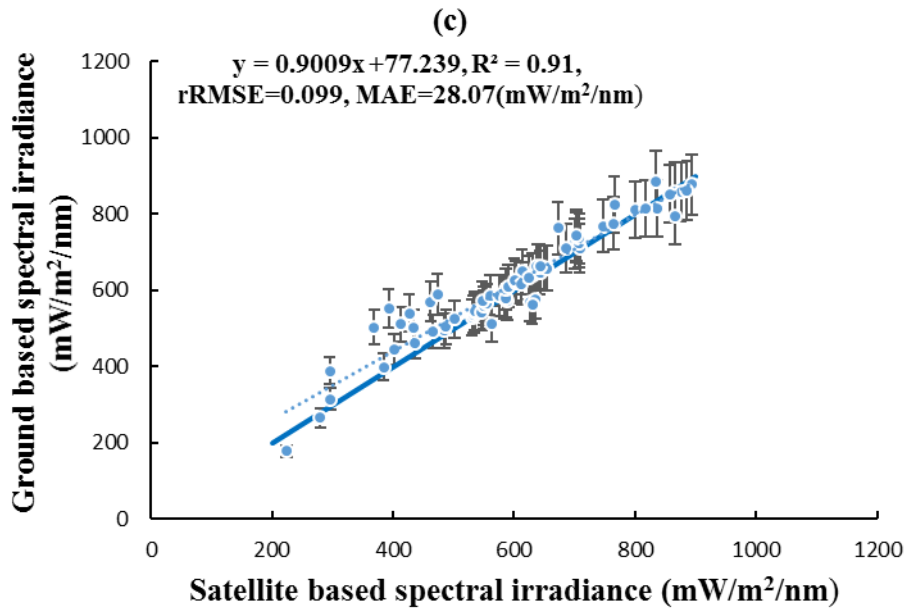


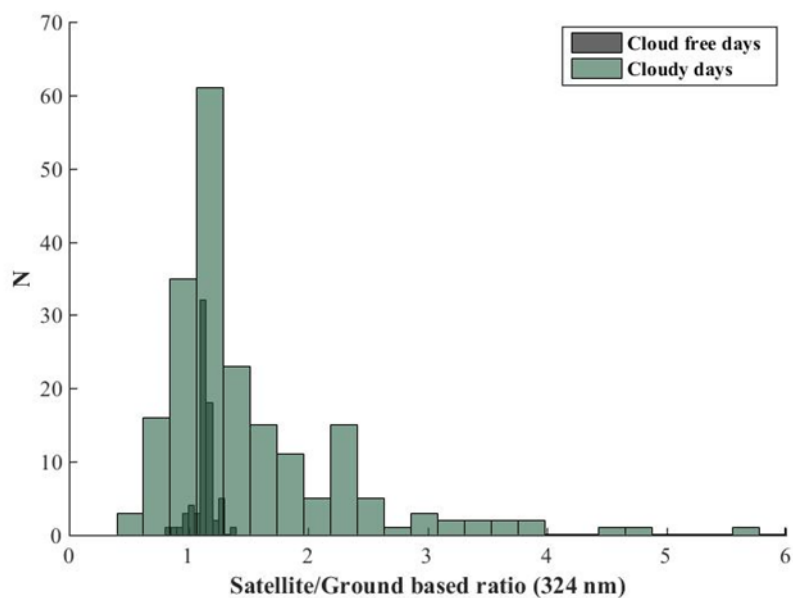
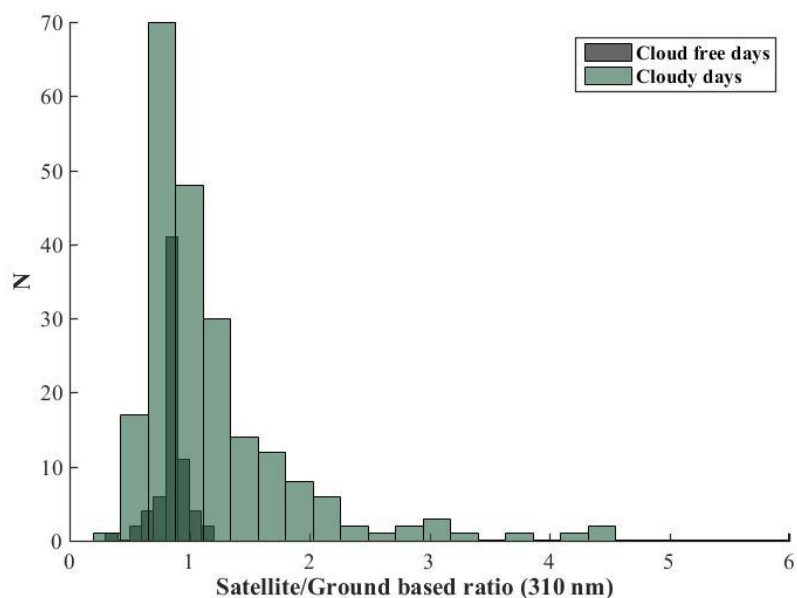
Figure 3.2 Cloud free days OMI and ground based spectroradiometer spectral irradiance comparison for (a) 310 nm, (b) 324 nm, (c) 380 nm ($n=71$ cloud free days). The error bars correspond to the $\pm 9\%$ error associated with the Bentham spectroradiometer data. The solid line in each graph is the 1:1 line.

The distribution of the ratio of satellite to ground based measured spectral irradiance is plotted in Figure 3.3 for both cloud free conditions (darker bars) and cloudy conditions (lighter bars). Figure 3.3 illustrates that most of the spectral irradiance from the OMI satellite exceeded the measured ground based data as noted previously by other researchers for the shorter wavelength erythema UV and UVB comparisons (Mateos et al. 2013). Median, first quartile and third quartile statistics are given in Table 3.1 for the distributions plotted in Figure 3.3.

Those ratios above one confirm that some satellite measurements over predict the UVA irradiance for most sky conditions, which displays a similar trend to shorter wavelength comparisons as seen in the literature. Those ratios below one may be the result of low aerosols in the research area which may be different to other research areas. Also seen in the Figure, the cloudy days have a much wider range of values with the median ratio generally being higher than one.

Table 3.1 The first quartile (Q1), median and third quartile (Q3) values for cloudy and cloud free days at 310, 324 and 380 nm.

	Q1	Median	Q3
Cloud free days (310 nm)	0.82	0.85	0.89
Cloud free days (324 nm)	1.11	1.13	1.16
Cloud free days (380 nm)	0.95	0.98	1.00
Cloudy days (310 nm)	0.83	0.99	1.34
Cloudy days (324 nm)	1.06	1.22	1.76
Cloudy days (380 nm)	0.90	1.07	1.66



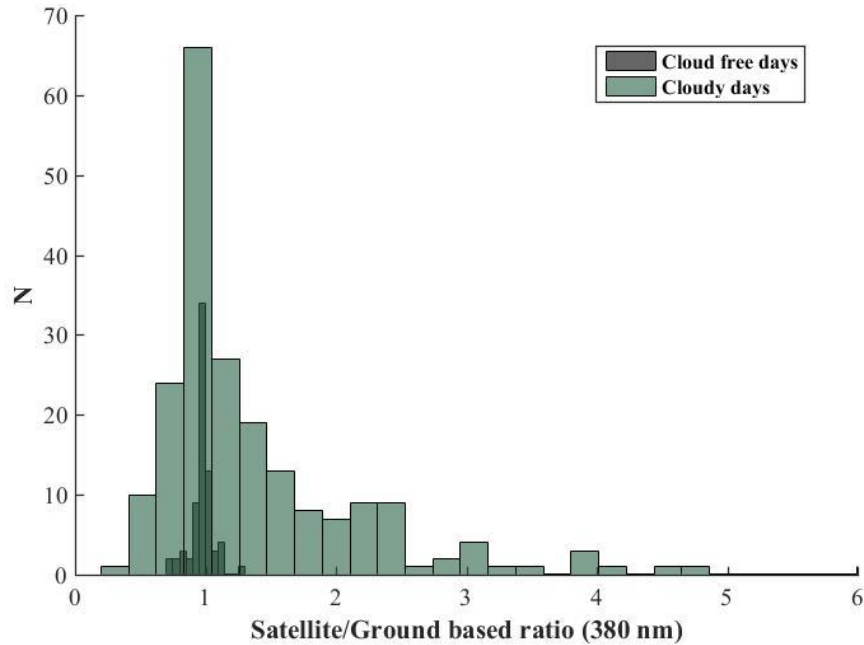


Figure 3.3 Histograms of the ratio of the satellite to ground-based spectral solar noon UV measurements for each of 310, 324 and 380 nm. The darker bars correspond to the measurements for the 71 cloud free days and the lighter bars correspond to 221 measurements on cloudy days. *N* is the number of values. For each graph, there are 2 or less values above the value of 6.

3.2.2 Broadband UVA

The broadband UVA solar noon irradiance, which are derived from the solar noon OMI spectral irradiance data have been reconstructed using Equation 2.1 and compared under cloud free days to ground based measurements. Figure 3.4 shows the UVA irradiance (W/m^2) modelled from the satellite spectral irradiance measurements ($\text{W}/\text{m}^2/\text{nm}$) at 310, 324 and 380 nm for solar noon compared to the broadband UVA data measured with the UVA Biometer on cloud free days in the period 1 January to 31 December 2009. The error bars represent the $\pm 10\%$ error associated with the ground based UVA Biometer data. There is a reasonable agreement between the solar noon UVA broadband irradiance from the measured ground based UVA Biometer instrument and the modelled UVA irradiance derived from satellite with an R^2 of 0.86. Figure 3.4 shows the satellite UVA evaluation is approximately 30% higher which can be accounted for by calibration to ground based instruments and in turn used for health applications where ground based data are not available. The spectroradiometer measurements at 310, 324, 380 nm were used in Equation 2.1 to calculate the UVA

and compared to the Biometer UVA. The dashed line is the fitted regression line and the solid line is the 1:1 line. The R^2 was 0.86 and the rRMSE was 0.085. The slope is 0.7 indicating that there is some difference between ground and satellite based data.

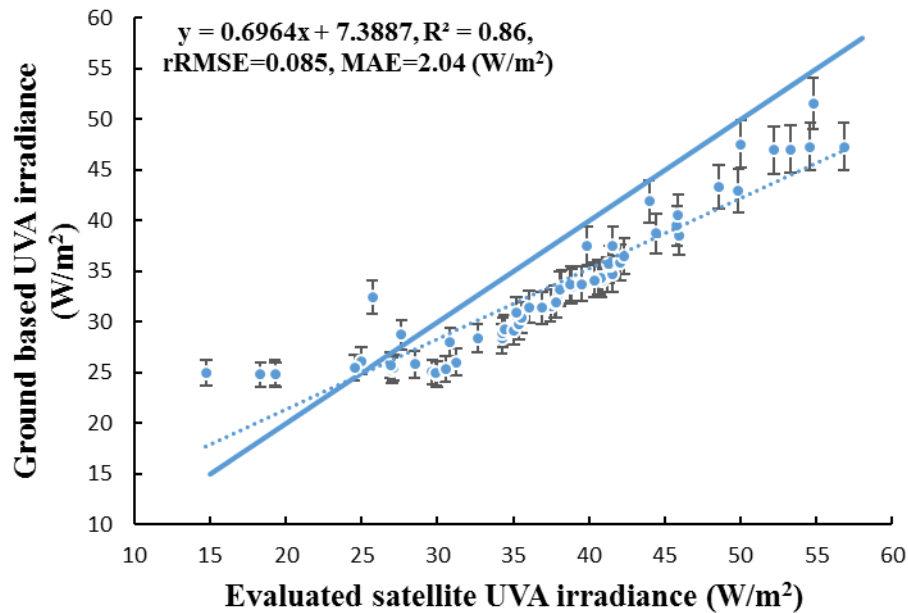


Figure 3.4 Comparison of the broadband UVA irradiance values evaluated from OMI spectral data and the UVA irradiance from the ground based measurements as derived from Equation 2.1 using the OMI spectral irradiances. The error bars are the $\pm 10\%$ error associated with the ground based data and the solid line is the 1:1 line.

3.3 CHAPTER SUMMARY

This chapter discussed the validation of the OMI UV satellite measurements at 310, 324 and 380 nm using ground based spectral UV data. The model developed in this research to calculate UVA irradiance from the satellite data has been validated to the ground based radiometer irradiance data. The following chapter applies the method evaluated to twelve years of data to evaluate UVA irradiance from OMI data including the influence of cloud on the UVA irradiance. The influence of aerosols at the research site on the UVA irradiance is also considered.

CHAPTER 4

INFLUENCE OF CLOUD ON THE SATELLITE AND GROUND BASED UVA MEASUREMENTS

4.1 OVERVIEW

This chapter provides the results of the comparisons of the OMI UV satellite measurements against ground-based spectral UV data including the influence of cloud for the 12 year period of 2004-2016. In addition, the chapter provides the results of the evaluated UVA irradiance from OMI data including the influence of cloud for the twelve years. Furthermore, this chapter considers the influence of aerosols on the UVA irradiance.

4.2 SPECTRAL UV IRRADIANCES AND THE INFLUENCES OF CLOUD

Figure 4.1, 4.2, 4.3 and 4.4 show the results of the comparisons between the solar noon ground based spectroradiometer data and the OMI satellite measurements for the three wavelengths of 310, 324 and 380 nm for all the cloud conditions, including obscured and not obscured conditions (0-2, 2-4, 4-6, and 6-8 okta). Ground based data (Bentham measurements) are taken over the 12 year period when there was available spectral data (2005, 2007, and 2008). For the cloud condition categories of 0-2 okta (Figure 4.1), there is a good correlation with an R^2 from 0.63 to 0.76 and an rRMSE ranging from 0.31 to 0.25 for the three wavelengths. For the > 2-4 okta category (Figure 4.2), there is a similar correlation to the 0-2 okta, particularly at the wavelength of 310 nm. For this category, the R^2 was from 0.57 to 0.74 and the rRMSE ranged from 0.41 to 0.32 for all three wavelengths. The measured spectral irradiance comparisons for > 4-6 okta and > 6-8 okta (Figure 4.3 and 4.3) showed lower correlation than the 0-4 okta cloud conditions, with R^2 values of 0.52 to 0.55 (> 4-6 okta) and 0.20 to 0.37 (> 6-8 okta). This is to be expected for these higher amounts of cloud cover.

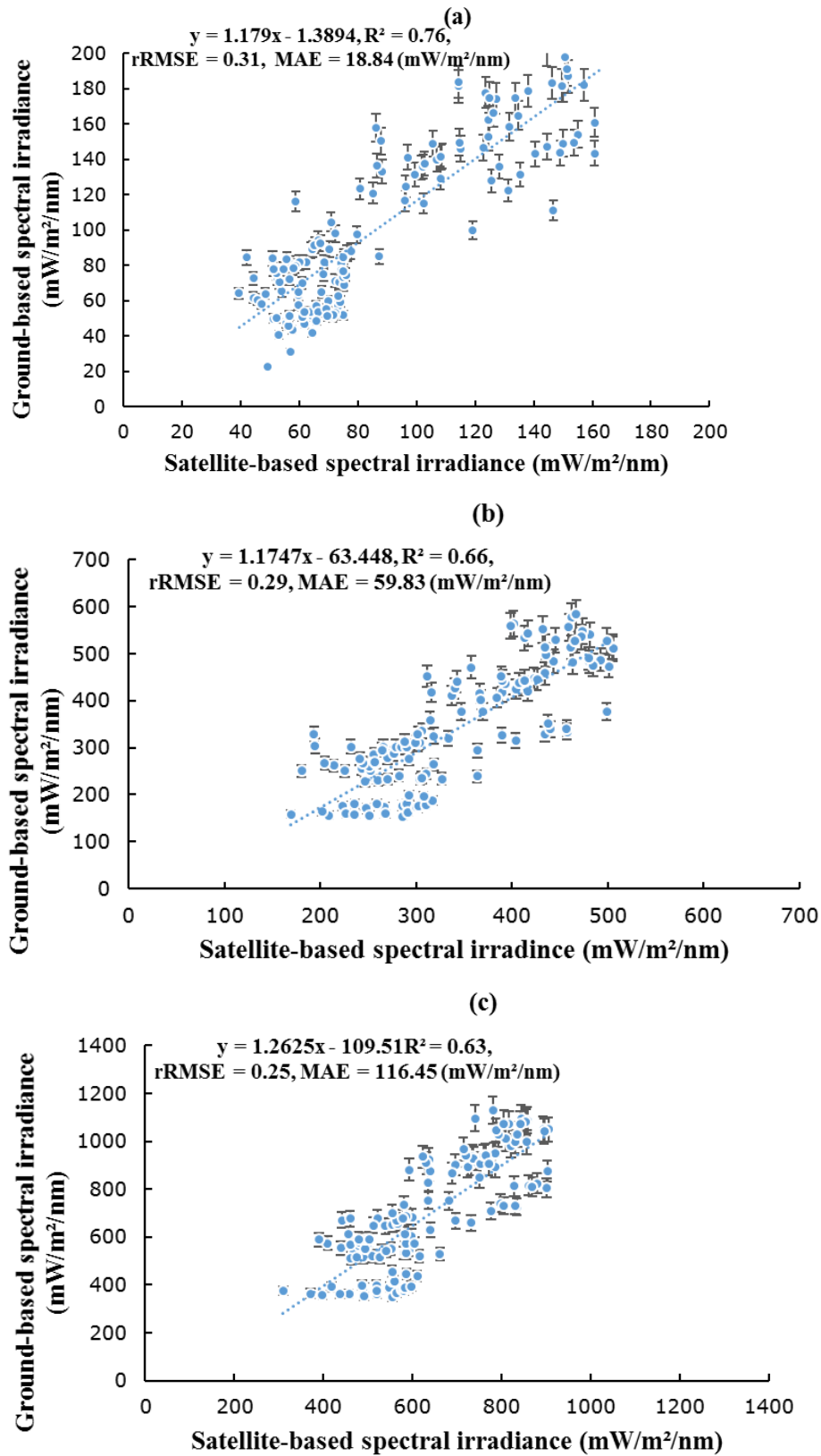


Figure 4.1 OMI and Bentham spectral irradiance comparison for (a) 310 nm, (b) 324 nm, (c) 380 nm, for the cloud cover of 0 to 2 okta.

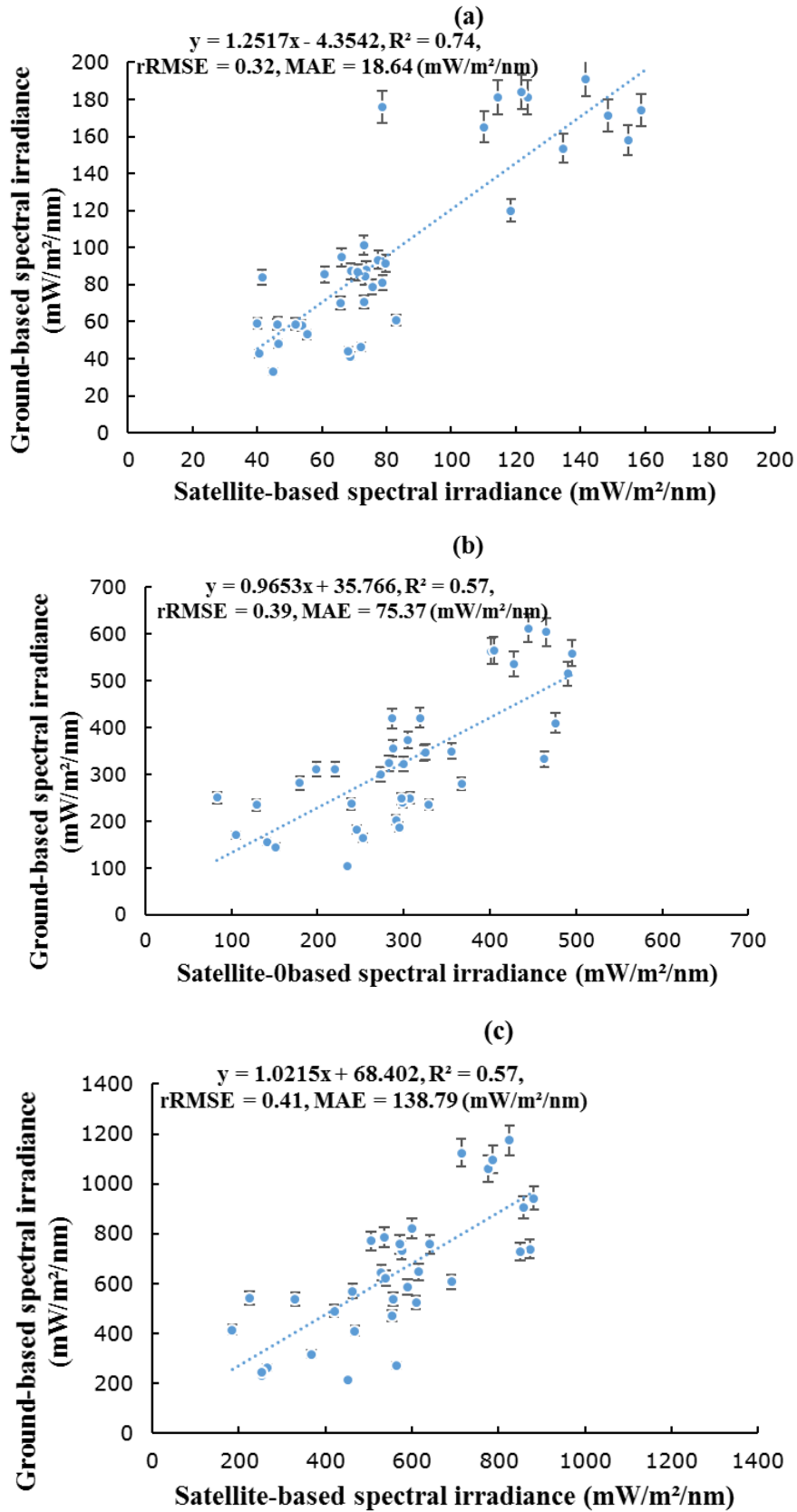


Figure 4.2 OMI and Bentham spectral irradiance comparison for (a) 310 nm, (b) 324 nm, (c) 380 nm, for the cloud cover of > 2 to 4 okta.

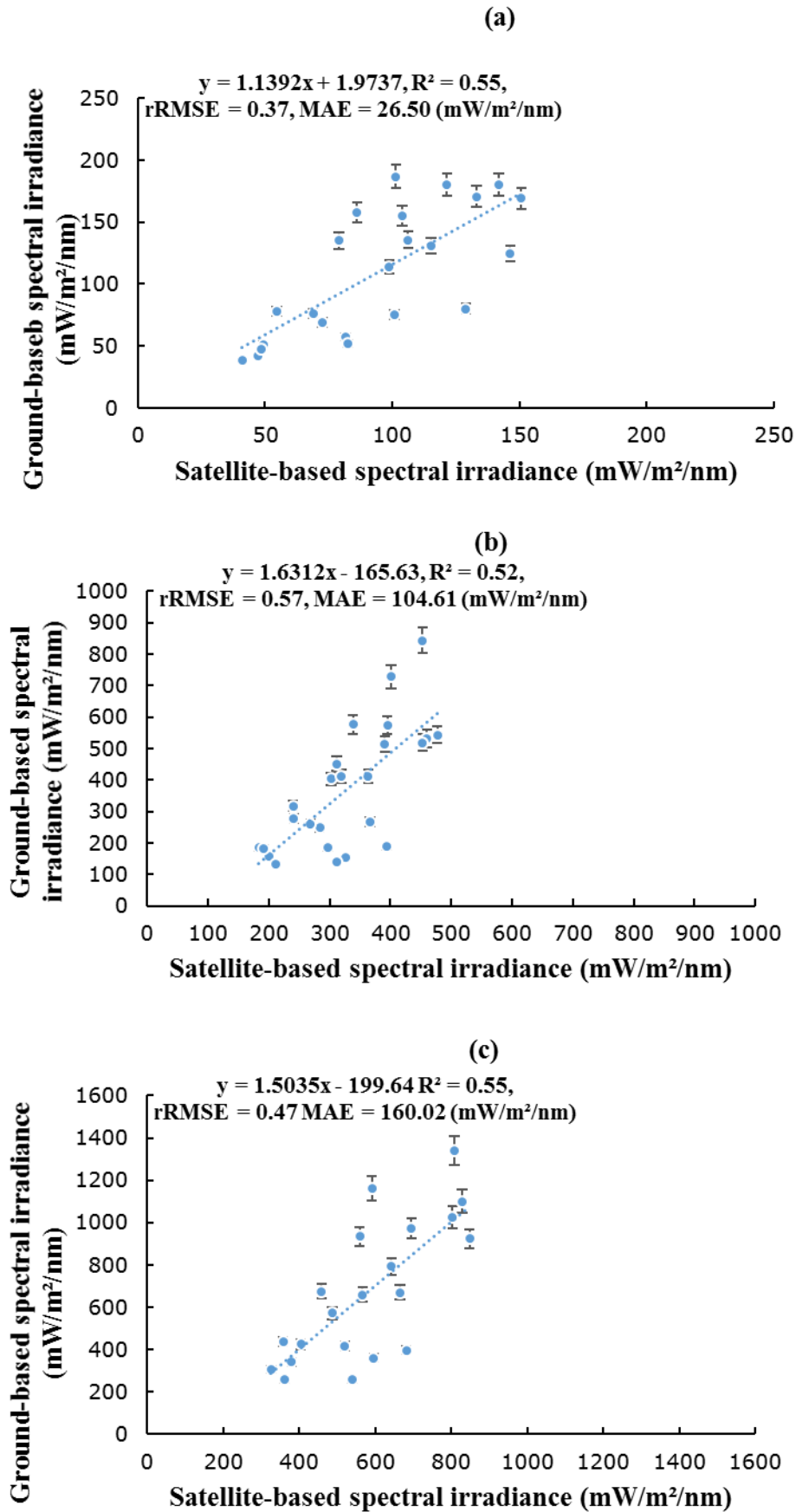


Figure 4.3 OMI and Bentham spectral irradiance comparison for (a) 310 nm, (b) 324 nm, (c) 380 nm, for the cloud cover of > 4 to 6 okta.

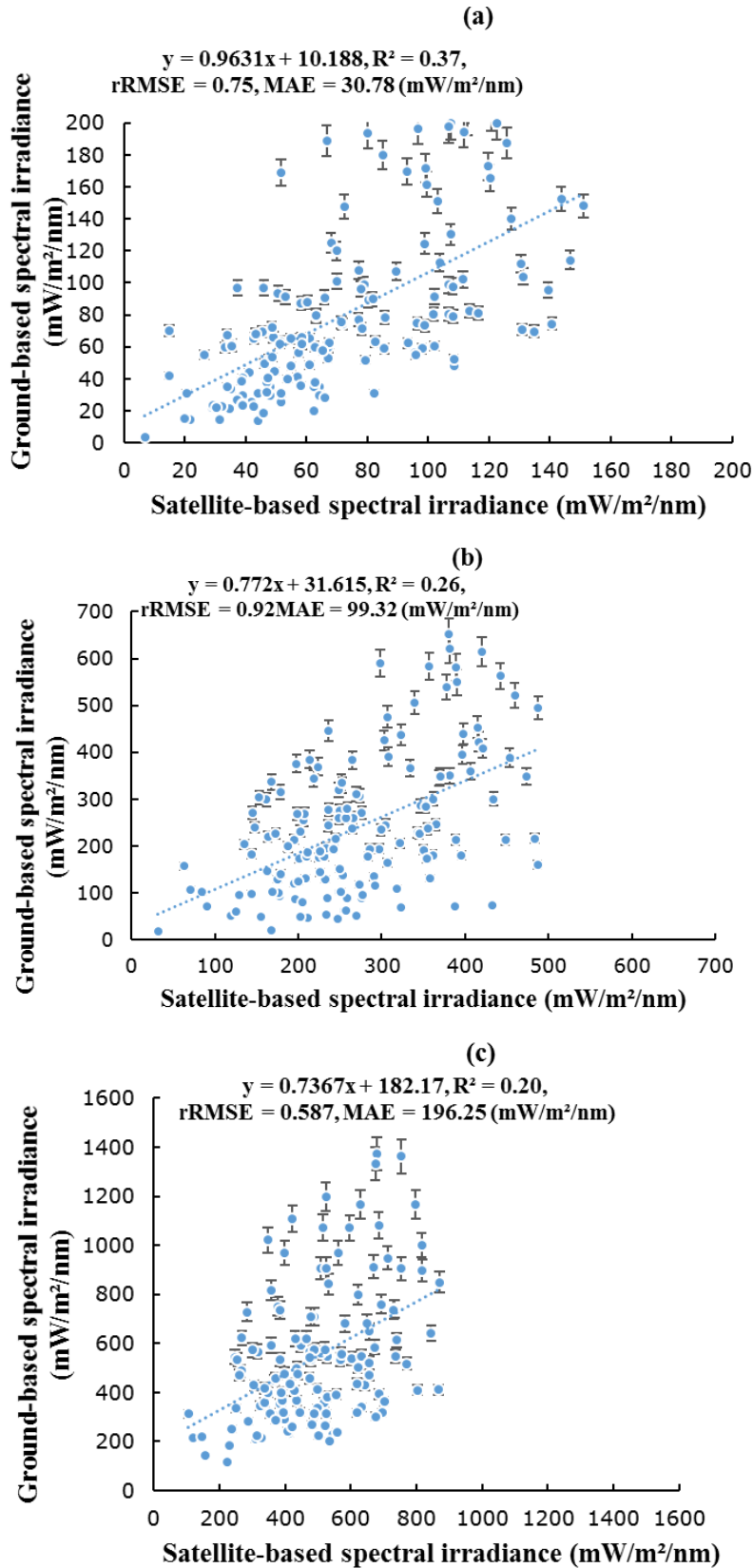


Figure 4.4 OMI and Bentham spectral irradiance comparison for (a) 310 nm, (b) 324 nm, (c) 380 nm, for the cloud cover of > 6 to 8 okta.

4.3 EVALUATED UVA IRRADIANCE OVER A TWELVE-YEAR PERIOD FROM OMI DATA INCLUDING THE INFLUENCE OF CLOUD

The research reported here extends the previous section by considering evaluation and validation of the broadband UVA irradiance derived from discrete OMI spectral irradiance measurements to the ground based data recorded from an independent radiometer over a long-term (decadal) period. Subsequently there remains limited information in the literature to develop an understanding of the direct seasonal influence of cloud. This is an important consideration, given the prevalence of cloud cover in the day-to-day environment. In this research, comparison of the OMI reconstructed solar noon UVA broadband irradiance with ground based measurements obtained from 2004 to 2016 are reported for all sky coverage conditions at the elevated regional sub-tropical Southern Hemisphere site of this research that is free from major sources of anthropogenic pollution (A Jebar et al. 2018a).

4.3.1 All Sky Conditions

Figure 4.5 shows the time series of the evaluated satellite broadband UVA irradiance at solar noon for the Toowoomba study site from October 2004 to December 2016 for all sky conditions. This included 3,861 values over 3,861 days from satellite based data representing 88% of the available days. The number of values available as recorded by the TSI, for the cloud free days in the period was 1,082 ($n = 1,082$). For cloudy days (> 2 octa), the number of values when there was available TSI data was 733 ($n=733$). The annual cyclical pattern of high and low irradiance with the changing seasons is seen in Figure 4.5 with the variation of the solar noon UVA irradiance changing annually between approximately 30 W/m^2 and 60 W/m^2 . The influence of absorption due to ozone is minimal in the UVA waveband. Additionally, the aerosol index over the measurement site is generally low due to unpolluted skies (see Section 4.4), apart from a small number of days that reported significant dust levels (Downs et al 2016). There is no snow at the sub-tropical site of the research, with no resulting large variation in the ground surface albedo. Consequently, measured reduction of the UVA irradiance below the cloud-free envelope is predominantly due to clouds.

A histogram of the complete set of the evaluated UVA irradiance is provided in Figure 4.6. The maximum solar noon UVA irradiance over this period is greater than 60 W/m^2

with the median solar noon UVA irradiance being 38.8 W/m^2 . The first and third quartile values are 30.8 and 48.4 W/m^2 respectively. The predominance of low amounts of cloud cover at the sub-tropical measurement site is evident in the positively skewed distribution of the 12 years data set toward higher noon time UVA irradiance measurements.

The total dataset, split by calendar year is presented as box and whisker plots in Figure 4.7. The line within each box is the median and the box is the data within quartiles one and three. The dashed line of the whiskers represents the range of the data up to ± 5 standard deviations, with two outliers. The box and whisker plot of 2004 is shifted to higher irradiance values due to only the last three months of the year being available. As this is the last two months of the austral spring and the first month of summer, the median is higher than that for the other years. For all but two years in the 12 year study period, the distribution of noon time annual solar UVA irradiance appears consistent. Red outliers in Figure 4.7 represent 26th of June 2007 and 7th of December 2011, which were completely overcast days, as determined from the TSI imager.

The solar noon UVA irradiance for the years of 2009 and 2010 are noteworthy due to the change in the climatic conditions between these two consecutive years. The year 2009 was a particularly dry year characterised by a severe dust storm in September 2009 (Downs, Bulter & Parisi 2016). Annual rainfall for 2009 totalled only 433 mm, a difference of 38.4% from the decadal mean for Toowoomba reported by the Australian Bureau of Meteorology of 703.1 mm. For 2009, the mean UVA irradiance was 40.4 Wm^2 and the median was 40.9 W/m^2 compared to the mean and median of the total remaining years of 38.9 W/m^2 and median 38.8 W/m^2 respectively. Mann-Whitney – u tests show that there was a statistically significant difference in the 2009 irradiance measurements compared to the total remaining years ($p < 0.0264$). Given that 2009 was drier than other years and employed to develop the method in Chapter 3, the research in this chapter reports on satellite to ground based measurements more typical of the sub-tropical climate experienced at the Toowoomba measurement site taken over a longer decadal time period.

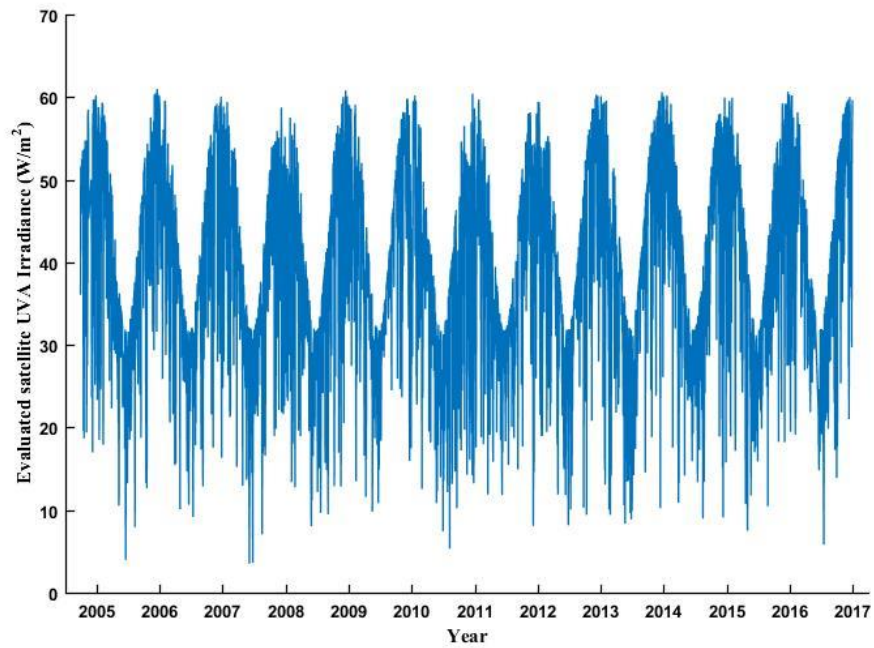


Figure 4.5 Time series of solar noontime UVA irradiance evaluated from the 310, 324 and 380 nm satellite data.

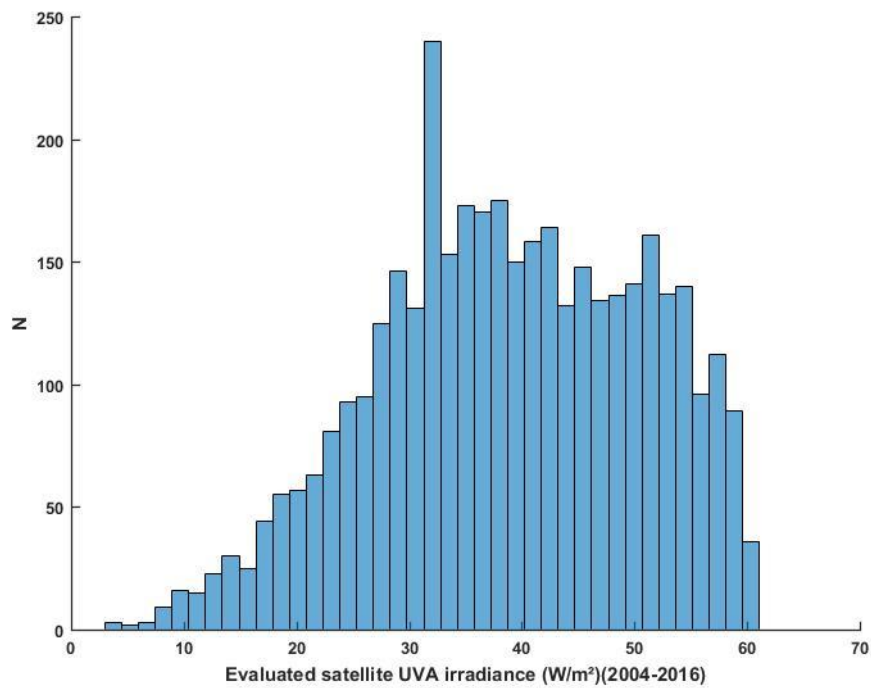


Figure 4.6 Distribution of the solar noon UV irradiance evaluated from the satellite data.

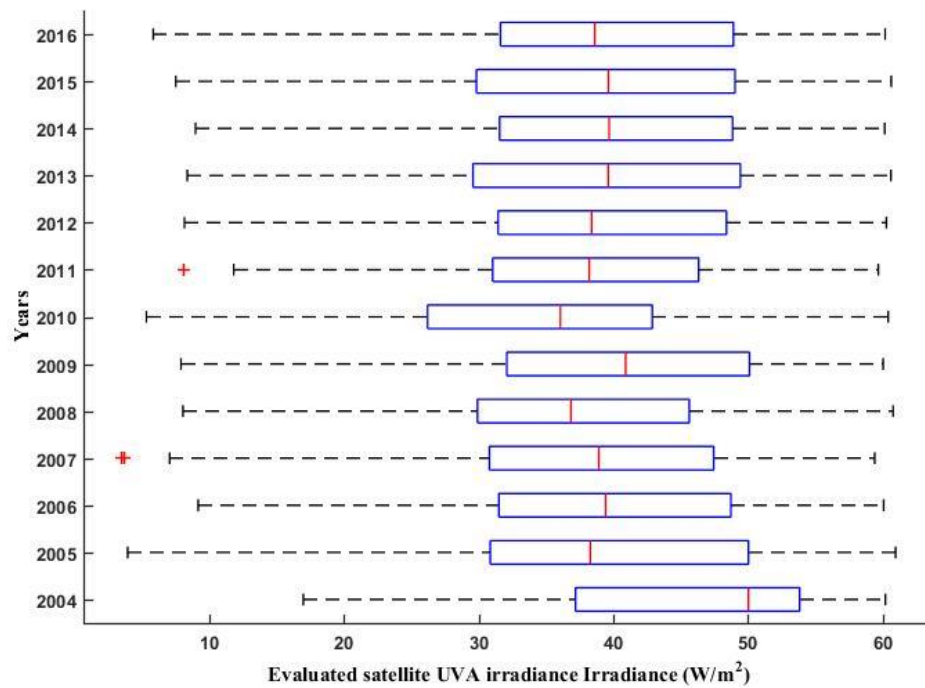


Figure 4.7 Box and whisker plots of the broadband UVA irradiance evaluated from the OMI spectral data from October 2004 to 31 December 2016 for all sky conditions. The line within each box is the median and the box is the data within quartiles one and three. The dashed line of the whiskers represents the range of the data up to ± 5 standard deviations, with two outliers. The dataset for 2004 is shifted to higher irradiance due to only the last three months of the year being available.

4.3.2 Cloud Data

Table 4.1 shows the number of occurrences of days with the different amounts of solar noon cloud cover from October 2004 to December 2016. At this sub-tropical site, the majority of the data (62.4%) is in the category of 0-2 octa, with a median of 0.1728 octa. The number of days in the two cloud categories of 0 to 2 and > 2 to 4 octa of cloud at solar noon was 1,285, representing 70.7% of the total number of study days. This means that the broadband UVA evaluation model from the OMI spectral data is applicable for approximately 70% of the days at the Toowoomba sub-tropical site. The number of the plotted cloud-free days (0 to 2 octa) is 1,262 as this takes into account the days when the Biometer data was employed to confirm a cloud free day (Long & Ackerman 2000). The number of the plotted data from > 2 to 8 octa was less than the total TSI data available due to missing Giovanni satellite data and Biometer data not available on some days. Figure 4.8 shows the time series of the TSI imager cloud

condition data as shown in the Table 4.1 at solar noon for the Toowoomba study site from October 2004 to December 2016. The gaps in the data are when the TSI was not operational.

Table 4.1 Distribution statistics of the cloud cover at solar noon for the 2004 to 2016 dataset (between 0 to 8 okta). Q1 is the first quartile of the range, Q3 is the third quartile of the range and N is a number of days with data in the respective category.

Octas	Q1	Median	Q3	n	n (plotted data)	n (obscured)
0-2	0.03	0.17	0.76	1082	1262(data from TSI and Biometer)	0
>2-4	2.45	2.86	3.43	203	150	115
>4-6	4.44	4.90	5.35	138	116	102
>6-8	7.21	7.99	8	392	352	368
0-8	0.10	1.13	5.02	1815	1880	585
2-8	3.73	6.26	8	733	618	585

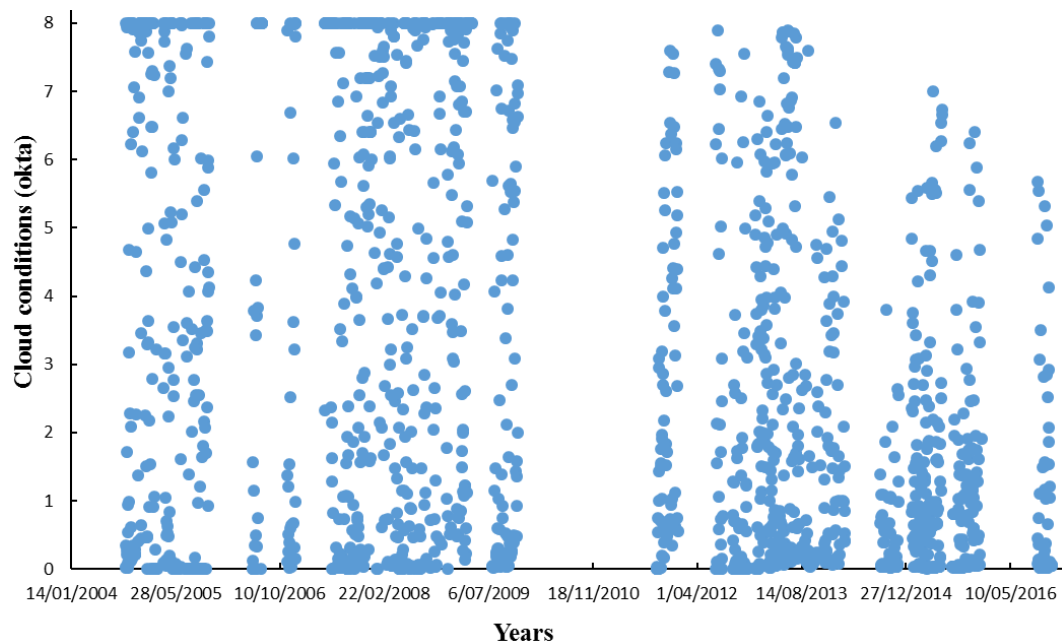


Figure 4.8 Time series of the cloud conditions from zero to eight okta for October 2004 to December 2016 as measured by the Total Sky Imager.

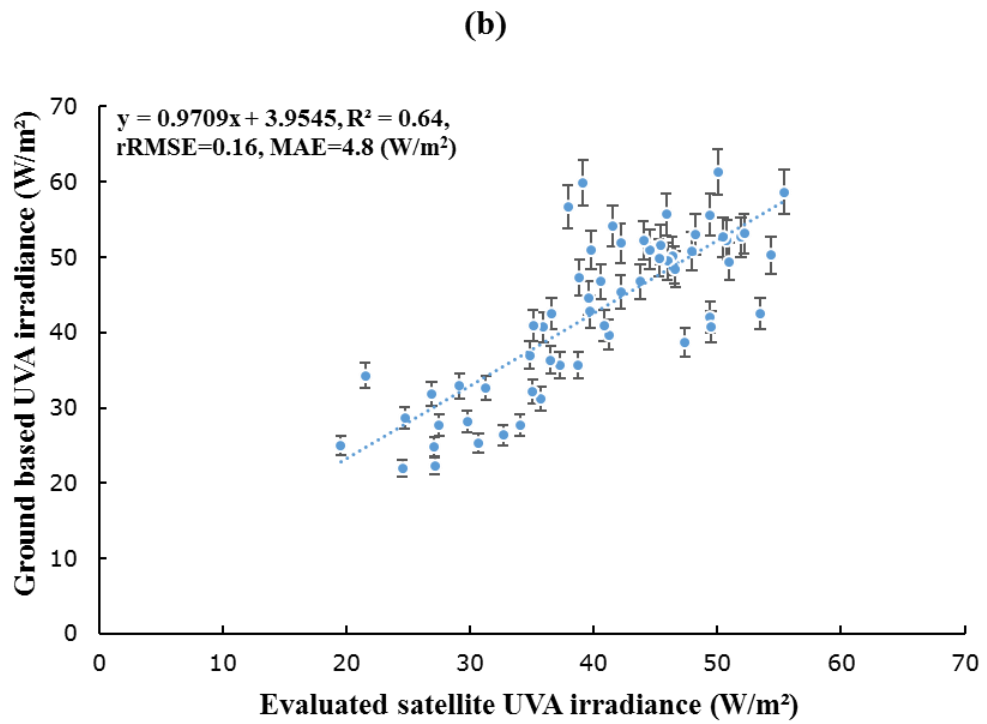
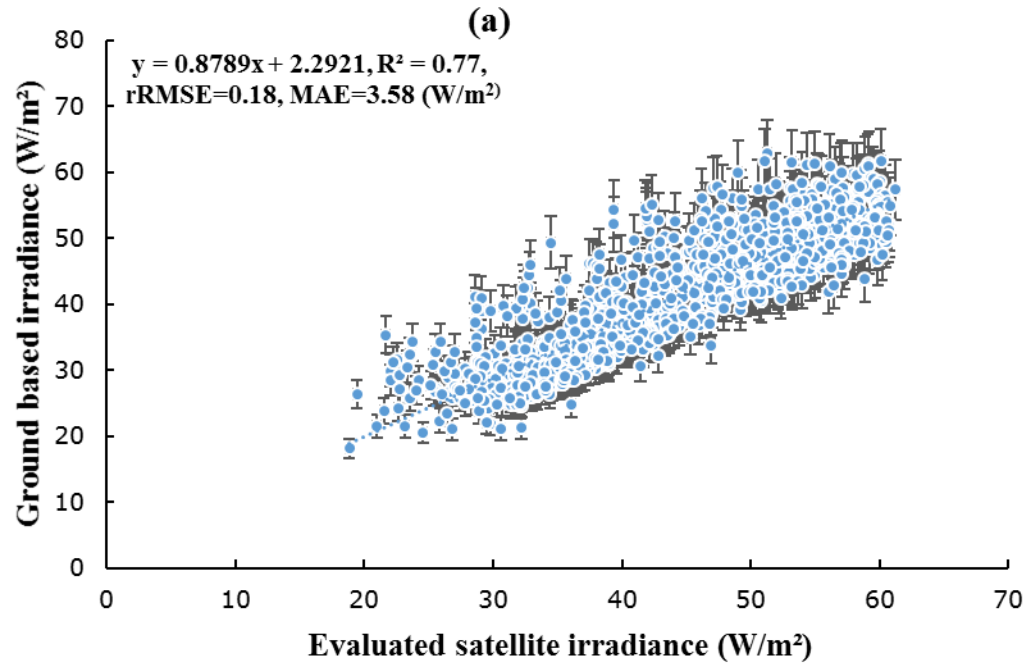
4.3.3 Sun Not Obscured Sky Conditions

The evaluated broadband UVA satellite irradiance at solar noon for the cases of when the solar disc was not obscured by cloud have been compared with the corresponding

broadband ground-based UVA irradiance recorded by the ground based radiometer at the research site over the 1 October 2004 to 31 December 2016 period. This data set of sun not obscured sky conditions is provided in Figure 4.9 for the four cloud cover categories of 0 to 2, > 2 to 4, > 4 to 6 and > 6 to 8 okta.

According to Figure, 4.9 (a), which shows data for sun not obscured sky conditions on days with ≤ 2 okta (65.7% of the available data), there is a correlation between the solar noon evaluated UVA satellite and the ground based irradiance values with an R^2 (coefficient of determination) of 0.77, and an rRMSE (relative root mean square error) of 18% and MAE (mean absolute error) of 3.58 (W/m^2). Figure 4.9 (b) shows the broadband UVA comparison between the satellite and the ground-based data when the quantity of cloud was from > 2 to 4 okta (7.8% of the available data). As expected, this figure shows lower correlation between the satellite and ground based data than the correlation for the 0 to 2 okta data in Figure 4.9 (a). However, despite the low number of data values there is comparable correlation between the data sets (R^2 is 0.64, rRMSE is 16% and MAE is 4.8 (W/m^2)).

Figure 4.9 (c) and 4.9 (d) for the cases of > 4 to 6 okta and > 6 to 8 okta show a poor correlation between the satellite and the ground based measurements due to the (50%-100% cloud coverage) with an R^2 of 0.31 and 0.4, an rRMSE of 53% and 25.5% and a MAE of 8.5 and 7.2 (W/m^2) respectively. Temporal differences between the cloud observation by satellite at about 1.00 pm and the actual cloud cover at solar noon for the ground-based measurements are likely to be a significant contributor to the poor correlation in these cloudy condition cases (Tanskanen et al 2007). In this case, the satellite over-prediction is greatest. A possible explanation could be due to differences in local cloud cover measured at noon and the sampled satellite data measured at a different time during the satellite overpass time. This is evident as a trend to a lower gradient with increasing cloud cover at noon. Additionally, there are likely variations in the local site cloud cover and satellite samples measured over the pixel size of 40 km \times 80 km.



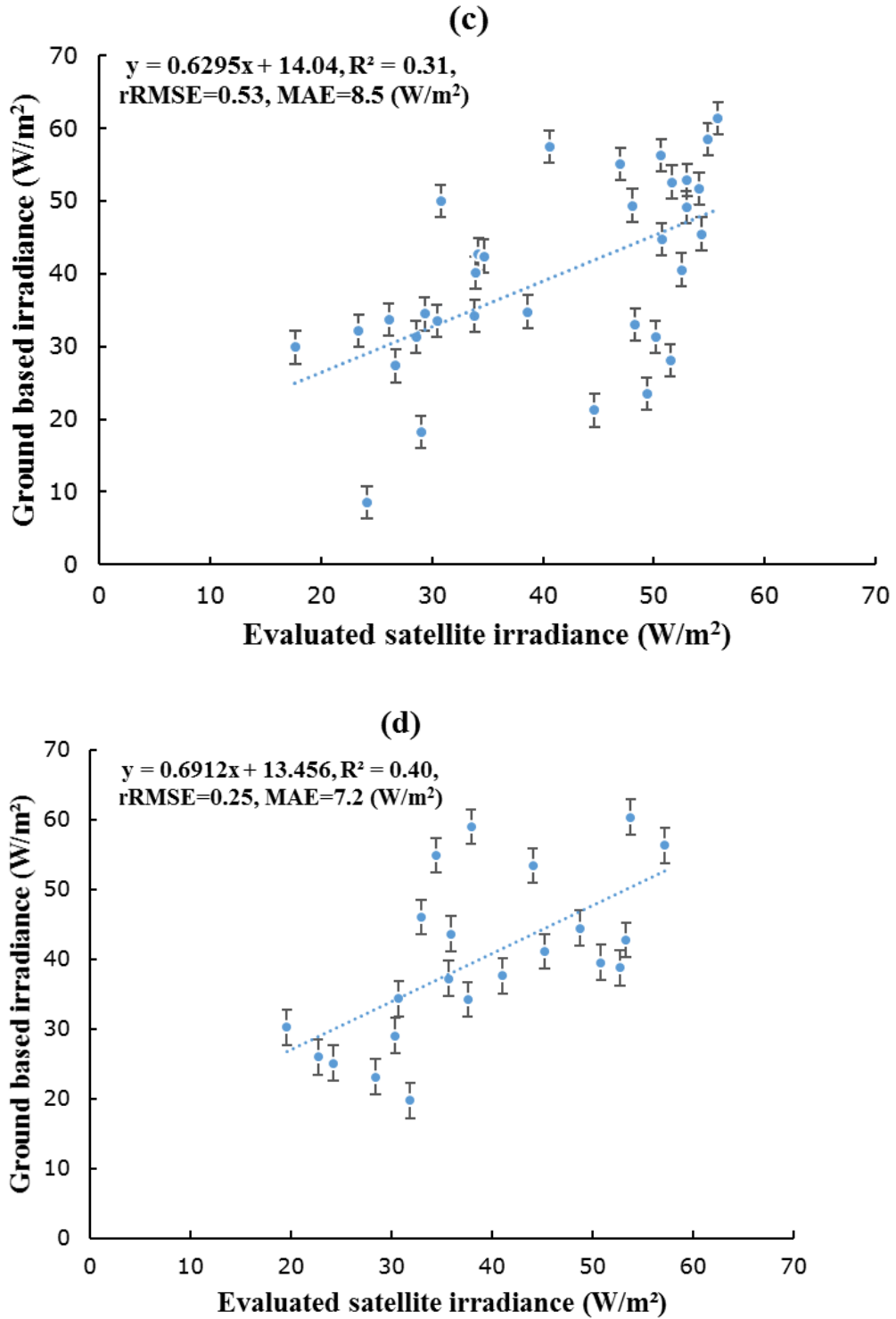
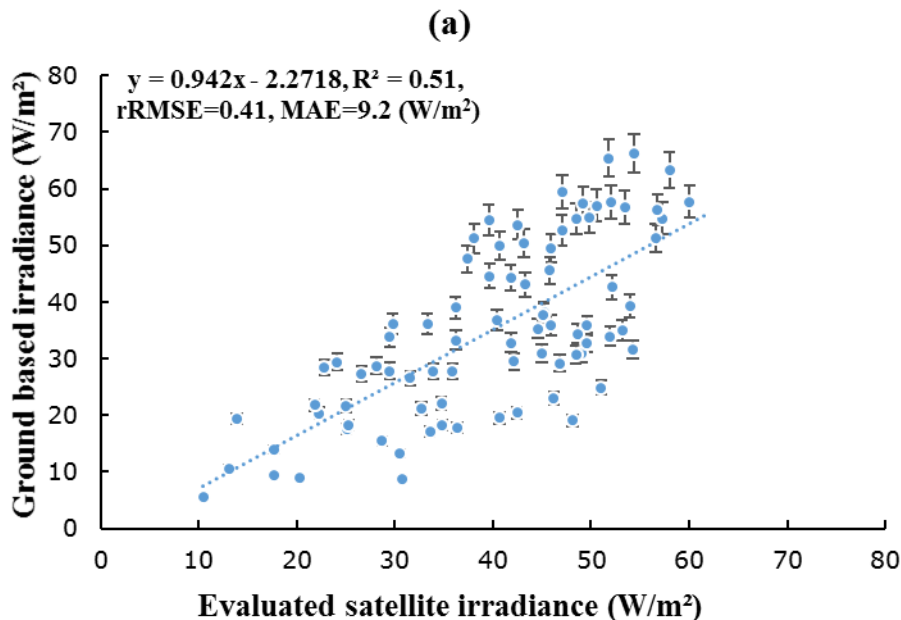


Figure 4.9 Comparison of the evaluated OMI satellite solar noon UVA irradiance with ground-based UVA data for the four categories of cloud cover of (a) 0 to 2, (b) > 2 to 4, (c) > 4 to 6 and (d) > 6 to 8 okta for sun non obscured sky conditions. The error bars are the $\pm 10\%$ error associated with the ground-based data. The dashed line is the fitted trend line.

4.3.4 Sun Obscured Sky Conditions

Figure 4.10 shows the data for sun obscured sky conditions in the three categories of cloud cover of > 2 to 4, > 4 to 6 and > 6 to 8 okta. Figure 4.10 (a) represents a comparison for > 2 to 4 okta. For this range of sky coverage, there is a weaker correlation compared to that with the sun not obscured data with an R^2 of 0.51, an rRMSE of 41% and a MAE of 9.2 (W/m^2). Figures 4.10 (b) (> 4 to 6 okta) and 4.10 (c) (> 6 to 8 okta) show there is a similarity in the correlation of the comparisons for the sun obscured and sun not obscured sky condition for the >4 okta cloud cases with a R^2 of 0.36 and 0.42, an rRMSE of 79% and 68% respectively and a MAE of 10.6 and 8.8 (W/m^2). For all three categories of sun obscured cloud conditions, the spread of the data about the fitted trend line increases with increasing solar noon irradiance. A possible explanation for this is due to the more noticeable relative amplification and attenuation by cloud with increasing irradiance. For cloud cover greater than 4 okta, the gradient of the graphs presented in Figure 4.10 (b) and 4.10 (c) is closer to unity than the sun not obscured graphs of Figure 4.9 (c) and 4.9 (d). When the sun is obscured, the attenuating cloud reduces the typical overestimation of the satellite UVA.



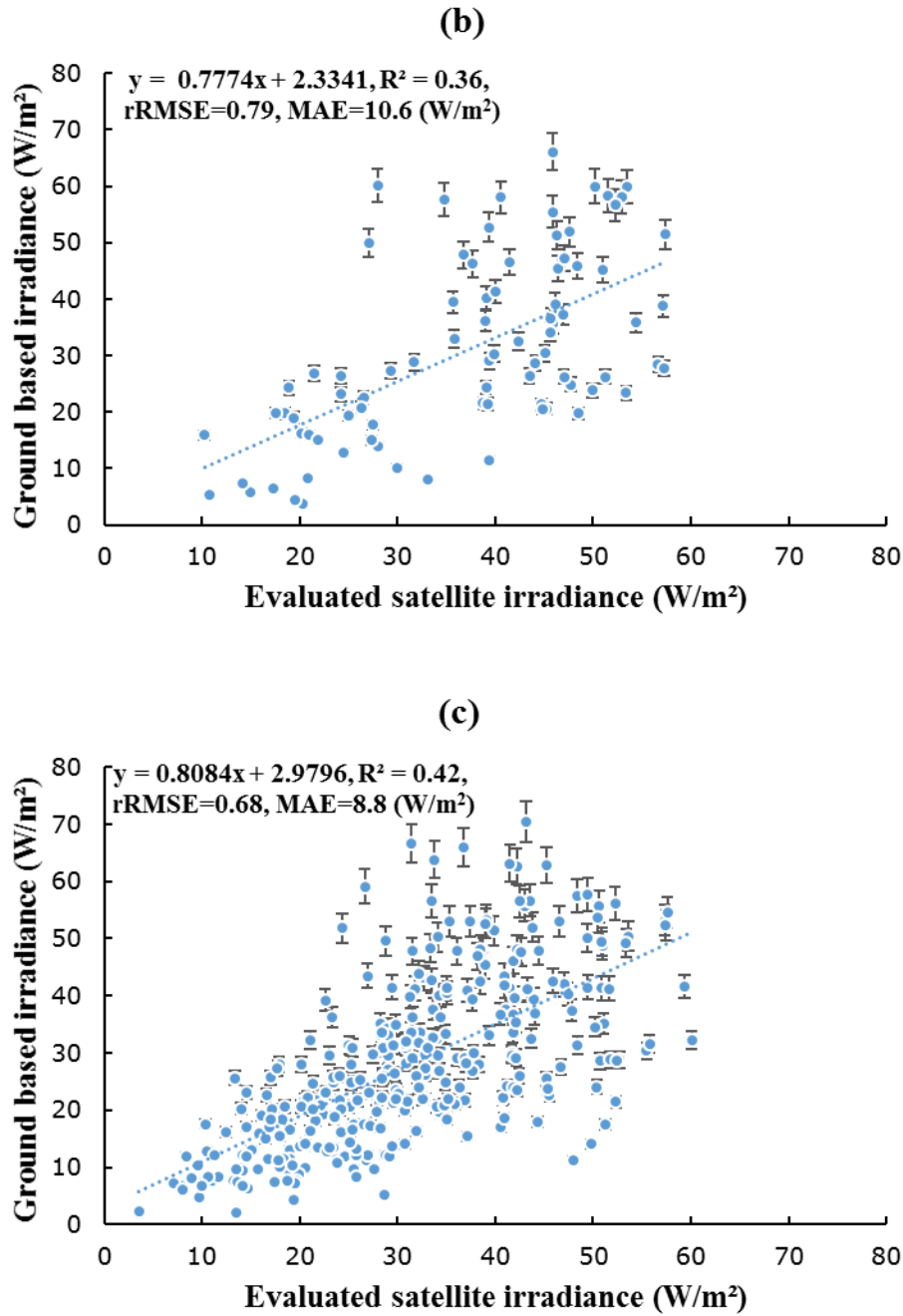


Figure 4.10 Comparison of the evaluated OMI satellite solar noon UVA irradiance with ground-based UVA data. The data are plotted for the three categories of the amount of cloud cover of (a) > 2 to 4, (b) > 4 to 6 and (c) > 6 to 8 oktas for sun obscured sky conditions. The error bars are the $\pm 10\%$ error associated with the ground-based data. The dashed line is the fitted trend line.

4.4 INFLUENCE OF AEROSOLS ON THE UV IRRADIANCE

Figure 4.11 shows the time series of a daily UV aerosol index and aerosol optical depth for the Toowoomba study site from October 2004 to December 2016. The aerosol index measures the difference between the transmission of different UV radiation wavelengths through an atmosphere containing aerosols and a pure molecular atmosphere (Buchard et al. 2015). Aerosol optical thickness is a measure of the attenuation due to scattering and absorption by aerosols through the atmosphere. Figure 4.11(a) shows the significant majority of the daily UV aerosol index are between 0.5 and 1.5 (97.8%). The daily UV aerosol average value is 0.76, the median is 0.69 and the standard deviation is 0.29. In Figure 4.11 (b), the majority of the aerosol optical depths are less than 0.7. The spike to 1.5 in September 2009 is due to a severe dust storm over one day. The aerosol optical depth average value is 0.24, the median is 0.22 and the standard deviation is 0.14.

Daily UV aerosol index and aerosol optical depth for the Toowoomba study site are low as a comparison with high aerosol regions such as some regions in the Northern Hemisphere. For example, in Iraq, the daily UV aerosol index average value is 1.44 and the aerosol optical depth average value is 0.66 (<<http://giovanni.gsfc.nasa.gov/giovanni/>>). In North Africa, the UV aerosol index reached 2.6 in 2006 (Torres, Ahn & Chen 2013) and in China the aerosol optical depth average was over 0.43 (Xin et al 2007). Based on the low aerosol levels over the site of the research, apart from one day in September 2009 in the 12 year period, aerosols have a significantly lower impact on the UVA irradiance compared to cloud cover.

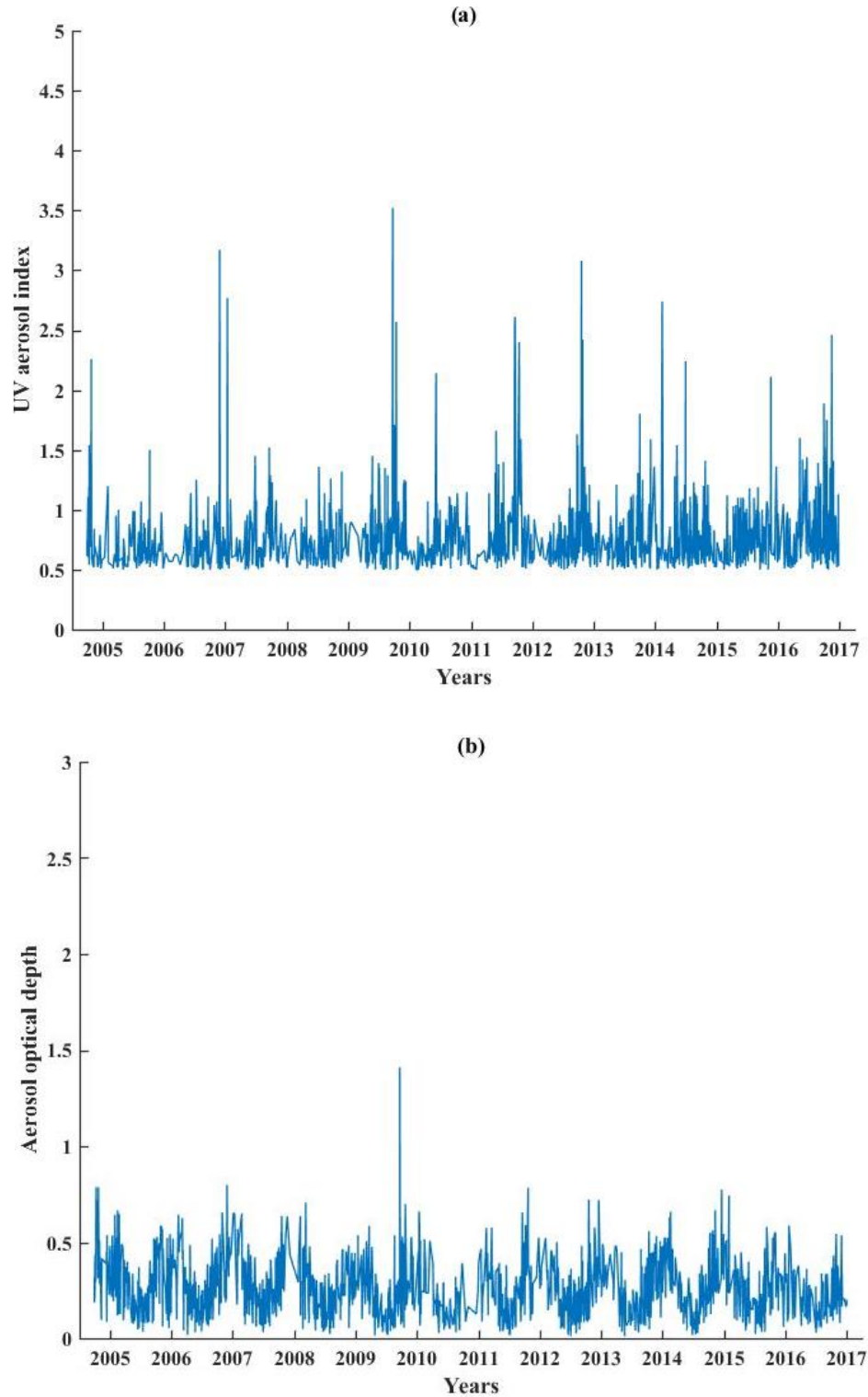


Figure 4.11 (a) The time series of the daily UV aerosol index and (b) the aerosol optical depth for the Toowoomba study site from October 2004 to December 2016.

4.5 CHAPTER SUMMARY

This chapter presented results and discussed the comparisons of the OMI UV satellite measurements against ground-based spectral UV data and the evaluated UVA irradiance from OMI data including the influence of cloud over a 12 year period. In addition, the level of aerosols over the research area have been considered in this chapter. The following chapter provides the evaluation of the total daily UVA exposure from OMI UVA irradiance data for both cloud free days and cloudy days and investigates the influence of cloud on total daily UVA exposure.

CHAPTER 5

EVALUATION OF THE TOTAL DAILY UVA EXPOSURES

5.1 OVERVIEW

This chapter provides the results and discussion on the method developed for the evaluation of the total daily UVA exposure from OMI UVA irradiance data for cloud free days over 12 years period. The total daily UVA exposures are also calculated for cloudy days and the influence of cloud on total daily UVA exposure are investigated. This involves the use of a 10 year data set for the development of the method for cloudy days and 2 year validation data set.

5.2 TOTAL DAILY UVA EXPOSURE EVALUATED FROM SOLAR NOON OMI SATELLITE SPECTRAL IRRADIANCE FOR CLOUD FREE DAYS

Data retrieved from satellites is often limited between one and several local passes per day, making the full evaluation of the daily variation in the solar UV exposures challenging. However, the risks of UV radiation are linked to accumulating UV exposure over a long term (Lavker et al. 1995). This requires the evaluation of total daily UV exposures from the irradiance derived at the satellite over pass time. Langston (2017) recently derived annual erythemally weighted exposure integrals from single pass satellite noontime UVB irradiance estimates. Under cloud-free conditions, Diffey (2009) presented a technique to derive the daily UV erythemal exposure integral from the forecast maximum UV index by application of a Gaussian distribution function. In the research in this chapter, the total daily UVA exposures are derived from a dataset of cloud free surface exposures measured daily as a time series extending over 12 years. The daily exposure integrals are presented here with reference to an expression that can be applied to derive the cloud free UVA integral from single noontime measurements of the solar UVA irradiance. The developed technique may be applied where noontime irradiance is measured from a remote sensing platform to estimate upper daily (cloud-free) UVA exposure integrals.

The total daily satellite broadband UVA exposures derived from OMI satellite and calculated by using Equation (2.6) have been reconstructed for the days that were totally cloud free during daylight hours in the period February 2005 to December 2016. These days are referred to as cloud free and the number in each month are provided in

Table 5.1. At the Southern Hemisphere sub-tropical site of this research, the highest proportion of cloud free days occurred between May and October, corresponding to late autumn, winter and the first half of spring.

Figure 5.1 shows the total daily UVA exposures evaluated for the cloud free days between February 2005 to December 2016. There is a good correlation between the total daily UVA exposures from the measured ground-based UVA Biometer instrument and the total daily satellite UVA exposures with an R^2 of 0.9, rRMSE of 0.07 and MAE of 56.9 kJ/m². The error bars are the error related with the ground-based UVA measurements and the dashed line is the fitted regression line. The slope is 0.7 indicating that there is some difference between ground and satellite based data. The developed method provides the total daily exposure for cloud free days. It enables the total daily exposures to be evaluated at sites when there is no ground-based UVA radiometer.

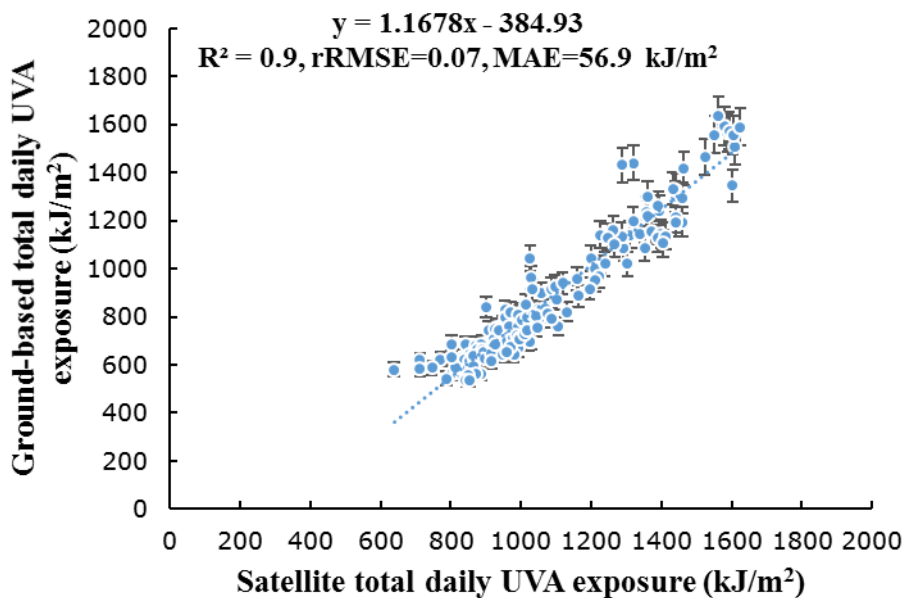


Figure 5.1 Comparison of satellite derived cloud free daily UVA exposure versus surface measured UVA exposure. The error bars represent the variation in surface UVA measurements ($\pm 10\%$).

5.3 INFLUENCE OF CLOUD ON OMI SATELLITE TOTAL DAILY UVA EXPOSURES OVER A TWELVE YEAR PERIOD

In the UVA waveband, the GOME-2 satellite data provides the UVA daily maximum irradiance and the total daily UVA exposure. A comparison has been provided between this data and that from a ground-based spectroradiometer at a Southern Hemisphere site (Parisi et al. 2017). However, the earlier launched OMI (Ozone Monitoring Instrument) does not provide the total daily UVA exposure integral and it is important to have information on UV exposures, as the risk of some sun related disorders is related to cumulative exposure. Solar UV radiation is subject to many factors, which determine and influence the irradiance that reaches the earth's surface (Madronich et al. 1998). Surface solar radiation is particularly sensitive to cloud (An and Wang 2015) which can be measured by both ground-based and satellite based instruments (Fontana et al. 2013).

Previous research has addressed the influence of cloud to make comparisons between ground-based and OMI satellite based solar noon UVA irradiance for different amounts of cloud cover at a Southern Hemisphere site (A Jebar et al., 2018). No previous research has considered the influence of cloud on the total daily UVA exposures evaluated from OMI satellite spectral irradiance data. The research in this chapter reports on the development and validation of the method to evaluate the UVA exposures from the solar noon irradiance and the influence of cloud on the OMI satellite total daily UVA exposures evaluated from the OMI solar noon spectral irradiance for the sub-tropical study site.

5.3.1 Cloud and Fractions of Maximum Daily Exposure

Table 5.1 shows the number of days in the different cloud categories for the cases of solar disc obscured and solar disc not obscured. The number of days in each category represent the days when there was available sky camera data at solar noon. This table presents the average over the ten years of the fraction, F of maximum daily exposure used in equation (2.6) for all categories.

According to this table, there is an inverse relationship between the fraction of the maximum daily exposure and the amount of cloud cover. In addition, the values of the fraction of maximum daily exposure for the sun not obscured sky conditions are bigger than the values of the fraction of maximum daily exposure for the sun obscured sky conditions. The decrease in the value of F (calculated in section 2.4) with the increase in cloud cover and with the sun obscured is due to the total daily UVA exposures decreasing with the cloud cover compared to the maximum daily exposures.

Table 5.1 Number of days in each category of cloud cover between zero and eight okta and the average of the fraction of the maximum daily exposure for all categories.

CATEGORIES OF THE CLOUD AMOUNT (OKTA) FOR SUN NOT OBSCURED SKY CONDITIONS	NUMBER OF DAYS	FRACTIONS OF MAXIMUM DAILY EXPOSURE (F)	CATEGORIES OF THE CLOUD AMOUNT (OKTA) FOR SUN OBSCURED SKY CONDITIONS	NUMBER OF DAYS	FRACTIONS OF MAXIMUM DAILY EXPOSURE (F)
0-2	712	0.50			
>2-4	38	0.45	>2-4	62	0.41
>4-6	29	0.42	>4-6	64	0.39
>6-8	19	0.42	>6-8	299	0.37

5.3.2 All Sky Conditions

Figure 5.2 shows the time series of the satellite total daily UVA exposures evaluated from the three OMI solar noon spectral irradiances for the study site from October 2004 to the end of 2016 for all sky conditions. This includes the 10 year data set and 2 year validation set. This figure has 3,511 daily UVA exposures based on when there was OMI satellite data available. The pattern of peaks and troughs in the exposures due to the seasons is shown in this figure, with a variation between approximately 840 kJ/m² and 1600 kJ/m². Superimposed on the seasonal pattern is the influence due to cloud.

The time series is then sub-divided according to cloud cover categories as box and whiskers plots in Figure 5.3. Figure 5.3 (a) shows the total daily satellite UVA exposure at all sky conditions. Figure 5.3 (b) represents total daily satellite UVA exposure of the time series for the four cloud amount categories (0-2, > 2-4, > 4-6 and > 6-8 okta) for sun not obscured sky conditions. Figure 5.3 (c) represents total daily satellite UVA exposure at the three cloud amount categories (> 2-4, > 4-6, and > 6-8 okta) for sun obscured sky conditions.

The median of the total daily satellite UVA exposure is reduced from about 1100 kJ/m² to less than 600 (54.5%) kJ/m² with the amount of cloud (Figure 5.3 (a)). Figures 5.3 (b) and Figure 5.3 (c), show, as expected, that the increase of the amount of cloud reduces the total daily satellite UVA exposure. In Figures 5.3 (b), the median for > 4 to 6 okta is higher than that for > 2 to 4 okta possibly due to the sample set, but in general the trend is decreasing UVA exposure with increasing cloud cover which is as expected. Additionally, the medians are generally lower for the sun obscured cases compared to the sun not obscured cases.

Figure 5.4 presents the total daily satellite UVA dataset as box and whisker plots for each of the years (from 2004 to 2016). For each year, the horizontal line is the median for each year, the box represents the 1st and 3rd quartile and the dashed line represents the range of the satellite data. Except for 2004 where there are only three months of satellite based data available (to compare to the ground-based data), the distribution of the annual medians of the total daily UVA exposures appears consistent. In this figure, 2010 has a lower median, and 1st and 3rd quartiles due to the above average annual rainfall of 1161 mm compared to the average annual Toowoomba rainfall of 679.75 mm, and correspondingly higher amounts of cloud.

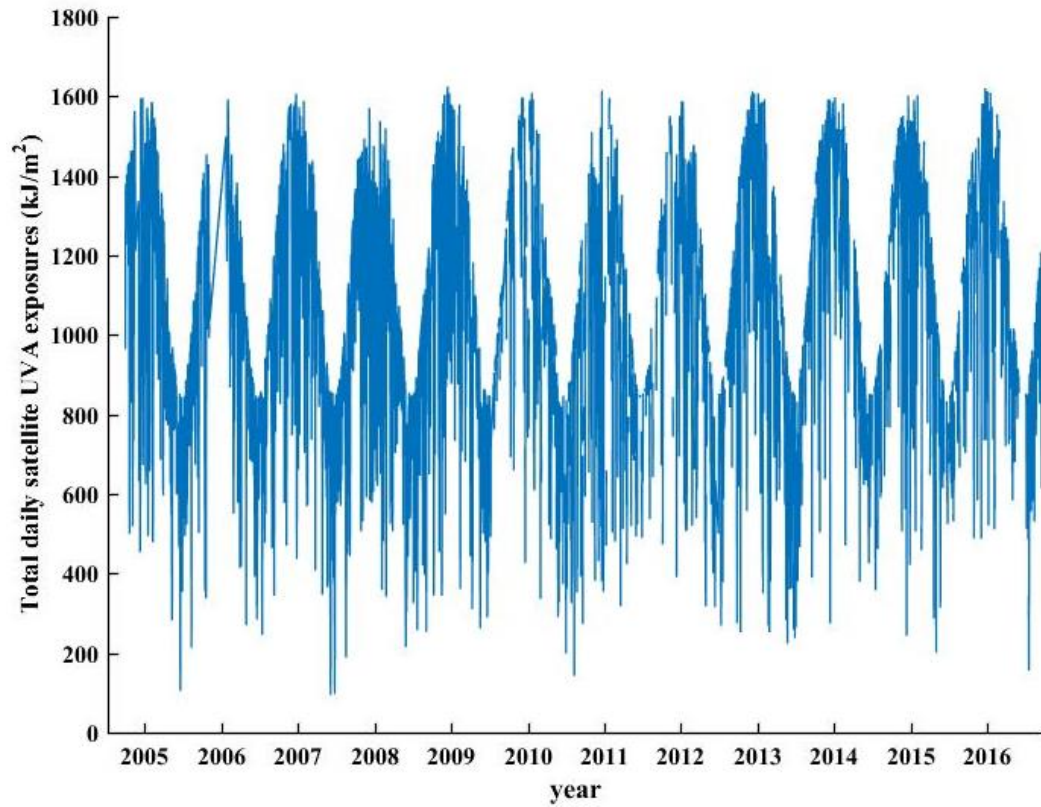
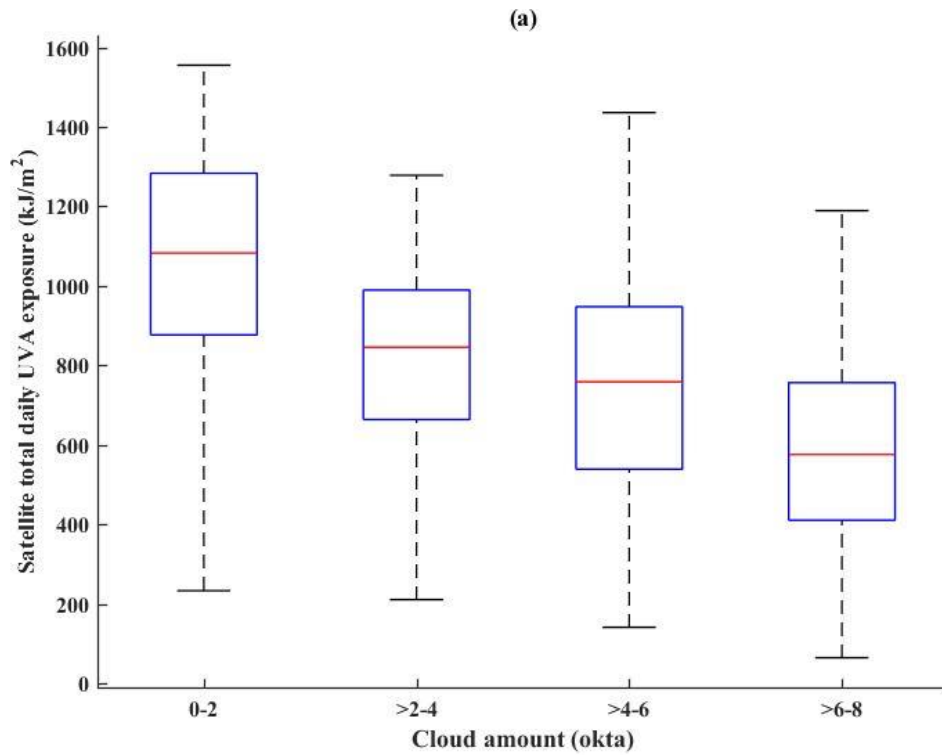


Figure 5.2 Time series of satellite total daily UVA exposures evaluated from the OMI solar noon spectral irradiance values.



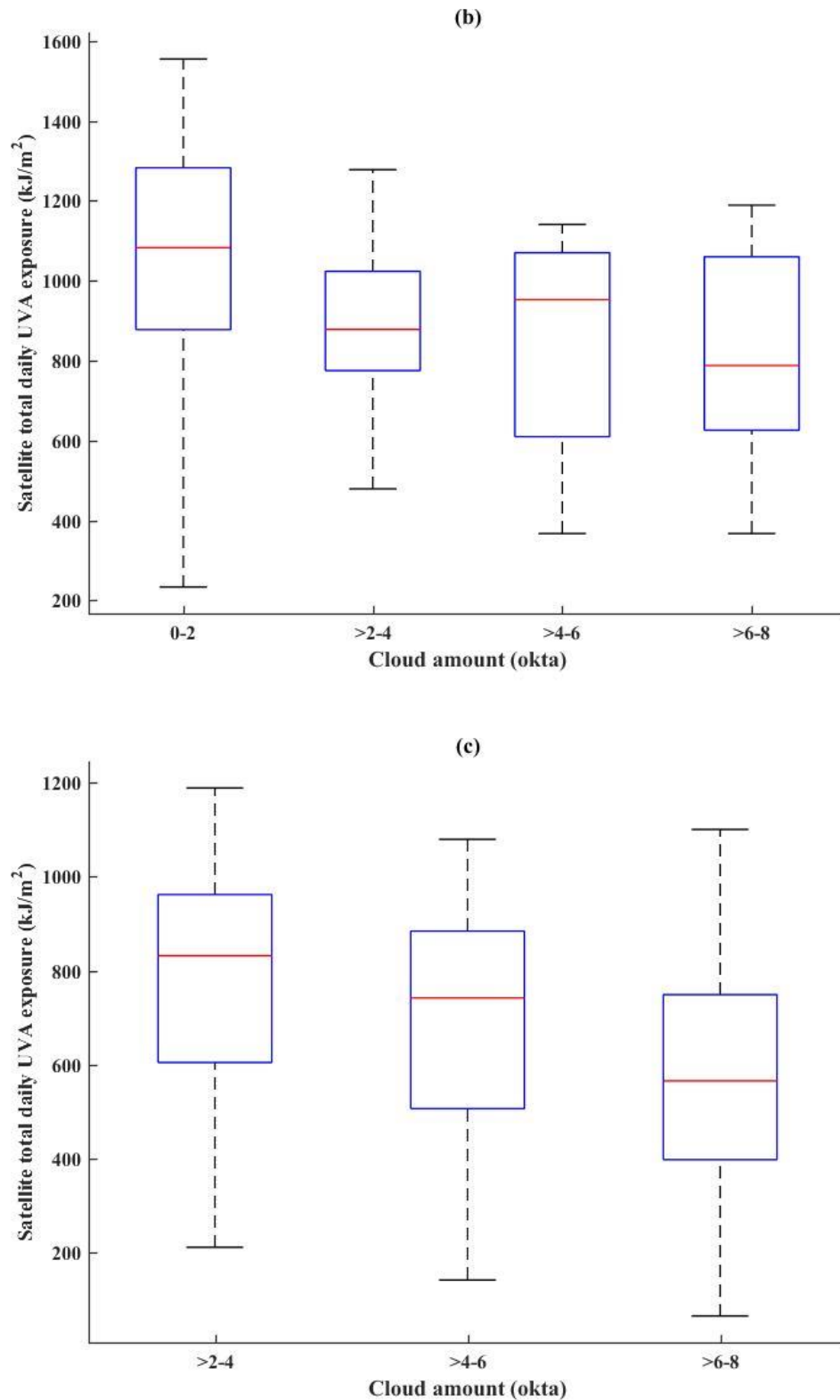


Figure 5.3 (a) The total daily satellite UVA exposure for all sky conditions. (b) The total daily satellite UVA exposure at the four cloud amount categories (0-2, > 2-4, > 4-6 and > 6-8 okta) for sun not obscured sky conditions. (c) Total daily satellite UVA

exposure at the three cloud amount categories ($> 2-4$, $> 4-6$, and $> 6-8$ okta) for sun obscured sky conditions. The horizontal line in each box and whisker is the median, the box is the $Q1$ and $Q3$ range and the dashed vertical line is the range of values.

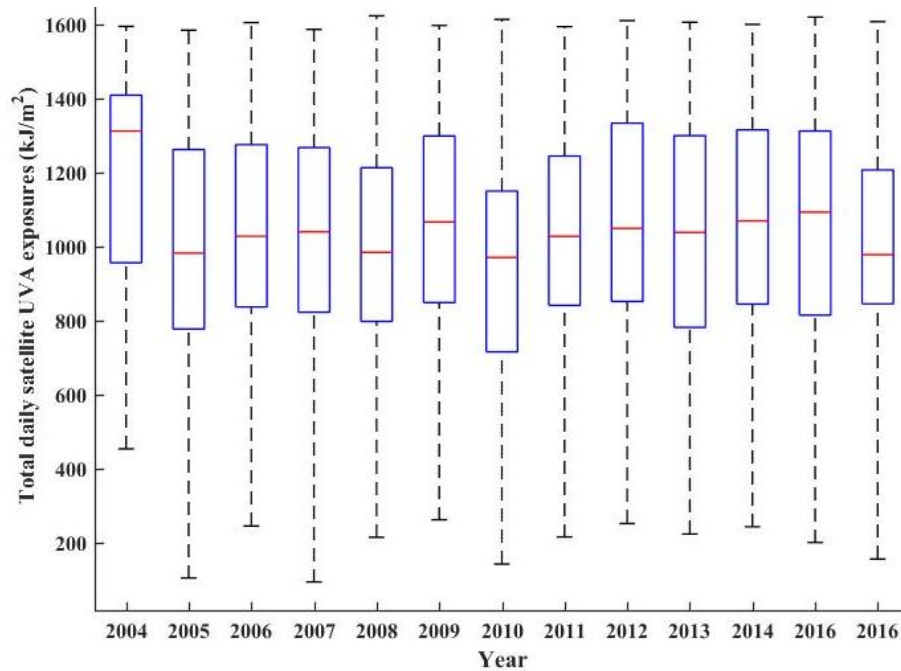
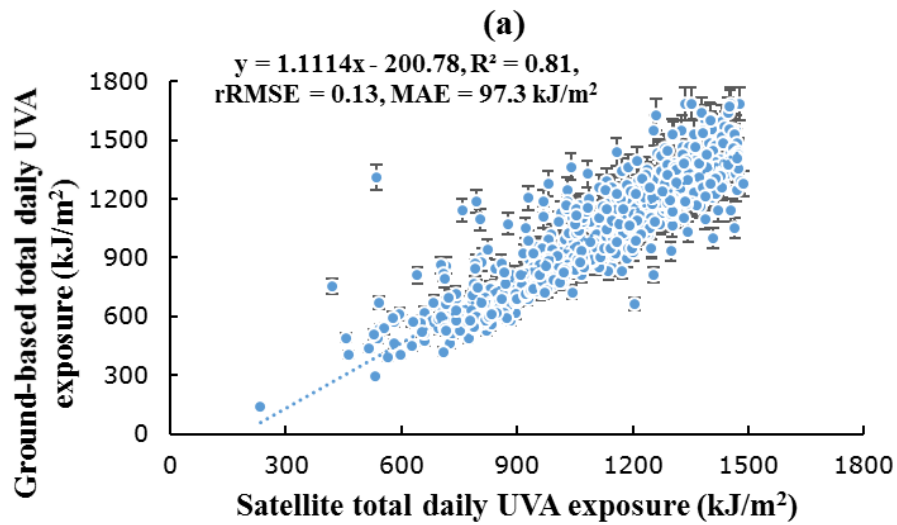


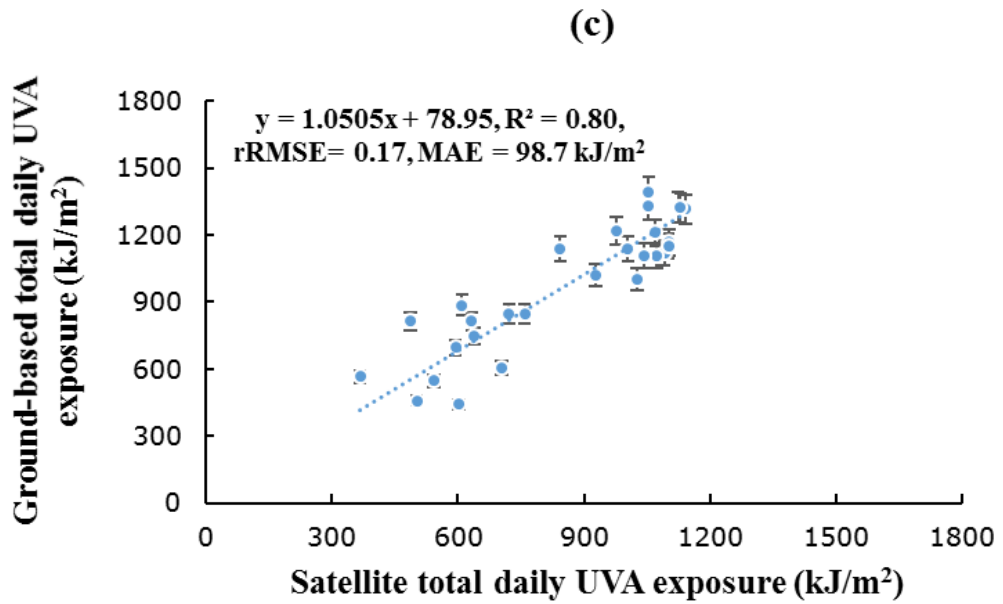
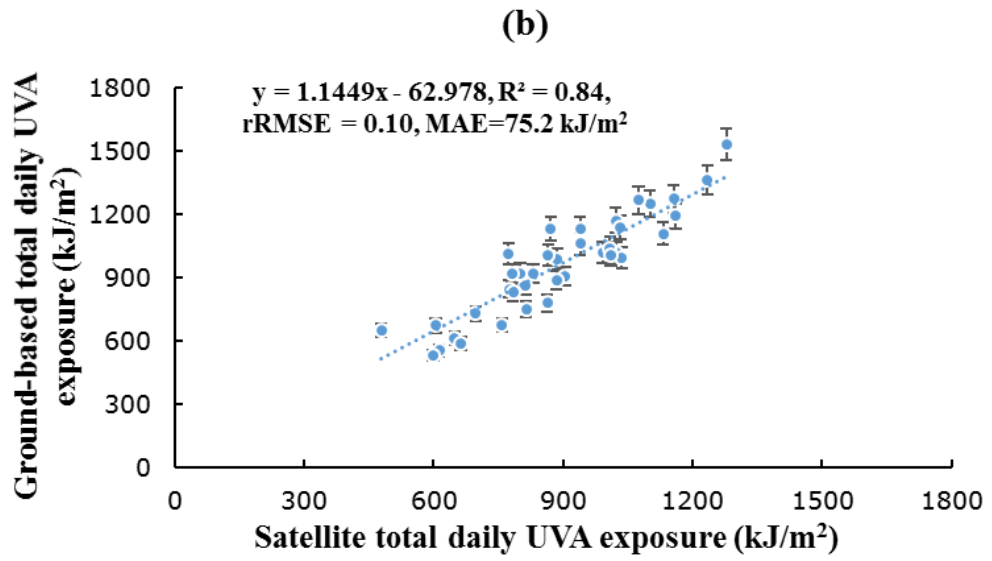
Figure 5.4 Box and whisker plots for each year of satellite total daily UVA exposures data October 2004 to December 2016.

5.3.3 Sun Not Obscured Sky Conditions

The total daily UVA satellite exposures calculated from the satellite solar noon UVA irradiance for the cases of when the sun was not obscured by cloud have been compared with total daily ground-based UVA exposure at the measurement site over the period of 1 October 2004 to the end of December 2014 (Figure 5.5). The comparisons between the two data sets for the sun not obscured sky conditions are shown in Figure 5.5, for the cloudy days in the four cloud cover categories of 0 to 2, > 2 to 4, > 4 to 6 and > 6 to 8 okta. The dashed lines are the regression lines fitted to the data and the error bars represent the $\pm 10\%$ uncertainty associated with the measured ground-based data.

When the amount of cloud was 0-2 and > 2 to 4 okta as shown in Figure 5.5 (a) and (b), there is a reasonable correlation between the total daily UVA satellite exposures evaluated from the OMI spectral irradiance measurements at solar noon and total daily ground-based UVA exposures with an R^2 of 0.81 and 0.84, rRMSE of 0.13 and 0.10, MAE of 97.3 and 75.2 kJ/m² respectively. For the cloudy days of more than 4 okta, Figure 5.5 (c) shows a good agreement between the satellite and ground based total daily UVA exposure with R^2 of 0.80, an rRMSE of 0.17 and MAE of 98.7 kJ/m² when the amount of cloud was > 4 to 6 okta. The use of the respective values of F for each category of cloud cover is likely contributing to this agreement. Similarly, for the days with > 6 to 8 okta, Figure 5.5 (d) shows a reasonable correlation between the satellite and ground based total daily UVA exposures with R^2 of 0.84, an rRMSE of 0.10 and MAE of 87.8 kJ/m².





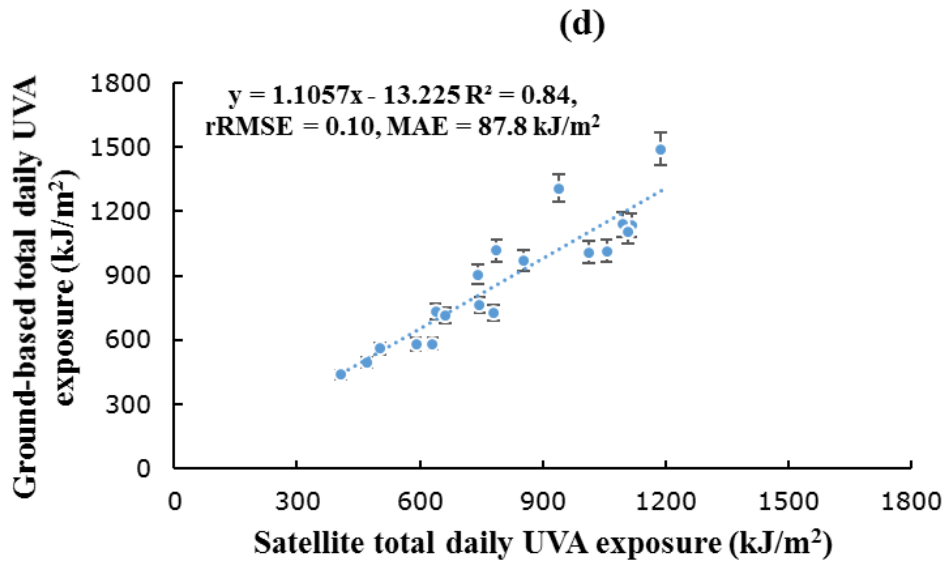


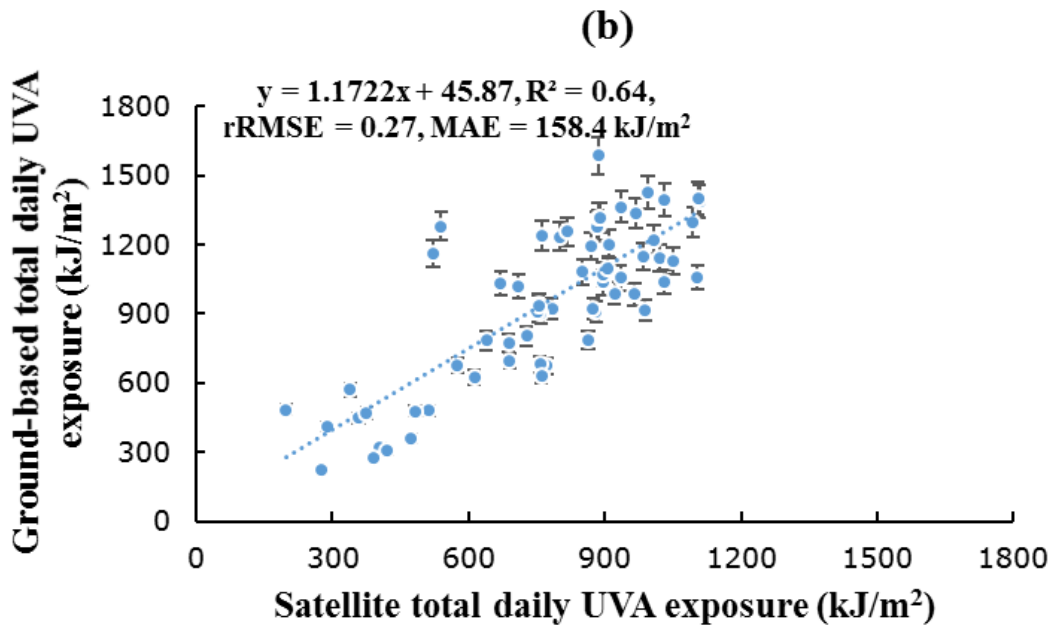
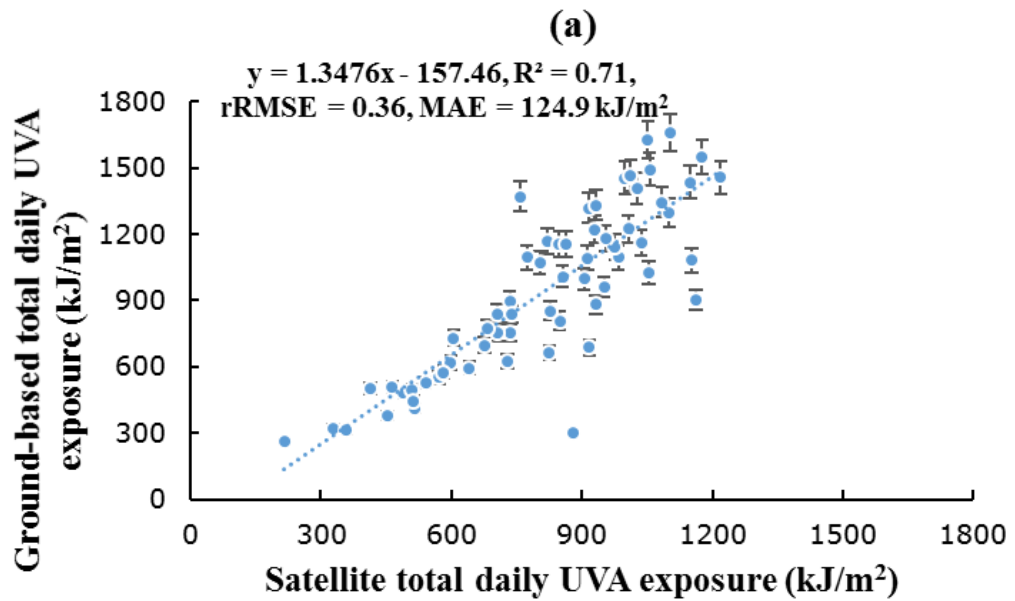
Figure 5.5 Comparison of the 2004 to 2014 satellite total daily UVA exposure evaluated from the OMI spectral irradiance evaluated at solar noon with the ground based total daily UVA exposure for the four categories of cloud cover of (a) 0 to 2, (b) > 2 to 4, (c) > 4 to 6 and (d) > 6 to 8 okta for solar disc non-obscured sky conditions. The dashed lines are the regression lines fitted to the data and the error bars correspond to the $\pm 10\%$ error associated with the ground-based data.

5.3.4 Sun Obscured Sky Conditions

Figure 5.6 shows the comparison of the satellite total daily UVA exposure evaluated from the OMI spectral irradiance and the ground-based total daily UVA exposure for sun obscured sky conditions. These are separated into the three cloud cover categories of > 2 to 4, > 4 to 6 and > 6 to 8 okta with the dashed line representing the fitted regression line.

For the sun obscured cases in Figure 5.6 (a), there is a good correlation between the satellite and ground based total daily UVA exposure with an R^2 of 0.71, rRMSE of 0.36 and MAE of 124.9 kJ/m². This figure shows a smaller R^2 compared to the sun not obscured cases due to the influence of cloud over the sun. In Figure 5.6 (b), even though, the cloud cover is >4 to 6 okta, the correlation is still reasonable with R^2 of 0.64, an rRMSE of 0.27 and MAE of 158.4 kJ/m². For the category of > 6 to 8 okta sky coverage shown in Figure 5.6 (c), the correlation is slightly weaker compared with the sun not obscured cases with the same cloud coverage with an R^2 of 0.75, an rRMSE

of 0.29 and MAE of 133.3 kJ/m². The larger rRMSE for the three cases of cloud cover > 2 to 4, > 4 to 6 and > 6 to 8 okta is expected because the cloud conditions used to determine the cloud categories are at solar noon and this amount of cloud cover, whether the sun is obscured or not, is often variable during the day.



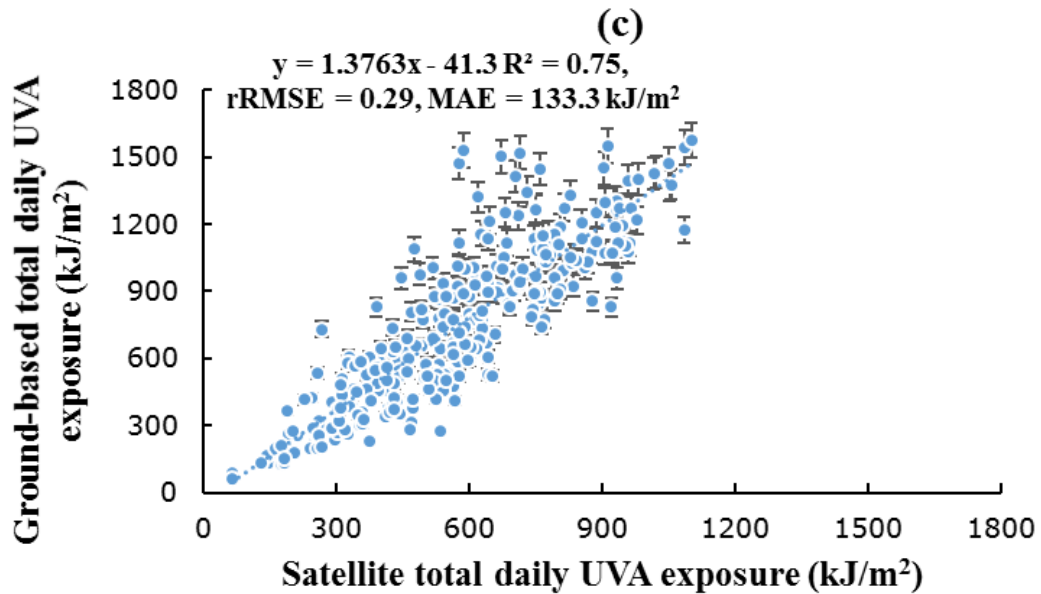


Figure 5.6 Comparison of the satellite total daily UVA exposure for 2004 to 2014 evaluated from the three OMI spectral irradiance with the ground-based total daily UVA exposure for the three categories of cloud cover of (a) > 2 to 4, (b) > 4 to 6 and > 6 to 8 okta for sun obscured sky conditions. The dashed lines are the regression lines fitted to the data and the error bars represent the $\pm 10\%$ errors with the measured ground based data.

5.3.5 Model Validation

The model was developed using the OMI satellite based solar noon UVA irradiance data set from 2004 to 2014 for the sun not obscured cases (N=210) and the sun obscured cases (N=32). The dataset from 2015 to 2016 was used to validate the developed model. Figure 5.7 shows the comparison of the satellite total daily UVA exposure and the ground-based total daily UVA exposure for sun not obscured and for sun obscured sky conditions for the 2015 and 2016 data set.

In Figure 5.7 (a), the validation comparison has a good correlation with an MAE of 84.2 kJ/m^2 (10%) for the sun not obscured cases. Figure 5.7 (b) shows the validation for the sun obscured cloudy days which has a reasonable agreement with an MAE of 138.4 kJ/m^2 (30%). This larger MAE compared to the sun not obscured cases is due to the variability of the sun obscured cloud influence on the solar UVA.

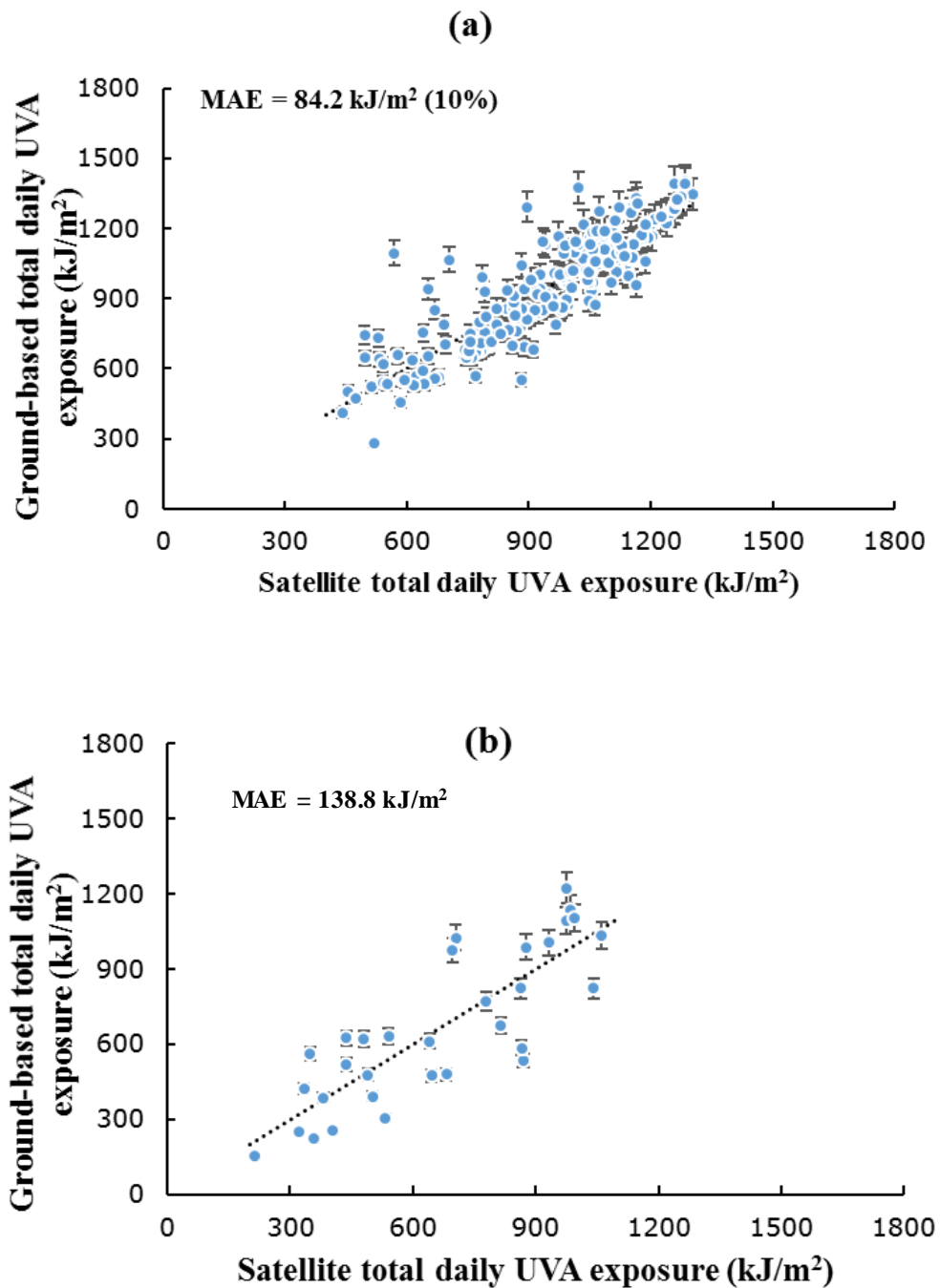


Figure 5.7 Validation of the satellite total daily UVA exposure evaluated from the three OMI spectral irradiances with the ground-based total daily UVA exposure for the two categories of (a) sun not obscured cloudy days and (b) sun obscured cloudy days for the 2015 and 2016 data set. The dashed line in each graph is the 1:1 line.

5.4 CHAPTER SUMMARY

This chapter presented and discussed the development of the method to evaluate total daily UVA exposures from solar noon OMI satellite irradiance. This was developed and validated for clear skies and for cloudy skies with the sun both obscured and not obscured. The following chapter provides the conclusions for the research in this thesis.

CHAPTER 6

CONCLUSION

6.1 OVERVIEW

This chapter presents the conclusions of the research on the OMI satellite spectral data validation, the method developed to evaluate the UVA irradiances, the evaluation of the satellite UVA irradiance values, the method developed to calculate the total daily satellite UVA exposure and the evaluation of these daily UVA exposures for totally cloud free days and for cloudy days.

6.2 SPECTRAL AND BROADBAND SURFACE BASED MEASUREMENTS TO VALIDATE OMI UV SATELLITE DATA

The cloud free solar noon spectral irradiance from OMI data for 2009 have been compared with ground based spectral spectroradiometer data at the three wavelengths provided by the OMI satellite data (310, 324, 380 nm) for a sub-tropical Southern Hemisphere site. These comparisons show a clear correlation for these wavelengths and with an R^2 of 0.89 or better in each waveband. These comparisons include the $\pm 9\%$ absolute error in the spectroradiometer ground based data and the errors in the spatial averaging of the satellite pixel data. In this research, the ratio of the spectral irradiances from satellite compared to the ground based measurements has shown that for the cloud free cases at 324 nm, the median is greater than one. The corresponding median at 310 nm is less than one and it is very close to one at 380 nm. For the cloudy days, the ratios had a much wider range of values with the median ratio being higher than one for 324 nm and 380 nm and approaches one for 310 nm. The observed spread in the cloud-affected data was largely due to the temporal nature of local cloud cover and differences between the satellite overpass time and solar noon and the spatial averaging of the satellite data over the satellite pixel. The models developed accounted for this over-estimation at the sub-tropical research site and are essential for any data correlation between satellite and ground based measurements.

Additionally, this research developed and validated a method to compare, evaluate and validate the broadband UVA solar noon irradiance derived from OMI satellite spectral data at 310, 324 and 380 nm for cloud free days with ground based broadband data taken from a UVA Biometer. There is reasonable agreement between the modelled UVA irradiance derived from OMI and the solar noon UVA broadband irradiance from the UVA Biometer with an R^2 of 0.86. Thus, it is possible to use this

Chapter 6 Conclusion

method to evaluate broadband UVA irradiances at solar noon from the OMI data at 310, 324 and 380 nm.

6.3 UVA IRRADIANCE OVER A TWELVE-YEAR PERIOD FROM OMI DATA INCLUDING THE INFLUENCE OF CLOUD

The broadband UVA solar noon irradiance derived from the OMI satellite spectral UV irradiance at the three wavelengths 310 nm, 324 nm and 380 nm have provided a long-term data series of over 12 years at a sub-tropical Southern Hemisphere site. This study has applied this model for both sun not obscured and sun obscured sky conditions. For sun not obscured sky conditions, four categories of the amount of cloud cover of 0 to 2, > 2 to 4, > 4 to 6 and > 6 to 8 okta have been used to investigate the comparison between remote estimates of the broadband surface UVA evaluated from the satellite UVA spectral irradiances and local ground based measurements. These categories showed an inverse relationship between the amount of cloud and the correlation for the satellite and ground based data. In this case, the evaluated broadband UVA satellite irradiance model is likely to be less suitable for cloudy sky conditions of more than four okta. For sun obscured sky conditions, an increasing of the cloud amount led to lower correlation of the satellite derived UVA irradiance model than for sun not obscured sky conditions. There was also an observed increase in the spread of the data with increasing UVA irradiance. Investigation on the effect of cloud on the satellite derived UVA irradiance has shown that the model is valid for sun not obscured conditions with cloud of up to four okta (with an $R^2 = 0.77$, and an $rRMSE = 18\%$ for coverage 0 to 2 okta and $R^2 = 0.64$ and $rRMSE = 16\%$ for > 2 to 4 okta). At the sub-tropical site of this research, the satellite derived UVA irradiances can be calibrated to surface measurements for most conditions, accounting for approximately 71% of the days having 4 okta or less of cloud in the 12 year study period.

6.4 TOTAL DAILY UVA EXPOSURE EVALUATED FROM SOLAR NOON OMI SATELLITE SPECTRAL IRRADIANCE FOR CLOUD FREE DAYS

A new method has been developed for the accurate calculation of total daily UVA exposure integrals under cloud free conditions. Terrestrial UVA surface exposures exhibit diurnal exposure patterns that vary predominately as a function of SZA, which,

Chapter 6 Conclusion

in the absence of cloud are not greatly affected by total ozone column. Normalised exposure variations in the UVA were utilised in this research to find a reliable exposure integral applicable over a range of conditions. This technique may be applied to estimate daily UVA exposure integrals in remote locations that do not have access to surface UVA radiometers. This has the potential to extend the range of surface radiation parameters able to be derived from OMI and other remote satellite platforms, providing new information on surface exposures that affect a range of terrestrial and marine ecosystems as well as having implications for human health.

6.5 INFLUENCE OF CLOUD ON OMI SATELLITE TOTAL DAILY UVA EXPOSURES OVER A TWELVE YEAR PERIOD

This research has employed the developed technique to calculate the total daily UVA exposures from the broadband UVA irradiances derived from the three OMI satellite spectral irradiance at solar noon to provide a comparison between total daily UVA satellite exposure data and total daily UVA ground based exposure data over a 10 year time period. The techniques developed and the quantity of data collected have enabled the influence of cloud on the total daily UVA satellite exposures to be considered. This has been for all cloud conditions for different cloud cover for the solar disc not obscured and solar disc obscured cases. For the sun not obscured sky conditions, the cloud cover categories of 0 to 2, > 2 to 4, > 4 to 6 and > 6 to 8 okta have been considered. In addition, for the case of the solar disc obscured sky conditions, the cloud categories of > 2 to 4, > 4 to 6 and > 6 to 8 okta have been considered.

For all cloud cover categories of sun not obscured data, there is a good correlation in the model between the total daily UVA satellite exposure data and the total daily UVA ground based exposure data, with R^2 values of better than 0.8 and rRMSE values of 0.17 or less. The > 2 to 4 okta coverage data with the sun obscured days provided an R^2 value of 0.71 and rRMSE value of 0.36. The model validation using a two year data set provided an MAE of 84.2 kJ/m² (10%) and 138.8 kJ/m² (30%) respectively for the cases of sun not obscured and sun obscured sky conditions. At the Southern Hemisphere site of this research, the total daily UVA exposures were calculated from the OMI satellite spectral irradiance for sun not obscured cloudy days and for sun

Chapter 6 Conclusion

obscured days, with further research required to compare the OMI satellite derived total daily UVA exposures to ground based data at other sites.

6.6 CONCLUSION

In this research, firstly, the cloud free solar noon spectral irradiance from OMI have been compared with ground based spectroradiometer spectral data at three wavelengths (310, 324, 380 nm) for a subtropical Southern Hemisphere site. These comparisons show a clear correlation for these wavelengths. Secondly, this research has developed a method to evaluate and validate the broadband UVA solar noon irradiance derived from OMI satellite spectral data at 310, 324 and 380 nm for cloud free days against ground based broadband data taken from a UVA Biometer. In addition, the broadband UVA solar noon irradiance have been calculated for a long term data series of over 12 years and applied for the sky conditions of sun not obscured and sun obscured. According to the results, the developed method will be suitable for cloudy sky conditions of less than four okta.

This research has also developed and validated a technique to calculate the total daily UVA exposures from the broadband UVA irradiance derived from OMI satellite spectral irradiance at solar noon to provide a comparison between total daily UVA satellite exposure data and total daily UVA ground based exposure data. The model parameters have been evaluated for different cloud cover conditions for the totally cloud free days and cloudy days at sun not obscured and sun obscured cases. The model has been developed using the data set from 2004 to 2014. The rest of the dataset from 2015 to 2016 has been used to test the developed model, providing a MAE of 10% for sun not obscured days and 30% of sun obscured days. This research has provided a method to use the OMI satellite data to calculate the total daily UVA exposures. The hypothesis “The OMI discrete spectral UV irradiances can be used as a proxy for broadband surface UVA irradiance and total daily UVA exposure” has been confirmed in this research.

6.7 FUTURE WORKS

Further evaluation and examination of the OMI satellite UV measurements should be undertaken to provide a better understanding about the relationship of UVA to disease/damage to the body, such as the following:

- Applying this project at different sites in the world such as in the Middle East, Africa and South America and taking in consideration different influencing factors, like aerosols, albedo and drought.
- Evaluation and validation of a method to reconstruct the UV spectrum from the OMI satellite data at 310, 324 and 380 nm and that is weighted with different action spectra against ground based spectroradiometer data located at any other sites, for example, Middle Eastern, African and American sites.
- Using the correlation between the satellite and ground based measurements to examine the effects of the UV radiation on the vitamin D effective UV.
- Use the OMI satellite data to investigate and analyse the influence of UV radiation in causing cataracts.
- Examination of the influence of UV irradiance on crop damage at other sites by using the satellite data.

The reconstruction of the broadband UVA irradiance and total daily exposures from the OMI data will allow a number of future research projects. They will make a significant contribution to photobiology by providing new research data on surface irradiance and exposures. These research data will be vital in research on the UVA effects for a range of terrestrial and marine ecosystems as well as the implications for human health.

REFERENCES

References

A Jebar, MA, Parisi, AV, Downs, NJ and Turner, JF 2017, 'Validation of OMI UV satellite data using spectral and broadband surface based measurements at a Queensland site', *Photochemistry and Photobiology*, Vol. 93, no. 5, pp.1289-1293.

A Jebar, MA, Parisi, AV, Downs, NJ, and Turner, JF, 2018a, 'Evaluated UVA irradiances over a twelve year period at a sub-tropical site from ozone monitoring instrument data including the influence of cloud'. *Photochemistry and photobiology*. doi: [10.1111/php.12948](https://doi.org/10.1111/php.12948).

A Jebar, M.A, Parisi, A.V, Downs, NJ and Turner, JF 2018b, 'Influence of cloud on OMI satellite total daily UVA exposures over a 12-year period at a Southern Hemisphere Site', Submitted to *International Journal of Remote Sensing*.

Ackerman, SA., Holz, RE, Frey, R, Eloranta, EW, Maddux, BC and McGill, M 2008, 'Cloud detection with MODIS. Part II: validation', *Journal of Atmospheric and Oceanic Technology*, Vol. 25, no. 7, pp.1073-1086.

Agar, NS, Halliday, GM, Barnetson, RS, Ananthaswamy, HN, Wheeler, M and Jones, AM 2004, 'The basal layer in human squamous tumors harbors more UVA than UVB fingerprint mutations: a role for UVA in human skin carcinogenesis'. *Proceedings of the National Academy of Sciences of the United States of America*, Vol. 101, no. 14, pp.4954-4959.

Amaro-Ortiz, A, Yan, B and D'Orazio, JA 2014, 'Ultraviolet radiation, aging and the skin: prevention of damage by topical cAMP manipulation', *Molecules*, Vol. 19, no. 5, pp.6202-6219.

Ambach, W and Blumthaler, M 1993, 'Biological effectiveness of solar UV radiation in humans', *Experientia*, Vol.49, no.9, pp.747-753.

An, N and Wang, K 2015, 'A comparison of MODIS-derived cloud fraction with surface observations at five SURFRAD sites', *Journal of Applied Meteorology and Climatology*, Vol. 54, no. 5, pp.1009-1020.

References

Anav, A, Rafanelli, C, Di Menno, I and Di Menno, M 2004, 'An algorithm to evaluate solar irradiance and effective dose rates using spectral UV irradiance at four selected wavelengths', *Radiation Protection Dosimetry*, Vol. 111, no. 3, pp.239-250.

Andrady, AL, Hamid, SH, Hu, X and Torikai, A 1998, 'Effects of increased solar ultraviolet radiation on materials', *Journal of Photochemistry and Photobiology B: Biology*, Vol. 46, no. 1, pp.96-103.

Antón, M, Loyola, D, Clerbaux, C, López, M, Vilaplana, JM, Banón, M, Hadji-Lazaro, J, Valks, P, Hao, N, Zimmer, W and Coheur, PF 2011, 'Validation of the Metop-A total ozone data from GOME-2 and IASI using reference ground-based measurements at the Iberian Peninsula', *Remote Sensing of Environment*, Vol. 115, no. 6, pp.1380-1386.

Arola, A, Kalliskota, S, Den Outer, PN, Edvardsen, K, Hansen, G, Koskela, T, Martin, TJ, Matthijsen, J, Meerkoetter, R, Peeters, P and Seckmeyer, G 2002, 'Assessment of four methods to estimate surface UV radiation using satellite data, by comparison with ground measurements from four stations in Europe', *Journal of Geophysical Research: Atmospheres*, Vol. 107, no. D16. <https://doi.org/10.1029/2001JD000462>

Australian Institute of Health and Welfare 2017, Summary pages for selected cancers 2017, viewed August 2017 <<http://www.aihw.gov.au/cancer/cancer-in-australia-2017/summary-pages-for-selected-cancers/#t17>>.

Bais, AF, McKenzie, RL, Bernhard, G, Aucamp, PJ, Ilyas, M, Madronich, S and Tourpali, K 2015, 'Ozone depletion and climate change: Impacts on UV radiation', *Photochemical & Photobiological Sciences*, Vol. 14, no. 1, pp.19-52.

Bais, AF, Tourpali, K, Kazantzidis, A, Akiyoshi, H, Bekki, S, Braesicke, P, Chipperfield, MP, Dameris, M, Eyring, V, Garny, H and Iachetti, D 2011, 'Projections of UV radiation changes in the 21st century: Impact of ozone recovery and cloud effects', *Atmospheric Chemistry and Physics*, Vol. 11, no. 15, pp.7533-7545.

References

Balis, D, Kroon, M, Koukouli, M.E, Brinkma, E.J, Labow, G, Veeffkind, JP and McPeters, RD 2007, 'Validation of Ozone Monitoring Instrument total ozone column measurements using Brewer and Dobson spectrophotometer ground-based observations', *Journal of Geophysical Research: Atmospheres*, Vol. 112, no. D24. <https://doi.org/10.1029/2007JD008796>.

Basher, R.E 1982, 'Ozone absorption coefficients' role in Dobson instrument ozone measurement accuracy', *Geophysical Research Letters*, Vol. 9, no. 11, pp.1235-1238.

Behar-Cohen, F, Martinsons, C, Viénot, F, Zissis, G, Barlier-Salsi, A, Cesarini, JP, Enouf, O, Garcia, M, Picaud, S and Attia, D 2011, 'Light-emitting diodes (LED) for domestic lighting: Any risks for the eye', *Progress in Retinal and Eye Research*, Vol. 30, no. 4, pp.239-257.

Bernhard, G, Arola, A, Dahlback, A, Fioletov, V, Heikkilä, A, Johnsen, B, Koskela, T, Lakkala, K, Svendby, T and Tamminen, J 2015, 'Comparison of OMI UV observations with ground-based measurements at high northern latitudes', *Atmospheric Chemistry and Physics*, Vol. 15, no. 13, pp.7391-7412.

Blumthaler, M, Ambach, W and Ellinger, R 1997, 'Increase in solar UV radiation with altitude', *Journal of Photochemistry and Photobiology B: Biology*, Vol. 39, no. 2, pp.130-134.

Bramstedt, K, Gleason, J, Loyola, D, Thomas, W, Bracher, A, Weber, M and Burrows, JP 2003, 'Comparison of total ozone from the satellite instruments GOME and TOMS with measurements from the Dobson network 1996–2000', *Atmospheric Chemistry and Physics*, Vol. 3, no. 5, pp.1409-1419.

Buchard, V, Brogniez, C, Auriol, F, Bonnel, B, Lenoble, J, Tanskanen, A, Bojkov, B and Veeffkind, P 2008, 'Comparison of OMI ozone and UV irradiance data with ground-based measurements at two French sites', *Atmospheric Chemistry and Physics*, Vol. 8, no. 16, pp.4517-4528.

References

Buchard, V, da Silva, AM, Colarco, PR, Darmenov, A, Randles, CA, Govindaraju, R., Torres, O, Campbell, J and Spurr, R 2015, 'Using the OMI aerosol index and absorption aerosol optical depth to evaluate the NASA MERRA Aerosol Reanalysis', *Atmospheric Chemistry and Physics*, Vol. 15, no. 10, p.5743.

Buntoung, S and Webb, AR 2010, 'Comparison of erythemal UV irradiances from Ozone Monitoring Instrument (OMI) and ground-based data at four Thai stations', *Journal of Geophysical Research: Atmospheres*, Vol. 115, no. D18. <https://doi.org/10.1029/2009JD013567>.

Burrows, JP, Weber, M, Buchwitz, M, Rozanov, V, Ladstätter-Weissenmayer, A, Richter, A, DeBeek, R., Hoogen, R, Bramstedt, K, Eichmann, KU and Eisinger, M 1999, 'The global ozone monitoring experiment (GOME): Mission concept and first scientific results', *Journal of the Atmospheric Sciences*, Vol. 56, no. 2, pp.151-175.

Cachorro, VE, Toledano, C, Antón, M, Berjón, A, Frutos, A.D, Vilaplana, JM, Arola, A and Krotkov, NA 2010, 'Comparison of UV irradiances from Aura/Ozone Monitoring Instrument (OMI) with Brewer measurements at El Arenosillo (Spain)– Part 2: analysis of site aerosol influence', *Atmospheric Chemistry and Physics*, Vol. 10, no. 23, pp.11867-11880.

Cadet, JM, Bencherif, H, Portafaix, T, Lamy, K, Ncongwane, K, Coetzee, GJ and Wright, CY 2017, 'Comparison of Ground-Based and Satellite-Derived Solar UV Index Levels at Six South African Sites', *International Journal of Environmental Research and Public Health*, Vol. 14, no. 11, p.1384.

Calbó, J, D, Pagès, and J-A González 2005, 'Empirical studies of cloud effects on UV radiation. A review', *Rev. Geophys.*, Vol. 43, RG2002, doi: 10.1029/2004RG000155.

Calbó, J, González, JA and Pagès, D 2001, 'A method for sky-condition classification from ground-based solar radiation measurements', *Journal of Applied Meteorology*, Vol. 40, no. 12, pp.2193-2199.

References

Calbó, J and Sabburg, J 2008, 'Feature extraction from whole-sky ground-based images for cloud-type recognition', *Journal of Atmospheric and Oceanic Technology*, Vol. 25no. 1, pp.3-14.

Caldwell, MM, Björn, LO, Bornman, JF, Flint, SD, Kulandaivelu, G, Teramura, AH and Tevini, M 1998, 'Effects of increased solar ultraviolet radiation on terrestrial ecosystems', *Journal of Photochemistry and Photobiology B: Biology*, Vol. 46, no. 1, pp.40-52.

Callies, J, Corpaccioli, E, Eisinger, M, Lefebvre, A, Hahne, A, Munro, R and Perez-Albinana, A 2000, 'Ozone monitoring by GOME-2 on the METOP satellites'. In *Atmospheric Ozone. Proceedings of the Quadrennial Ozone Symposium, Sapporo, Japan*.

CIE (International Commission on Illumination) 1987, 'A reference action spectrum for ultraviolet induced erythema in human skin', *CIE-Journal*, Vol. 5, no. 1, pp. 17–22.

CIE(International Commission on Illumination) 1998, 'Erythema reference action spectrum and standard erythema dose', *CIE S*, Vol. 7, p.E1998.

CIE (International Commission on Illumination) 2006, 'Action spectrum for the production of previtamin D₃ in human skin', *CIE-174*.

CIE (International Commission on Illumination) 2014, 'Rationalizing nomenclature for UV doses and effects on humans', *CIE-209*. ISBN 978-3-902842-35-0.

De Gruijl, F.R. 1999, 'Skin cancer and solar UV radiation', *European Journal of Cancer*, Vol. 35, no. 14, pp.2003-2009.

De Miguel, A, Román, R, Bilbao, J and Mateos, D 2011, 'Evolution of erythemal and total shortwave solar radiation in Valladolid, Spain: effects of atmospheric factors', *Journal of Atmospheric and Solar-Terrestrial Physics*, Vol. 73, no. 5, pp.578-586.

References

Di Sarra, A, Disterhoft, P and DeLuisi, JJ 2002, 'On the Importance of spectral responsivity of Robertson-Berger-type ultraviolet radiometers for long-term observations', *Photochemistry and Photobiology*, Vol. 76, no. 1, pp.64-72.

Diffey, B 2009, 'A simple technique for estimating daily ambient erythemal ultraviolet from the ultraviolet index', *Photodermatology, Photoimmunology & Photomedicine*, Vol. 25, no. 4, pp.227-229.

Diffey, B.L 2002a, 'What is light?', *Photodermatology, Photoimmunology & Photomedicine*, Vol. 18, no. 2, pp.68-74.

Diffey, BL 2002b, 'Sources and measurement of ultraviolet radiation', *Methods*, Vol. 28, no. 1, pp.4-13.

Diffey, BL 1991, 'Solar ultraviolet radiation effects on biological systems', *Physics in Medicine and Biology*, vol. 36, no. 3, pp. 299–328.

Doran, CM, Ling, R, Byrnes, J, Crane, M, Searles, A Perez, D & Shakeshaft, A 2015, 'Estimating the economic costs of skin cancer in New South Wales, Australia', *BMC Public Health*, 15:952, doi.org/10.1186/s12889-015-2267-3.

D'Orazio, J, Jarrett, S, Amaro-Ortiz, A and Scott, T 2013, 'UV radiation and the skin', *International Journal of Molecular Sciences*, Vol. 14, no. 6, pp.12222-12248.

Downs, N, Butler, H and Parisi, AV 2016, 'Solar ultraviolet attenuation during the Australian (Red Dawn) dust event of 23 September 2009', *Bulletin of the American Meteorological Society*, 98, pp.2039-2050.

Feister, U and Grewe, R 1995, 'Spectral albedo measurements in the UV and visible region over different types of surfaces', *Photochemistry and Photobiology*, Vol. 62, no. 4, pp.736-744.

References

Feng, Y, Ramanathan, V and Kotamarthi, VR 2013, 'Brown carbon: a significant atmospheric absorber of solar radiation', *Atmospheric Chemistry and Physics*, Vol. 13, no. 17, pp.8607-8621.

Frederick, JE, Snell, HE and Haywood, EK 1989, 'Solar ultraviolet radiation at the earth's surface', *Photochemistry and Photobiology*, Vol. 50, no. 4, pp.443-450.

Fioletov, VE, Kerr, JB and Wardle, DI 1997, 'Relationship between total ozone and spectral UV irradiance from Brewer observations and its use for derivation of total ozone from UV measurements', *Geophysical Research Letters*, Vol. 24, no. 23, pp.2997-3000.

Fioletov, VE, Kerr, JB, Wardle, DI, Krotkov, N and Herman, JR 2002, 'Comparison of Brewer ultraviolet irradiance measurements with total ozone mapping spectrometer satellite retrievals', *Optical Engineering*, Vol. 41, no. 12, pp.3051-3061.

Fioletov, VE, Kimlin, MG, Krotkov, N, McArthur, LB, Kerr, JB, Wardle, DI, Herman, JR, Meltzer, R, Mathews, TW and Kaurola, J 2004, 'UV index climatology over the United States and Canada from ground-based and satellite estimates', *Journal of Geophysical Research: Atmospheres*, Vol. 109(D22).
<https://doi.org/10.1029/2004JD004820>

Fishman, J and Brackett, VG 1997, 'The climatological distribution of tropospheric ozone derived from satellite measurements using version 7 Total Ozone Mapping Spectrometer and Stratospheric Aerosol and Gas Experiment data sets', *Journal of Geophysical Research: Atmospheres*, Vol. 102(D15), pp.19275-19278.

Fishman, J, Wozniak, AE and Creilson, JK 2003, 'Global distribution of tropospheric ozone from satellite measurements using the empirically corrected tropospheric ozone residual technique: Identification of the regional aspects of air pollution', *Atmospheric Chemistry and Physics*, Vol. 3, no. 4, pp.893-907.

References

Fitzpatrick, TB, 1988. 'The validity and practicality of sun-reactive skin types I through VI'. *Archives of dermatology*, Vol 124, no. 6, pp.869-871.

Fontana, F, Lugrin, D, Seiz, G, Meier, M and Foppa, N 2013, 'Intercomparison of satellite-and ground-based cloud fraction over Switzerland (2000–2012)', *Atmospheric Research*, Vol. 128, pp.1-12.

Fountoulakis, I, Bais, AF, Tourpali, K, Fragkos, K and Misios, S 2014, 'Projected changes in solar UV radiation in the Arctic and sub-Arctic Oceans: Effects from changes in reflectivity, ice transmittance, clouds, and ozone', *Journal of Geophysical Research: Atmospheres*, Vol. 119, no. 13, pp.8073-8090.

Freeman, SE, Gange, RW, Sutherland, JC, Matzinger, EA and Sutherland, BM 1987, 'Production of pyrimidine dimers in DNA of human skin exposed in situ to UVA radiation', *Journal of Investigative Dermatology*, Vol. 88, no. 4, pp.430-433.

Frey, R.A, Ackerman, SA, Liu, Y, Strabala, KI, Zhang, H, Key, JR and Wang, X 2008, 'Cloud detection with MODIS. Part I: Improvements in the MODIS cloud mask for collection 5', *Journal of Atmospheric and Oceanic Technology*, Vol, 25, no. 7, pp.1057-1072.

Gallagher, RP and Lee, TK 2006, 'Adverse effects of ultraviolet radiation: a brief review', *Progress in Biophysics and Molecular Biology*, Vol. 92, no. 1, pp.119-131.

Gao, W, Slusser, J, Gibson, J, Scott, G, Bigelow, D, Kerr, J and McArthur, B 2001, 'Direct-Sun column ozone retrieval by the ultraviolet multifilter rotating shadow-band radiometer and comparison with those from Brewer and Dobson spectrophotometers', *Applied Optics*, Vol. 40, no. 19, pp.3149-3155.

Gies, P 2003, 'Australia has more than enough solar UV radiation', *Clinical and Experimental Optometry*, Vol. 86, no. 2, pp.71-73.

Gies, P, Klekociuk, A, Tully, M, Henderson, S, Javorniczky, J, King, K, Lemus-Deschamps, L and Makin, J 2013, 'Low ozone over Southern Australia in August 2011

References

and its impact on solar ultraviolet radiation levels', *Photochemistry and Photobiology*, Vol. 89, no. 4, pp.984-994.

Gies, P, Roy, C, Javorniczky, J, Henderson, S, Lemus-Deschamps, L and Driscoll, C 2004, 'Global Solar UV Index: Australian Measurements, Forecasts and Comparison with the UK', *Photochemistry and Photobiology*, Vol. 79, no. 1, pp.32-39.

Grant, WB 2007, 'Roles of solar UV radiation and vitamin D in human health and how to obtain vitamin D', *Expert Review of Dermatology*, Vol. 2, no. 5, pp.563-577.

Grobner, J, Blumthaler, M and Ambach, W 1996, 'Experimental investigation of spectral global irradiance measurement errors due to a non-ideal cosine response', *Geophysical Research Letters*, Vol. 23, no. 18, pp.2493-2496.

Häder, DP, Kumar, HD, Smith, RC and Worrest, RC 2007, 'Effects of solar UV radiation on aquatic ecosystems and interactions with climate change', *Photochemical and Photobiological Sciences*, Vol. 6, no. 3, pp.267-285.

Herman, J, DeLand, MT, Huang, LK, Labow, G, Larko, D, Lloyd, SA, Mao, J, Qin, W and Weaver, C 2013, 'A net decrease in the Earth's cloud, aerosol, and surface 340 nm reflectivity during the past 33 year (1979–2011)', *Atmospheric Chemistry and Physics*, Vol. 13, no. 16, pp.8505-8524.

Herman, JR, Bhartia, PK, Torres, O, Hsu, C, Seftor, C and Celarier, E 1997, 'Global distribution of UV-absorbing aerosols from Nimbus 7/TOMS data', *Journal of Geophysical Research: Atmospheres*, Vol. 102, no. D14, pp.16911-16922.

Herman, JR, Krotkov, N, Celarier, E, Larko, D and Labow, G 1999, 'Distribution of UV radiation at the Earth's surface from TOMS-measured UV-backscattered radiances', *Journal of Geophysical Research: Atmospheres*, Vol. 104, no. D10, pp.12059-12076.

Hollosy, F 2002, 'Effects of ultraviolet radiation on plant cells', *Micron*, Vol. 33, no. 2, pp.179-197.

References

Honigsmann, H 2002, 'Erythema and pigmentation', *Photodermatology, Photoimmunology & Photomedicine*, Vol. 18, no. 2, pp.75-81.

Hsu, NC, Herman, JR, Torres, O, Holben, BN, Tanre, D, Eck, TF, Smirnov, A, Chatenet, B and Lavenu, F 1999, 'Comparisons of the TOMS aerosol index with Sun-photometer aerosol optical thickness: Results and applications', *Journal of Geophysical Research: Atmospheres*, Vol. 104, no. D6, pp.6269-6279.

Ialongo, I, Arola, A, Kujanpää, J and Tamminen, J 2011, 'Use of satellite erythemal UV products in analysing the global UV changes', *Atmospheric Chemistry and Physics*, Vol. 11, no. 18, pp.9649-9658.

Ialongo, I, Buchard, V, Brogniez, C, Casale, GR and Siani, AM 2010, 'Aerosol Single Scattering Albedo retrieval in the UV range: an application to OMI satellite validation', *Atmospheric Chemistry and Physics*, Vol. 10, no. 2, pp.331-340.

Ialongo, I, Casale, GR and Siani, AM 2008, 'Comparison of total ozone and erythemal UV data from OMI with ground-based measurements at Rome station', *Atmospheric Chemistry and Physics*, Vol. 8, no. 12, pp.3283-3289.

Internetworks 2018, Print your solar noon calendar, viewed September 2016, <<http://www.solar-noon.com/>>.

Igoe, D and Parisi, AV 2014, 'Broadband direct UVA irradiance measurement for clear skies evaluated using a smartphone', *Radiation Protection Dosimetry*, Vol. 167, no. 4, pp.485-489.

Jablonski, NG and Chaplin, G 2012, 'Human skin pigmentation, migration and disease susceptibility', *Philosophical Transactions of the Royal Society B*, Vol. 367, no. 1590, pp.785-792.

Jégou, F, Godin-Beekmann, S, Corrêa, MP, Brogniez, C, Auriol, F, Peuch, VH, Haefelin, M, Pazmino, A, Saiag, P, Goutail, F and Mahé, E 2011, 'Validity of satellite

References

measurements used for the monitoring of UV radiation risk on health', *Atmospheric Chemistry and Physics*, Vol. 11, no. 24, pp.13377-13394.

Juzeniene, A, Brekke, P, Dahlback, A, Andersson-Engels, S, Reichrath, J, Moan, K, Holick, MF, Grant, WB and Moan, J 2011, 'Solar radiation and human health', *Reports on Progress in Physics*, Vol. 74, no. 6, p.066701.

Kalliskota, S, Kaurola, J, Taalas, P, Herman, JR., Celarier, EA and Krotkov, NA 2000, 'Comparison of daily UV doses estimated from Nimbus 7/TOMS measurements and ground-based spectroradiometric data'. *Journal of Geophysical Research: Atmospheres*, Vol. 105, no. D4, pp.5059-5067.

Kaufman, YJ, Koren, I, Remer, LA, Tanré, D, Ginoux, P and Fan, S 2005, 'Dust transport and deposition observed from the Terra-Moderate Resolution Imaging Spectroradiometer (MODIS) spacecraft over the Atlantic Ocean', *Journal of Geophysical Research: Atmospheres*, Vol. 110, no. D10.

Kazadzis, S, Bais, A, Arola, A, Krotkov, N, Kouremeti, N and Meleti, C 2009, 'Ozone Monitoring Instrument spectral UV irradiance products: comparison with ground based measurements at an urban environment', *Atmospheric Chemistry and Physics*, Vol. 9, no. 2, pp.585-594.

Kazantzidis, A, Bais, AF, Gröbner, J, Herman, JR., Kazadzis, S, Krotkov, N, Kyrö, E, Den Outer, PN, Garane, K, Görts, P and Lakkala, K 2006, 'Comparison of satellite-derived UV irradiances with ground-based measurements at four European stations', *Journal of Geophysical Research: Atmospheres*, Vol. 111(D13).

Kazantzidis, A, Eleftheratos, K and Zerefos, CS 2011, 'Effects of cirrus cloudiness on solar irradiance in four spectral bands', *Atmospheric Research*, Vol. 102, no. 4, pp.452-459.

Kerr, JB 2005, 'Understanding the factors that affect surface ultraviolet radiation', *Optical Engineering*, Vol. 44, no. 4, pp.041002-041002.

References

Kerr, JB, Seckmeyer, G, Bais, AF, Bernhard, G, Blumthaler, M, Diaz, SB, Krotkov, N, Lubin, D, McKenzie, RL, Sabziparvar, AA and Verdebout, J 2002, 'Surface ultraviolet radiation: Past and future', *Scientific Assessment of Ozone Depletion*, pp.5-1.

King, MD, Menzel, WP, Kaufman, YJ, Tanré, D, Gao, BC, Platnick, S, Ackerman, SA, Remer, LA, Pincus, R and Hubanks, PA 2003, 'Cloud and aerosol properties, precipitable water, and profiles of temperature and water vapor from MODIS', *IEEE Transactions on Geoscience and Remote Sensing*, Vol. 41, no. 2, pp.442-458.

Kohler, U 1999, 'A comparison of the new filter ozonometer MICROTOPS II with Dobson and Brewer spectrometers at Hohenpeissenberg', *Geophysical Research Letters*, Vol. 26, no. 10, pp.1385-1388.

Kozmin, S, Slezak, G, Reynaud-Angelin, A, Elie, C, De Rycke, Y, Boiteux, S and Sage, E 2005, 'UVA radiation is highly mutagenic in cells that are unable to repair 7, 8-dihydro-8-oxoguanine in *Saccharomyces cerevisiae*', *Proceedings of the National Academy of Sciences of the United States of America*, Vol. 102, no. 38, pp.13538-13543.

Kramer, LJ, Leigh, RJ, Remedios, JJ and Monks, PS 2008, 'Comparison of OMI and ground-based in situ and MAX-DOAS measurements of tropospheric nitrogen dioxide in an urban area', *Journal of Geophysical Research: Atmospheres*, Vol. 113, no. D16.

Krutmann, J 2000, 'Ultraviolet A radiation-induced biological effects in human skin: relevance for photoaging and photodermatosis', *Journal of Dermatological Science*, 23, pp.S22-S26.

Kujanpää, J and Kalakoski, N 2015, 'Operational surface UV radiation product from GOME-2 and AVHRR/3 data'. *Atmospheric Measurement Techniques*, Vol. 8, no. 10, pp.4399-4414.

Langston, M, Dennis, L, Lynch, C, Roe, D and Brown, H 2017, 'Temporal trends in satellite-derived erythemal UVB and implications for ambient sun exposure

References

assessment', *International Journal of Environmental Research and Public Health*, Vol. 14, no. 2, pp.176.

Lavker, RM, Gerberick, GF, Veres, D, Irwin, CJ and Kaidbey, KH 1995, 'Cumulative effects from repeated exposures to suberythemal doses of UVB and UVA in human skin', *Journal of the American Academy of Dermatology*, Vol. 32, no. 1, pp.53-62.

Levy, RC, Remer, LA, Tanré, D, Mattoo, S and Kaufman, YJ 2009, 'Algorithm for remote sensing of tropospheric aerosol over dark targets from MODIS: collections 005 and 051: Revision 2; Feb 2009', <http://modisatmos.gsfc.nasa.gov/_docs/ATBD_MOD04_C005_rev2.pdf>.

Long, C N and Ackerman T P 2000, 'Identification of clear skies from broadband pyranometer measurements and calculation of downwelling shortwave cloud effects', *Journal of Geophysical Research: Atmospheres*, Vol. 105, pp.15609-15626.

Long, CN, Sabburg, JM, Calbó, J and Pages, D 2006, 'Retrieving cloud characteristics from ground-based daytime color all-sky images', *Journal of Atmospheric and Oceanic Technology*, Vol. 23, no. 5, pp.633-652.

Madronich, S and Flocke, S 1999, 'The role of solar radiation in atmospheric chemistry', In *Environmental Photochemistry*, Springer, Berlin, Heidelberg, pp. 1-26

Madronich, S, McKenzie, RL, Björn, LO and Caldwell, MM 1998, 'Changes in biologically active ultraviolet radiation reaching the Earth's surface', *Journal of Photochemistry and Photobiology B: Biology*, Vol. 46, no. 1-3, pp.5-19.

Mateos, D, Bilbao, J, Kudish, AI, Parisi, AV, Carbajal, G, Di Sarra, A, Román, R and De Miguel, A 2013, 'Validation of OMI satellite erythemal daily dose retrievals using ground-based measurements from fourteen stations', *Remote Sensing of Environment*, Vol. 128, pp.1-10.

McCluney, WR, 2014. *Introduction to Radiometry and Photometry*. Artech House, Boston, London.

References

McKenzie, RL, Aucamp, PJ, Bais, AF, Björn, LO, Ilyas, M and Madronich, S 2011, 'Ozone depletion and climate change: impacts on UV radiation', *Photochemical and Photobiological Sciences*, Vol. 10, no. 2, pp.182-198.

McKenzie, RL, Seckmeyer, G, Bais, AF, Kerr, JB, and Madronich, S 2001, 'Satellite retrievals of erythemal UV dose compared with ground-based measurements at northern and southern mid-latitudes', *Journal of Geophysical Research*, Vol. 106, no. D20, pp.24-051.

McKenzie, RL, Weinreis, C, Johnston, PV, Liley, B, Shiona, H, Kotkamp, M, Smale, D, Takegawa, N and Kondo, Y 2008, 'Effects of urban pollution on UV spectral irradiances', *Atmospheric Chemistry and Physics Discussions*, Vol. 8, no. 2, pp.7149-7188.

Meloni, D, Di Sarra, A, Herman, JR, Monteleone, F and Piacentino, S 2005, 'Comparison of ground-based and Total Ozone Mapping Spectrometer erythemal UV doses at the island of Lampedusa in the period 1998–2003: Role of tropospheric aerosols', *Journal of Geophysical Research: Atmospheres*, Vol. 110(D1). <https://doi.org/10.1029/2004JD005283>

Miller, SA, Hamilton, SL, Wester, UG. and Cyr, WH 1998, 'An analysis of UVA emissions from sunlamps and the potential importance for melanoma', *Photochemistry and Photobiology*, Vol. 68, no. 1, pp.63-70.

Moyal, DD and Fourtanier, AM 2002, 'Effects of UVA radiation on an established immune response in humans and sunscreen efficacy', *Experimental Dermatology*, Vol. 11, no. s1, pp.28-32.

Munro, R, Lang, R, Klaes, D, Poli, G, Retscher, C, Lindstrot, R, Huckle, R, Lacan, A, Grzegorski, M, Holdak, A and Kokhanovsky, A 2016, 'The GOME-2 instrument on the Metop series of satellites: instrument design, calibration, and level 1 data processing—an overview', *Atmospheric Measurement Techniques*, Vol. 9, no. 3, pp.1279-1301.

References

Narayanan, DL, Saladi, RN and Fox, JL 2010, 'Ultraviolet Radiation and Skin Cancer', *International Journal of Dermatology*, Vol. 49, no. 9, pp.978-986.

Natarajan, VT, Ganju, P, Ramkumar, A, Grover, R and Gokhale, RS 2014, 'Multifaceted pathways protect human skin from UV radiation', *Nature Chemical Biology*, Vol. 10, no. 7, p.542-551.

Neidecker, MV, Davis-Ajami, ML, Balkrishnan, R & Feldman, SR 2009, 'Pharmacoeconomic considerations in treating actinic keratosis'. *Pharmacoeconomics*, vol.27, pp.451-64.

Norman, AW 1998, 'Sunlight, season, skin pigmentation, vitamin D, and 25-hydroxyvitamin D: integral components of the vitamin D endocrine system', *The American Journal of Clinical Nutrition*, Vol. 67, no. 6, pp.1108-1110.

Parisi, A and Kimlin, MG 1997, 'Why do UV levels vary?', *Australasian Science*, Vol. 18, no. 2, pp.39-41.

Parisi, AV and Downs, N 2004, 'Cloud cover and horizontal plane eye damaging solar UV exposures', *International Journal of Biometeorology*, Vol. 49, no. 2, pp.130-136.

Parisi, AV, Downs, N, Turner, J and King, R 2017, 'Comparison of GOME-2 UVA Satellite Data to Ground-Based Spectroradiometer Measurements at a Subtropical Site', *IEEE Transactions on Geoscience and Remote Sensing*, Vol. 55, no. 6, pp.3145-3149.

Parisi, AV, Sabburg, J and Kimlin, MG, 2004. *Scattered and Filtered Solar UV Measurements*. Springer Science & Business Media.

Parisi, AV, Sabburg, J, Turner, J and Dunn, PK 2008, 'Cloud observations for the statistical evaluation of the UV index at Toowoomba, Australia', *International Journal of Biometeorology*, Vol. 52, no. 3, pp.159-166.

References

Paulescu, M, Paulescu, E, Gravila, P and Badescu, V 2012, *Weather Modelling and Forecasting of PV Systems Operation*, Springer Science & Business Media.

Paulescu, M, Paulescu, E, Gravila, P and Badescu, V 2013, 'Solar radiation measurements', In *Weather Modeling and Forecasting of PV Systems Operation*. pp. 17-42. Springer, London.

Petritoli, A, Bonasoni, P, Giovanelli, G, Ravegnani, F, Kostadinov, I, Bortoli, D, Weiss, A, Schaub, D, Richter, A and Fortezza, F 2004, 'First comparison between ground-based and satellite-borne measurements of tropospheric nitrogen dioxide in the Po basin', *Journal of Geophysical Research: Atmospheres*, Vol. 109(D15). <https://doi.org/10.1029/2004JD004547>

Piazena, H 1996, The effect of altitude upon the solar UV-B and UV-A irradiance in the tropical Chilean Andes. *Solar energy*, Vol. 57, no. 2, pp.133-140.

Pitkänen, MRA, Arola, A, Lakkala, K, Koskela, T and Lindfors, AV 2015, 'Comparing OMI UV index to ground-based measurements at two Finnish sites with focus on cloud-free and overcast conditions', *Atmospheric Measurement Techniques Discussions*, Vol. 8, no. 1, pp.487-516.

Platnick, S, King, MD, Ackerman, SA, Menzel, WP, Baum, BA, Riédi, JC and Frey, R.A 2003, 'The MODIS cloud products: Algorithms and examples from Terra', *IEEE Transactions on Geoscience and Remote Sensing*, Vol. 41, no. 2, pp.459-473.

Rass, K and Reichrath, J 2008, 'UV damage and DNA repair in malignant melanoma and nonmelanoma skin cancer' In *Sunlight, Vitamin D and Skin Cancer*, Springer New York, pp. 162-178

Ravanat, JL, Douki, T and Cadet, J 2001, 'Direct and indirect effects of UV radiation on DNA and its components', *Journal of Photochemistry and Photobiology B: Biology*, Vol. 63, no. (1-3), pp.88-102.

References

Reichrath, J and Nürnberg, B 2008, 'Understanding positive and negative effects of solar UV-radiation: A challenge and a fascinating perspective', *Solar radiation and human health. The Norwegian Academy of Science and Letters, Oslo*, pp.76-94.

Sabburg, J and Wong, J 2000, 'The effect of clouds on enhancing UVB irradiance at the earth's surface: a one year study', *Geophysical Research Letters*, Vol. 27, no. 20, pp.3337-3340.

Sabburg, JM and Long, CN 2004, 'Improved sky imaging for studies of enhanced UV irradiance', *Atmospheric Chemistry and Physics*, Vol. 4, no. 11/12, pp.2543-2552.

Sabburg, JM and Parisi, AV 2006, 'Spectral dependency of cloud enhanced UV irradiance', *Atmospheric Research*, Vol. 81, no. 3, pp.206-214.

Schwander, H, Koepke, P and Ruggaber, A, 1997, 'Uncertainties in modeled UV irradiances due to limited accuracy and availability of input data', *Journal of Geophysical Research: Atmospheres*, Vol. 102, no. D8, pp.9419-9429.

Segura, S, Estellés, V, Esteve, AR, Tena, F, Utrillas, MP and Martínez-Lozano, JA 2015, 'Assessment and application of MODIS ocean and land algorithms for the characterization of aerosol properties over a Mediterranean coastal site', *Atmospheric Research*, 157, pp.66-73.

Sharma, NP, Bhattarai, BK, Sapkota, B and Kjeldstad, B 2011, 'Comparison of Ground Based Measurements of Solar UV Index with Satellite Estimation at Four Sites of Nepal', *Journal of the Institute of Engineering*, Vol. 8, no. 3, pp.58-71.

Simic, S, Fitzka, M, Schmalwieser, A, Weihs, P and Hadzimustafic, J 2011, 'Factors affecting UV irradiance at selected wavelengths at Hoher Sonnblick', *Atmospheric Research*, Vol. 101, no. 4, pp.869-878.

Sivasakthivel, T and Reddy, KSK 2011 'Ozone layer depletion and its effects: a review', *International Journal of Environmental Science and Development*, Vol. 2, no. 1, p.30.

References

Smith, GJ, White, MG and Ryan, KG 1993, 'Seasonal trends in erythemal and carcinogenic Ultraviolet radiation at MID-southern latitudes 1989–1991', *Photochemistry and Photobiology*, Vol. 57, no. 3, pp.513-517.

Soehnge, H, Ouhtit, A and Ananthaswamy, ON 1997, 'Mechanisms of induction of skin cancer by UV radiation', *Frontiers Bioscience*, 2, pp.D538-D551.

Soulen, PF and Frederick, JE 1999, 'Estimating biologically active UV irradiance from satellite radiance measurements: A sensitivity study'. *Journal of Geophysical Research: Atmospheres*, 104(D4), pp.4117-4126.

Stamnes, K and Stamnes, J J 2008, 'Transport of Solar Radiation through the Atmosphere: Aspects Relevant for Health', *Solar Radiation and Human Health*, pp. 9-22.

Stubenrauch, CJ, Rossow, WB, Kinne, S, Ackerman, S, Cesana, G, Chepfer, H, Di Girolamo, L, Getzewich, B, Guignard, A, Heidinger, A and Maddux, BC 2013, 'Assessment of global cloud datasets from satellites: Project and database initiated by the GEWEX radiation panel', *Bulletin of the American Meteorological Society*, Vol. 94, no. 7, pp.1031-1049.

Tanskanen, A, Krotkov, NA., Herman, JR and Arola, A 2006, 'Surface ultraviolet irradiance from OMI' *IEEE transactions on Geoscience and Remote Sensing*, Vol. 44, no. 5, pp.1267-1271.

Tanskanen, A, Lindfors, A, Määttä, A, Krotkov, N, Herman, J, Kaurola, J, Koskela, T, Lakkala, K, Fioletov, V, Bernhard, G and McKenzie, R 2007, 'Validation of daily erythemal doses from Ozone Monitoring Instrument with ground-based UV measurement data', *Journal of Geophysical Research: Atmospheres*, 112(D24).

Thompson, AM, Witte, JC, McPeters, RD, Oltmans, SJ, Schmidlin, FJ, Logan, JA, Fujiwara, M, Kirchhoff, VW, Posny, F, Coetzee, GJ and Hoegger, B 2003, 'Southern Hemisphere Additional Ozonesondes (SHADOZ) 1998–2000 tropical ozone

References

climatology 1. Comparison with Total Ozone Mapping Spectrometer (TOMS) and ground-based measurements', *Journal of Geophysical Research: Atmospheres*, Vol. 108(D2). <https://doi.org/10.1029/2001JD000967>

Torres, O, Tanskanen, A, Veihelmann, B, Ahn, C, Braak, R, Bhartia, PK, Veeffkind, P and Levelt, P 2007, 'Aerosols and surface UV products from Ozone Monitoring Instrument observations: An overview', *Journal of Geophysical Research: Atmospheres*, Vol. 112(D24). <https://doi.org/10.1029/2007JD008809>

Torres, O, Ahn, C and Chen, Z 2013, 'Improvements to the OMI near-UV aerosol algorithm using A-train CALIOP and AIRS observations' *Atmospheric Measurement Techniques*, Vol. 6, no. 11, pp.3257-3270.

Torres, O, Bhartia, PK, Herman, JR, Ahmad, Z and Gleason, J 1998, 'Derivation of aerosol properties from satellite measurements of backscattered ultraviolet radiation: Theoretical basis', *Journal of Geophysical Research: Atmospheres*, Vol. 103, no. D14, pp.17099-17110.

Turner, J and Parisi, AV 2009, 'Measuring the influence of UV reflection from vertical metal surfaces on humans', *Photochemical & Photobiological Sciences*, Vol. 8, no.1, pp.62-69.

Udelhofen, PM., Gies, P, Roy, C and Randel, WJ 1999, 'Surface UV radiation over Australia, 1979–1992: effects of ozone and cloud cover changes on variations of UV radiation', *Journal of Geophysical Research: Atmospheres*, Vol. 104, no. D16, pp.19135-19159.

Van Roozendaal, M, Peeters, P, Roscoe, HK, De Backer, H, Jones, AE, Bartlett, L, Vaughan, G, Goutail, F, Pommereau, JP, Kyro, E and Wahlstrom, C 1998, 'Validation of ground-based visible measurements of total ozone by comparison with Dobson and Brewer spectrophotometers', *Journal of Atmospheric Chemistry*, Vol. 29, no. 1, pp.55-83.

References

Vanicek, K 2006, 'Differences between ground Dobson, Brewer and satellite TOMS-8, GOME-WFDOAS total ozone observations at Hradec Kralove, Czech', *Atmospheric Chemistry and Physics*, Vol. 6, no. 12, pp.5163-5171.

Veefkind, JP, de Haan, JF, Brinksma, EJ, Kroon, M and Levelt, PF 2006, 'Total ozone from the Ozone Monitoring Instrument (OMI) using the DOAS technique', *IEEE Transactions on Geoscience and Remote Sensing*, Vol. 44, no. 5, pp.1239-1244.

Veefkind, JP, de Leeuw, G, Stammes, P and Koелеmeijer, RB 2000, 'Regional distribution of aerosol over land, derived from ATSR-2 and GOME'. *Remote Sensing of Environment*, Vol. 74, no. 3, pp.377-386.

Viatte, C, Schneider, M, Redondas, A, Hase, F, Eremenko, M, Chelin, P, Flaud, JM, Blumenstock, T and Orphal, J 2011, 'Comparison of ground-based FTIR and Brewer O3 total column with data from two different IASI algorithms and from OMI and GOME-2 satellite instruments', *Atmospheric Measurements Technique*. Vol. 4, pp.535–546.

Vile, GF, Basu-Modak, S, Waltner, C and Tyrrell, RM 1994, 'Heme oxygenase 1 mediates an adaptive response to oxidative stress in human skin fibroblasts', *Proceedings of the National Academy of Sciences*, Vol. 91, no. 7, pp. 2607-2610.

Webb, AR and Engelsen, O 2006, 'Calculated ultraviolet exposure levels for a healthy vitamin D status', *Photochemistry and Photobiology*, Vol. 82, no. 6, pp.1697-1703.

Webb, AR and Holick, MF 1988, 'The role of sunlight in the cutaneous production of vitamin D₃' *Annual Review of Nutrition*, Vol. 8, no. 1, pp.375-399.

Weber, M, Burrows, JP and Cebula, RP 1998, 'GOME solar UV/VIS irradiance measurements between 1995 and 1997—First results on proxy solar activity studies', In *Solar Electromagnetic Radiation Study for Solar Cycle 22* . Springer Netherlands, pp. 63-77

References

Wenny, BN., Schafer, JS, DeLuisi, JJ, Saxena, V.K., Barnard, WF, Petropavlovskikh, IV and Vergamini, AJ 1998, 'A study of regional aerosol radiative properties and effects on ultraviolet-B radiation', *Journal of Geophysical Research: Atmospheres*, Vol. 103, no. D14, pp.17083-17097.

World Health Organization and International Commission on Non-Ionizing Radiation Protection 2002, 'Global solar UV index: a practical guide' (No. WHO/SDE/OEH/02.2). Geneva: World Health Organization.

Wright, CY, Norval, M, Summers, B, Davids, L, Coetzee, G and Oriowo, MO 2012, 'The impact of solar ultraviolet radiation on human health in sub-Saharan Africa', *South African Journal of Science*, Vol. 108, no. 11-12, pp.45-51.

Xin, J, Wang, Y, Li, Z, Wang, P, Hao, WM, Nordgren, BL, Wang, S, Liu, G, Wang, L, Wen, T and Sun, Y 2007, 'Aerosol optical depth (AOD) and Ångström exponent of aerosols observed by the Chinese Sun Hazemeter Network from August 2004 to September 2005', *Journal of Geophysical Research: Atmospheres*, Vol. 112, no. D5. <https://doi.org/10.1029/2006JD007075>

Xu, M, Liang, XZ, Gao, W and Krotkov, N 2010, 'Comparison of TOMS retrievals and UVMRP measurements of surface spectral UV radiation in the United States', *Atmospheric Chemistry and Physics*, Vol. 10, no. 18, p.8669.

Yankee Environmental Systems 2006, TSI-440 Total Sky Imager, viewed September 2016, <<http://www.yesinc.com/products/data/tsi440/index.html>>.

Zempila, MM, Fountoulakis, I, Taylor, M, Kazadzis, S, Arola, A, Koukouli, ME, Bais, A, Meleti, C and Balis, D 2018, Validation of OMI erythemal doses with multi-sensor ground-based measurements in Thessaloniki, Greece. *Atmospheric Environment*, Vol. 183, pp.106-121.

APPENDIX: Published Refereed Papers

A Jebar, MA, Parisi, AV, Downs, NJ and Turner, JF, 2017. 'Validation of OMI UV satellite data using spectral and broadband surface based measurements at a Queensland site'. *Photochemistry and Photobiology*, 93(5), pp.1289-1293.

A Jebar, MA, Parisi, AV, Downs, NJ, and Turner, JF, 2018a. 'Evaluated UVA irradiances over a twelve year period at a sub-tropical site from ozone monitoring instrument data including the influence of cloud'. *Photochemistry and photobiology*. doi: [10.1111/php.12948](https://doi.org/10.1111/php.12948).

A Jebar, M.A., Parisi, A.V., Downs, N.J. and Turner, J.F., 2018b. 'Influence of Cloud on OMI Satellite Total Daily UVA Exposures over a 12-year Period at a Southern Hemisphere Site'. Submitted to *International Journal of Remote Sensing*.

Validation of Ozone Monitoring Instrument UV Satellite Data Using Spectral and Broadband Surface Based Measurements at a Queensland Site

Mustapha A. A Jebar, Alfio V. Parisi*, Nathan J. Downs and Joanna F. Turner

Faculty of Health, Engineering and Sciences, University of Southern Queensland, Toowoomba, Qld, Australia

Received 18 January 2017, accepted 24 March 2017, DOI: 10.1111/php.12784

ABSTRACT

This research reconstructed and validated the broadband UVA irradiances derived from discrete spectral irradiance data retrieved from the Ozone Monitoring Instrument (OMI) satellite from 1 January to 31 December 2009. OMI data at solar noon were compared to ground-based spectral irradiances at Toowoomba (27°36' S 151°55' E), Australia, at 310, 324 and 380 nm for both cloud-free and all sky conditions. There was a strong relationship between the ground-based UV spectroradiometer data and satellite-based measurements with an R^2 of 0.89 or better in each waveband for cloud-free days. The data show an overestimate of the satellite-derived spectral irradiances compared to the ground-based data. The models developed for the subtropical site data account for this overestimation and are essential for any data correlation between satellite- and ground-based measurements. Additionally, this research has compared solar noon broadband UVA irradiances evaluated with a model and the discrete satellite spectral irradiances for the solar noon values of cloud-free days to those measured with a ground-based UVA radiometer. An R^2 of 0.86 was obtained confirming that for cloud-free days the broadband UVA can be evaluated from the OMI satellite spectral irradiances.

INTRODUCTION

The UV radiation waveband has been divided into three regions according to the wavelengths: UVC (100–280 nm), UVB (280–320 nm) and UVA (320–400 nm) (1). UVA has a longer wavelength, less energy and has lower biological effectiveness than short wavelength UV. The earth's surface is exposed to a significant quantity of solar UV radiation. The UV region makes up 8–9% of the available solar energy reaching the top of the atmosphere. Of this, UVA radiation makes up 6.3% and is transmitted to the earth's surface without absorption (although it is prone to scattering and attenuation). Because of its longer wavelength, UVA damage occurs to greater depths in biological systems including below the human epidermis skin (2). Regular exposure to small amounts of the UVA leads to significant damage and cutaneous alterations in the epidermis (3). UVA is therefore a health concern and must be accounted for in research that

investigates the relationship of UV exposure to chronic human disease.

The importance of the influence of UV radiation on the earth and the poor spatial coverage of ground-based observation stations have created a demand for satellite-based instrumentation. Approaches that depend on satellite data are suitable alternatives because satellites have the capability to determine important parameters over a wide area and provide accurate calculations in evaluating levels of UV irradiance where surface instrumentation is not available (4, 5). This requires correlating the satellite data to ground-based data to attain an improved evaluation of the UV derived from satellite measurements. There are several kinds of satellite instruments that monitor UV radiation at the earth's surface: TOMS (Total Ozone Mapping Spectrometer), GOME (Global Ozone Monitoring Experiment), MODIS (Moderate Resolution Imaging Spectrometer) and Ozone Monitoring Instrument (OMI) (6). This paper considers the data from OMI which is a generation of spectrometers placed in orbit by NASA on 14 July 2004.

OMI observes the upper layers of the atmosphere and covers the UV band and near-visible irradiance (270–500 nm) with high spatial ($13 \times 24 \text{ km}^2$ at nadir) and spectral resolution (0.5 nm). OMI was developed to monitor ozone columns, clouds, surface UV and gases (NO_2 , SO_2 , HCHO, BrO, OCIO). Thus, the primary objective of OMI is to monitor long-term changes in the UV (7–12). The OMI UV algorithm is a derivative of the TOMS (Total Ozone Mapping Spectrometer) UV-based algorithm as developed previously by NASA (11). This algorithm evaluates the surface irradiance under cloud-free conditions (E_{clear}). E_{clear} is then multiplied by the factor C_T (which is equal to the derived cloud fraction divided by the nonabsorbing aerosol transmittance factor) to estimate the terrestrial irradiance in the presence of cloud (13) where,

$$E_{\text{cloud}} = E_{\text{clear}} C_T \quad (1)$$

OMI does not cover the boundary layer of the atmosphere which means that absorption of aerosols in the lower atmosphere is not accounted for by the OMI algorithm. Consequently, the OMI algorithm typically overestimates the surface UV irradiance. Some researchers, Arola *et al.* (14), have applied a postcorrection to reduce this overestimation by taking into account aerosol absorption.

Mateos *et al.* (15) have estimated the differences between satellite and ground-based daily terrestrial erythemal irradiance. This was achieved by comparing the OMI measurements to six Spanish, three Argentinean, two Italian, two Israeli and one

*Corresponding author email: parisi@usq.edu.au (Alfio Parisi)
© 2017 The American Society of Photobiology

Australian ground station. The results have shown an overestimation of the satellite values where all these results were compared at low surface albedo conditions. This overestimation significantly depends on lower atmospheric cloud condition, ozone and aerosols. Spectral comparison at a Northern Hemisphere site with high levels of aerosols has found a higher overestimation of the satellite values at the shorter wavelength of 305 nm compared to that at 324 and 380 nm (16). Buntoung and Webb (17) have compared the results of erythral UV dose measurements between OMI and broadband instruments at four urban sites in Thailand. Satellite-derived OMI measurements show an overestimation under cloud-free conditions of the UV irradiance by 10–40% for urban sites. Ialongo *et al.* (18) have compared the differences of erythral dose rates (EDRs) and erythral daily doses (EDD) between OMI and ground-based instruments (Brewer and broadband radiometer measurements) that were located in Rome, Italy. Again, the results show OMI overestimation of the satellite-derived measurements compared with the Brewer and radiometer UV measurements. However, no previous research has compared the broadband unweighted UVA (320–400 nm) data derived from the OMI to ground-based instruments. The research in this paper will firstly compare the cloud-free solar noon spectral irradiances at three wavelengths from OMI with ground-based spectral spectroradiometer data. Using the spectral irradiances at these wavelengths, we develop a method to evaluate the broadband UVA solar noon irradiances derived from OMI satellite spectral data for cloud-free days and validate this against ground-based broadband data obtained from a radiometer at a Southern Hemisphere subtropical site.

METHODS

Ground-based data. The time period of the data collected in this research is 12 months beginning 1 January and ending 31 December 2009. Data were collected at the University of Southern Queensland, Toowoomba, Australia (27°36' S 151°55' E, elevation 693 m). The ground-based UVA data of this study were recorded by two instruments located at this site on a building roof with a relatively unobstructed view of the sky. Firstly, the spectral solar UV was recorded with a calibrated UV spectroradiometer (model DTM 300; Bentham Instruments, UK). Parisi and Downs (19) have described the structure, installation and operation of the Bentham spectroradiometer installed at this site. The calibration of the spectroradiometer is traceable to the UK standard and the error of the spectroradiometer data is estimated as $\pm 9\%$. The global UV spectra obtained from the Bentham spectroradiometer are recorded at 10 minute intervals, from 5:00 am to 7:00 pm daily with 0.5 nm increment scans taking <2 min to complete, beginning at 280 nm and ending at 400 nm. Secondly, the ground-based broadband unweighted UVA data were recorded with a UVA Biometer which was calibrated yearly to the spectroradiometer (model 501A; Solar Light Inc, PA). This instrument is temperature-stabilized at 25°C and records the broadband UVA exposures continuously every 5 min.

Ground-based cloud fraction data were obtained from a sky camera located at the same site. To identify the cloud conditions (cloudy or cloud-free sky), this study has used a Total Sky Imager (model TSI440; Yankee Environmental Systems, PA). This instrument is based on a CCD color camera recording images of the sky reflected on a half-sphere dome, providing an approximate 160° field of view (20). Image processing software running on a PC acquires images, processes the images to determine pixels that are either cloud or cloud-free and determines whether the solar disk is obscured (19, 21).

In this study, the TSI-440 instrument has missing data from 17 March to 22 July 2009 and from 25 November to 31 December 2009 due to a failure of the instrument network (73 days). Consequently, the broadband erythral UV Biometer data were used to determine whether the noon time sky was clear on these days. Here, the erythral UV exposures measured by a separate broadband Biometer (model 501; Solar light Inc,

PA) recording in 5 min daily intervals were employed to monitor noon time sky conditions. If the data monitored in this way formed part of a bell-shaped curve at noon, and met the mathematical criterion according to “The change in magnitude with time test” of Long and Ackerman (22), it was taken as a cloud-free sky. Days which did not fit the criterion of Long and Ackerman were not counted as cloud-free (Fig. 1a). Thus, if the curve was not smooth at noon, it was taken as cloudy (Fig. 1b).

OMI data. OMI satellite data were retrieved from the Giovanni website which is provided by NASA (<http://giovanni.gsfc.nasa.gov/giovanni/>). The Giovanni website provides the OMI spectral UV irradiances at solar noon from October 2004 until the current day. In this study, the OMI spectral irradiance data were collected for the three UV wavelengths of 310, 324 and 380 nm. The satellite data were collected from 1 January 2009 to 31 December 2009 and corresponds to the OMI satellite solar noon time-derived spectral irradiance. To make a comparison between satellite data (OMI) and ground-based Bentham spectroradiometer data, cloud-free days were selected by using information from the TSI images when the amount of cloud was determined as 2 okta (25% sky coverage) or less ($n = 71$). As explained previously, erythemally effective Biometer data were used for days with missing data from the TSI. Therefore, the total number of days in the 1 January to 31 December period classified as cloud-free was 71 (19.5% of the total number of days in the study period).

Derivation of satellite broadband UVA irradiance. This research has made a comparison of the solar noon broadband UVA irradiances evaluated from the satellite spectral data with the broadband UVA irradiance measured with the ground-based UVA Biometer. The satellite UVA irradiances were evaluated from the satellite spectral irradiances at 310, 324 and 380 nm for cloud-free days. The trapezoidal rule was applied between 310, 324 and 380 nm, with the spectral irradiance at 380 nm extended out to 400 nm (23, 24) to develop a model for the evaluation of the broadband UVA (W m^{-2}) from 320 to 400 nm as follows:

$$\text{UVA}_{\text{irrad}} = 0.57 S_{310} + 31.429 S_{324} + 48 S_{380} \quad (2)$$

where S_{310} , S_{324} and S_{380} are the spectral UV irradiance ($\text{W m}^{-2} \text{nm}^{-1}$) at the respective satellite wavelengths. This formula approximates the irradiance limits for summation from 320 to 400 nm to provide the broadband UVA.

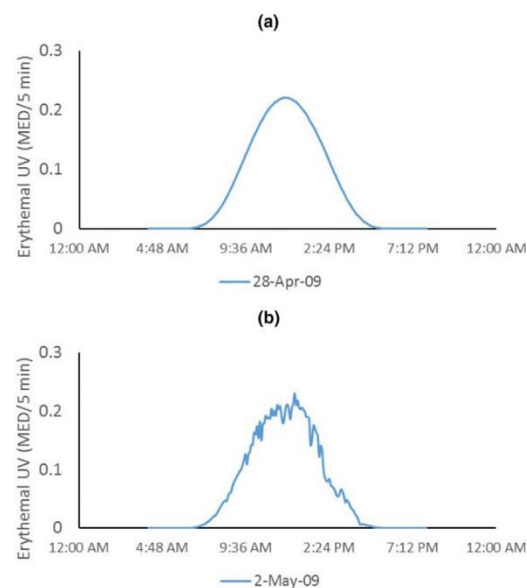


Figure 1. Time series of biometer erythral UV irradiance for determining cloud condition at solar noon, (a) cloud-free, (b) cloud-affected. [Color figure can be viewed at wileyonlinelibrary.com]

RESULTS AND DISCUSSION

Spectral data

The time series of the cloud-free spectral irradiances for the satellite data are shown in Fig. 2 for wavelengths 310, 324 and 380 nm. This figure shows that the signal increases from 310 to 380 nm because the measured UV irradiance increases with wavelength in the UVA spectrum.

The linear regression of ground-based to satellite-derived spectral irradiance on cloud-free days is shown in Fig. 3. The OMI data are a spatial average over a $1^{\circ} \times 1^{\circ}$ grid and the ground-based data are at a given point. Additionally, the OMI overpass time is not at noon and is based on the data collected at the overpass time to calculate the values for solar noon, showing the need to provide calibrations as in this paper to ground-based data. The error bars correspond to the $\pm 9\%$ error associated with the ground-based measurements (19). The average of the aerosol levels from the Giovanni website on these cloud-free days from the MODIS instrument on the Aqua and Terra satellites is 0.04 showing the relatively low aerosol level over the site. The error at 310 nm due to the OMI evaluation of the ozone levels is expected to be minimal as the mean relative difference between OMI and ground-based Dobson spectrophotometer ozone data for Brisbane (within 150 km of the site in this research) is within -1% (25). The satellite-measured spectral irradiance comparisons to the ground-based measurements show a clear correlation for the wavelengths of 310, 324 and 380 nm. There is a good comparison between satellite- and ground-based spectral irradiance measurements on cloud-free days for the three discrete wavelengths with R^2 of 0.89 or better in each waveband (Fig. 3). The R^2 value of 0.89 occurs for 310 nm where the magnitude of the spectral irradiance is the lowest. Sensitivity to ozone variations and instrument noise affect the sensitivity of the instrument at 310 nm, thereby increasing the uncertainty of the comparison at 310 nm.

The distribution of satellite- to ground-based measured spectral irradiance is plotted in Fig. 4 for cloud-free and all sky conditions. Figure 4 illustrates that most of the spectral irradiances

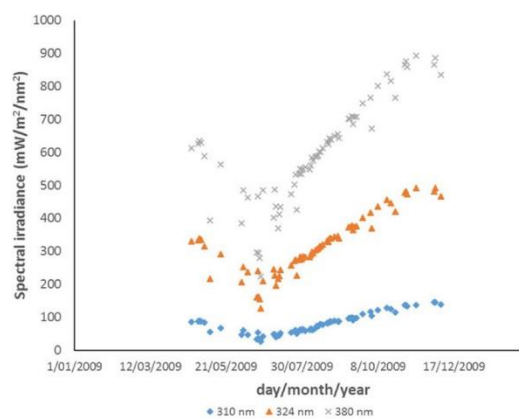


Figure 2. Time series of cloud-free spectral irradiance at 310, 324 and 380 nm for cloud-free days for the Ozone Monitoring Instrument (OMI) satellite data from 1 January 2009 to 31 December 2009.

from the OMI satellite exceed measured ground-based data as noted previously by other researchers for the shorter wavelength erythral UV and UVB comparisons (15). Median, first quartile and third quartile statistics are given in Table 1 for the same distribution plotted in Fig. 4.

Those ratios above 1 confirm that some satellite measurements overpredict the UVA irradiance for most sky conditions, which displays a similar trend to shorter wavelength comparisons as seen in the literature. Also seen in the Figure, the cloudy days have a much wider range of values with the median ratio generally being higher than one.

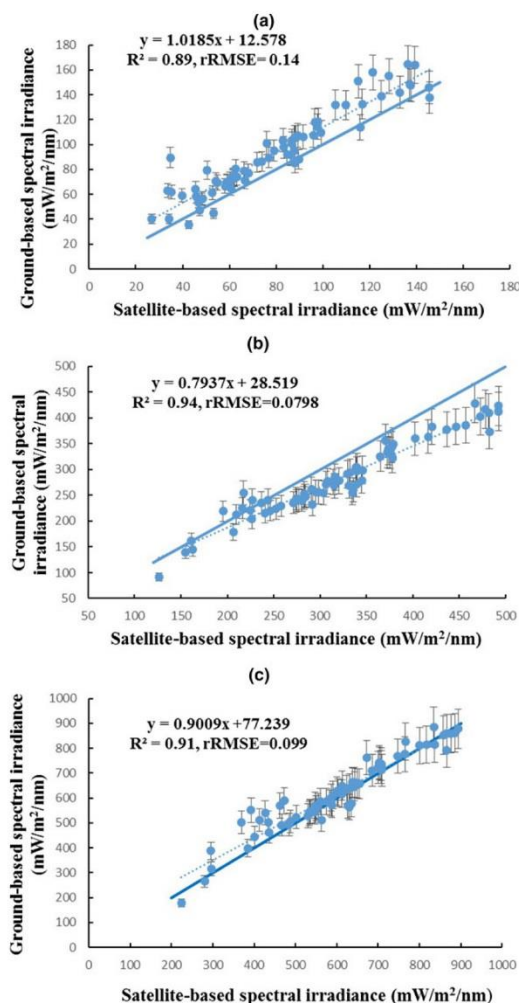


Figure 3. Cloud-free days' Ozone Monitoring Instrument (OMI) and Benthams spectral irradiance comparison for (a) 310 nm, (b) 324 nm, (c) 380 nm ($n = 71$ cloud-free days). The error bars correspond to the $\pm 9\%$ error associated with the Benthams spectroradiometer data. The solid line in each graph is the 1:1 line. The dotted line is the fitted regression line.

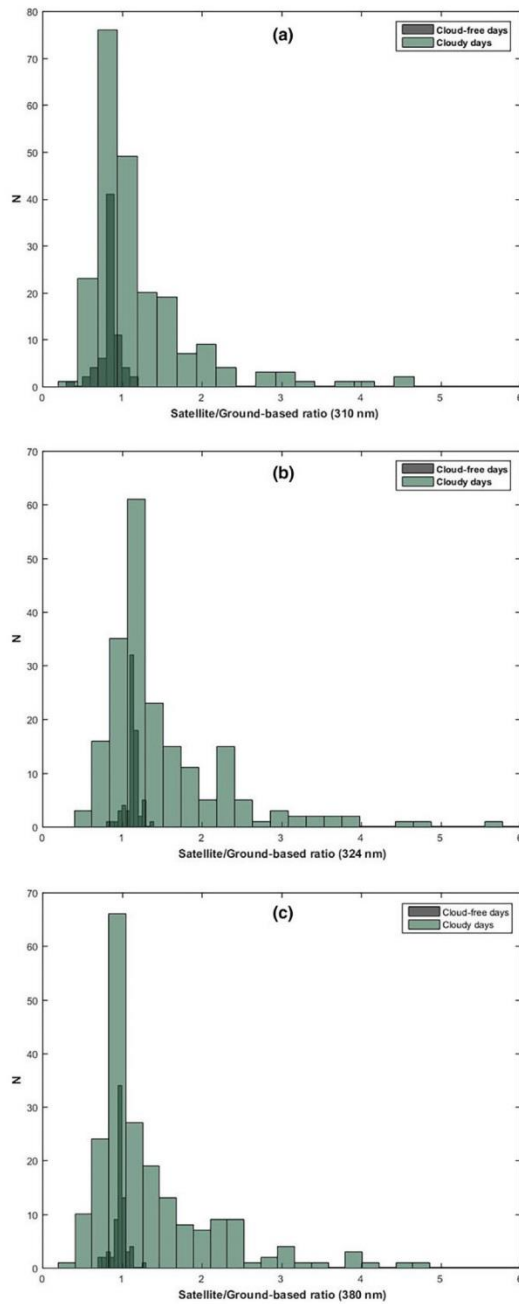


Figure 4. Histograms of the ratio of the satellite-based (Ozone Monitoring Instrument, OMI) to ground-based (Bentham) UV measurements for each of 310, 324 and 380 nm. Darker bars correspond to the measurements of 71 cloud-free days and lighter bars correspond to 221 cloudy day's measurements. *N* is the number of values. For each graph, there are 2 or less values above the value of 6. [Color figure can be viewed at wileyonlinelibrary.com]

Table 1. The first quartile (Q1), median and third quartile (Q3) for cloudy and cloud-free days at 310, 324 and 380 nm.

	Q1	Median	Q3
Cloud-free days (310 nm)	0.82	0.85	0.89
Cloud-free days (324 nm)	1.11	1.13	1.16
Cloud-free days (380 nm)	0.95	0.98	1.00
Cloudy days (310 nm)	0.83	0.99	1.34
Cloudy days (324 nm)	1.06	1.22	1.76
Cloudy days (380 nm)	0.90	1.07	1.66

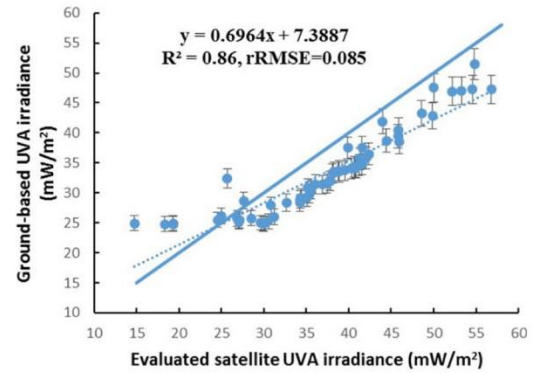


Figure 5. Comparison of the broadband UVA irradiances evaluated from Ozone Monitoring Instrument (OMI) spectral data and the UVA irradiance from the ground-based measurements were derived from Eq. 2 to use the OMI spectral irradiances. The error bars are the $\pm 10\%$ error associated with the ground-based data and the solid line is the 1:1 line. The dotted line is the fitted regression line.

Broadband UVA

Broadband UVA irradiances which are derived from the OMI data have been reconstructed and validated under cloud-free days using a mathematical model (Eq. 2). Figure 5 shows the UVA irradiances ($W m^{-2}$) modeled from the satellite spectral irradiances ($W m^{-2} nm^{-1}$) at 310, 324 and 380 nm for solar noon data measured on cloud-free days in the period 1 January to 31 December 2009. The error bars represent the $\pm 10\%$ error associated with the ground-based data. There is a reasonable agreement between the solar noon UVA broadband irradiance from the measured ground-based UVA Biometer instrument and the modeled UVA irradiance derived from satellite with an R^2 of 0.86. The figure shows the satellite UVA evaluation is approximately 30% higher which can be accounted for by calibration to ground-based instruments and in turn used for health applications where ground-based data are not available. The spectroradiometer measurements at 310, 324, 380 nm were used in Eq. (2) to calculate the UVA, and compared to the Biometer UVA, the R^2 was 0.89 and the rRMSE was 0.082.

CONCLUSION

The cloud-free solar noon spectral irradiances from OMI have been compared with a ground-based spectral spectroradiometer data at three wavelengths (310, 324, 380 nm) for a subtropical Southern Hemisphere site. These comparisons show a clear

correlation for these wavelengths and with an R^2 of 0.89 or better in each waveband. These comparisons include the $\pm 9\%$ absolute error in the spectroradiometer ground-based data and the errors in the spatial averaging of the satellite pixel data. In this paper, the ratio of the spectral irradiances from satellite compared to the ground-based measurements has showed that for the cloud-free cases at 324 nm, the median is higher than one. The corresponding median at 310 is <1 and it is very close to one at 380 nm. For the cloudy days, the ratios have a much wider range of values with the median ratio being higher than one for 324 and 380 nm and very close to one for 310 nm. The observed spread in the cloud-affected data is largely due to the temporal nature of local cloud cover and differences between the satellite overpass time and solar noon and the spatial averaging of the satellite data over the satellite pixel. The models developed account for this overestimation at the subtropical research site and are essential for any data correlation between satellite- and ground-based measurements. Additionally, this research has developed a method to evaluate and validate the broadband UVA solar noon irradiances derived from OMI satellite spectral data at 310, 324, 380 nm for cloud-free days against ground-based broadband data taken from a UVA Biometer. There is a reasonable agreement between the modeled UVA irradiance derived from OMI and the solar noon UVA broadband irradiance from the UVA Biometer with an R^2 of 0.86.

Acknowledgements—We acknowledge the OMI mission scientists and associated NASA personnel for the production of the data used in this research effort.

REFERENCES

- Parisi, A. V., J. Sabburg and M. G. Kimlin (2004) *Scattered and filtered solar UV measurements*. Springer Science & Business Media, New York.
- Stamnes, K. and J. J. Stamnes (2008) Transport of solar radiation through the atmosphere: aspects relevant for health. In *Solar Radiation and Human Health* (Edited by E. Bjertness), pp. 9–22. The Norwegian Academy of Science and Letters, Oslo.
- Lavker, R. M., G. F. Gerberick, D. Veres, C. J. Irwin and K. H. Kaidbey (1995) Cumulative effects from repeated exposures to suberythemal doses of UVB and UVA in human skin. *J. Am. Acad. Dermatol.* **32**, 53–62.
- Soulen, P. F. and J. E. Frederick (1999) Estimating biologically active UV irradiance from satellite radiance measurements: a sensitivity study. *J. Geophys. Res. Atmos.* **104**, 4117–4126.
- Paulescu, M., E. Paulescu, P. Gravila and V. Badescu (2012) *Weather modeling and forecasting of PV systems operation*. Springer Science & Business Media, New York.
- Bais, A., R. McKenzie, G. Bernhard, P. Aucamp, M. Ilyas, S. Madronich and K. Tourpali (2015) Ozone depletion and climate change: impacts on UV radiation. *Photochem. Photobiol. Sci.* **14**, 19–52.
- Bernhard, G., A. Arola, A. Dahlback, V. Fioletov, A. Heikkilä, B. Johnsen, T. Koskela, K. Lakkala, T. Svendby and J. Tamminen (2015) Comparison of OMI UV observations with ground-based measurements at high northern latitudes. *Atmos. Chem. Phys.* **15**, 7391–7412.
- Pitkänen, M., A. Arola, K. Lakkala, T. Koskela and A. Lindfors (2015) Comparing OMI UV index to ground-based measurements at two Finnish sites with focus on cloud-free and overcast conditions. *Atmos. Meas. Tech. Discuss.* **8**, 487–516.
- Torres, O., A. Tanskanen, B. Veihelmann, C. Ahn, R. Braak, P. K. Bhartia, P. Veeffkind and P. Levelt (2007) Aerosols and surface UV products from ozone monitoring instrument observations: an overview. *J. Geophys. Res. Atmos.* **112**, D24S47. <https://doi.org/10.1029/2007JD008809>.
- Veeffkind, J. P., J. F. de Haan, E. J. Brinksma, M. Kroon and P. F. Levelt (2006) Total ozone from the ozone monitoring instrument (OMI) using the DOAS technique. *IEEE Trans. Geosci. Remote Sens.* **44**, 1239–1244.
- Ialongo, I., V. Buchard, C. Brogniez, G. Casale and A. Siani (2010) Aerosol single scattering Albedo retrieval in the UV range: an application to OMI satellite validation. *Atmos. Chem. Phys.* **10**, 331–340.
- Jégou, F., S. Godin-Beekmann, M. Corrêa, C. Brogniez, F. Auriol, V. Peuch, M. Haeffelin, A. Pazmino, P. Saiag and F. Goutail (2011) Validity of satellite measurements used for the monitoring of UV radiation risk on health. *Atmos. Chem. Phys.* **11**, 13377–13394.
- Tanskanen, A., N. A. Krotkov, J. R. Herman and A. Arola (2006) Surface ultraviolet irradiance from OMI. *IEEE Trans. Geosci. Remote Sens.* **44**, 1267–1271.
- Arola, A., S. Kazadzis, A. Lindfors, N. Krotkov, J. Kujanpää, J. Tamminen, A. Bais, A. Di Sarra, J. Villaplana and C. Brogniez (2009) A new approach to correct for absorbing aerosols in OMI UV. *Geophys. Res. Lett.* **36**, L22805. <https://doi.org/10.1029/2009GL041137>.
- Mateos, D., J. Bilbao, A. Kudish, A. V. Parisi, G. Carbajal, A. Di Sarra, R. Román and A. De Miguel (2013) Validation of OMI satellite erythemal daily dose retrievals using ground-based measurements from fourteen stations. *Remote Sens. Environ.* **128**, 1–10.
- Kazadzis, S., A. Bais, A. Arola, N. Krotkov, N. Kouremeti and C. Meleti (2009) Ozone monitoring instrument spectral UV irradiance products: comparison with ground based measurements at an urban environment. *Atmos. Chem. Phys.* **9**, 585–594.
- Buntoung, S. and A. Webb (2010) Comparison of erythemal UV irradiances from ozone monitoring instrument (OMI) and ground based data at four Thai stations. *J. Geophys. Res. Atmos.* **115**, D18215. <https://doi.org/10.1029/2009JD013567>.
- Ialongo, I., G. Casale and A. Siani (2008) Comparison of total ozone and erythemal UV data from OMI with ground-based measurements at Rome station. *Atmos. Chem. Phys.* **8**, 3283–3289.
- Parisi, A. V. and N. Downs (2004) Cloud cover and horizontal plane eye damaging solar UV exposures. *Int. J. Biometeorol.* **49**, 130–136.
- Sabburg, J. and C. N. Long (2004) Improved sky imaging for studies of enhanced UV irradiance. *Atmos. Chem. Phys.* **4**, 2543–2552.
- Yankee Environmental Systems (2006) TSI-440 Total Sky Imager. Available at: <http://www.yesinc.com/products/data/tsi440/index.html>. Accessed on 1 September 2016.
- Long, C. N. and T. P. Ackerman (2000) Identification of clear skies from broadband pyranometer measurements and calculation of downwelling shortwave cloud effects. *J. Geophys. Res. Atmos.* **105**, 15609–15626.
- Anav, A., C. Rafanelli, I. Di Menno and M. Di Menno (2004) An algorithm to evaluate solar irradiance and effective dose rates using spectral UV irradiance at four selected wavelengths. *Radiat. Prot. Dosimetry.* **111**, 239–250.
- Igoe, D. and A. V. Parisi (2014) Broadband direct UVA irradiance measurement for clear skies evaluated using a smartphone. *Radiat. Prot. Dosimetry.* **167**, 485–489.
- Balis, D., M. Kroon, M. E. Koukouli, E. J. Brinksma, G. Labow, J. P. Veeffkind and R. D. McPeters (2007) Validation of ozone monitoring instrument total ozone column measurements using Brewer and Dobson spectrophotometer ground-based observations. *J. Geophys. Res.* **112**, D24546.

Evaluated UVA Irradiances over a Twelve-year Period at a Subtropical Site from Ozone Monitoring Instrument Data Including the Influence of Cloud

Mustapha A. A Jebar, Alfio V. Parisi* , Nathan J. Downs and Joanna F. Turner 

Faculty of Health, Engineering and Sciences, University of Southern Queensland, Toowoomba, Qld, Australia

Received 27 March 2018, accepted 25 May 2018, DOI: 10.1111/php.12948

ABSTRACT

This research investigated the influence of cloud on the broadband UVA solar noon irradiances evaluated from the solar noon satellite-based OMI spectral UV data that were compared to the irradiances of a ground-based radiometer from 1 October 2004 to 31 December 2016. The correlation between ground-based radiometer data and the evaluated OMI broadband UVA data evaluated with a model were dependent on whether or not the solar disk was obscured by the presence of cloud and the total sky cloud fraction. For conditions when the sun was not obscured by cloud, the evaluated satellite and the ground-based UVA irradiance correlation was best for cloud cover between 0 and 2 octa ($R^2 = 0.77$) and the worst for high cloud cover of >4–8 octa (R^2 between 0.3 and 0.4). The R^2 reduced with increasing cloud amount and showed significantly weaker correlation when the sun was obscured. The correlation between the evaluated satellite broadband UVA and the ground-based measurements over the twelve years for total cloud cover conditions of 4 or less octa confirmed that the broadband UVA satellite evaluation model for the OMI spectral data is valid for approximately 71% of the days at the Southern Hemisphere subtropical study site.

INTRODUCTION

The earth's surface is exposed to a significant quantity of solar ultraviolet (UV) radiation, with 8–9% of the available total global solar irradiance reaching the top of the earth's atmosphere (1). Of this radiation, UVA radiation (defined here as the greatest portion of UVA, specifically from 320 to 400 nm) is the dominant component making up 6.3% of the available irradiance and, unlike the shorter wavelength UVB (280 to 320 nm), which is strongly attenuated by stratospheric ozone, is mostly transmitted to the earth's surface without absorption. UVA, however, is prone to scattering and attenuation by aerosols, water droplets, and ice crystals in tropospheric cloud layers and experiences natural fluctuations in magnitude depending on total cloud fraction and cloud optical depth.

UV radiation, including UVA is potentially damaging to several biological systems on the earth affecting human health, aquatic ecosystems, and plant species (2–7). In addition, solar ultraviolet, especially UVB radiation, negatively affects physical

material properties by photodegradation that lead to a decrease in the quality of materials such as wood, paper, biopolymers, and plastics (polymers) (8). Consequently, this could decrease the outdoor service life of these materials. Satellite-based monitoring of UV and the associated atmospheric influencing factors play an important role by providing ongoing measurements of wide spatially diverse regions not able to be monitored at the surface locally. Effective satellite monitoring that takes into account variation in local atmospheric profiles that affect surface measurements requires validation to ground-based UV monitoring stations (9).

Kazantzidis *et al.* (2006) (10) have conducted a comparison between the Total Ozone Mapping Spectrometer (TOMS) UV data and four-ground stations in Europe depending on the cloud conditions. This study has shown a 15% overestimation for TOMS when the value of cloud optical depth is lower than five for most conditions. Cloud optical depth is a measure of the amount of attenuation of the solar radiation as it passes through the atmosphere due to the influence by clouds (11). It depends on the thickness of the cloud, the moisture content and makeup and size of the cloud particles (12). Anton *et al.* (2011) (13) have measured simultaneous total ozone column (TOC) data which were taken from the GOME-2 (Global Ozone Monitoring Experiment) and Infrared Atmospheric Sounding Interferometer (IASI) satellites compared to five calibrated Brewer instruments located on the Iberian Peninsula in Spain. This study showed GOME-2 provides a slight underestimation of the Brewer ozone data by 1.6%. In contrast, IASI clearly overestimated Brewer surface measurements by 4.4%. These differences are attributed to the differences between the vertical sensitivity of IASI and GOME-2. However, in general, the performance of GOME-2 and IASI present an excellent agreement of column ozone data with ground-based instruments, especially in cloud-free conditions. Cochorro *et al.* (2010) (14) have addressed the comparison between the satellite-based TOMS and Ozone Monitoring Instrument (OMI), with Brewer instruments located at a station in the south of Spain. The measurements were taken from 2004 to 2008 for three wavelengths: two wavelengths within the UVB range (305, 310 nm) and one within the UVA range (324 nm). In this case, Brewer measurements overestimated satellite data from 10 to 15% for all UV wavelengths and included an approximate 13% overestimation of the erythemal UV. Many factors were attributed to this difference including cloud conditions, aerosols, ozone, and solar elevation. Kazadzis *et al.* (2009) (15) have presented a comparison of the UV measurements of OMI and ground-based instruments located in urban areas

*Corresponding author email: parisi@usq.edu.au (Alfio Parisi)
© 2018 The American Society of Photobiology

(Thessaloniki, Greece). This study considered data from 2004 to 2007. The results showed a large OMI overestimation in the UVB where 305 nm was overestimated by 30% for all sky conditions (clear and cloudy), with lower overestimation in the more abundant surface UVA with overestimates at 324 and 380 nm reaching 20% and 16%, respectively. Kerr *et al.* (2002) (16) have provided a comparison between UV measurements of Brewer instruments, located in different Canadian areas and UV measurements of TOMS, with differences ranging from 3% to 11%. This study attributed these differences to many predictable factors that could affect the results such as solar zenith angle (SZA), clouds, angular response error, calibration errors, local microclimate, and aerosols. McKenzie *et al.* (2001) (17) focused on the differences in UV dose measurements between satellite (TOMS) and ground-based instruments in the southern and northern hemisphere. This study found that the values of ground-based instruments were less than the satellite values at most surface sites while in some unpolluted sites there was satisfactory agreement between satellite and ground-based measurements. In addition, southern hemisphere sites have better agreement due to lower ozone and less pollution. These differences were attributed to the effects of ozone, aerosols, and local cloud conditions.

Of all the atmospheric factors, influencing the satellite-based monitoring of surface UV irradiance; cloud is perhaps the most significant influencing factor. The physical influences of atmospheric scattering, refraction, and reflection are enhanced by the presence of cloud (18). Water and ice particles that make up clouds scatter solar radiation contributing to the diffuse UV that reaches the earth's surface (19). In recent years, studies have assessed the radiative contribution of clouds to the global surface irradiance because of the potential climatological importance of energy budgets to global warming. As a result, it has been found that clouds either attenuate or enhance the amount of UV radiation that reaches the earth's surface. However, in general, the influence of clouds is more explicit in the longer wavelength visible spectrum than for UV radiation, due to the predominance of longer wavelength visible radiation in the direct solar spectrum and following scattering according to Rayleigh's criterion. So, in contrast to visible radiation, the level of diffuse UV radiation can still be high, even though the sky may be covered completely and optically dim (20). The attenuating impact of clouds on the solar UV at a certain wavelength can be accounted for using a cloud modification factor (CMF) (21), defined here as;

$$CMF = \frac{E(\lambda)_w}{E(\lambda)_k} \quad (1)$$

This is the ratio between the measured UV irradiance under cloud cover, $E(\lambda)_w$ and the UV irradiance expected for cloud-free conditions, $E(\lambda)_k$. It is difficult to quantify the effects of clouds accurately because of the spatial and temporal inhomogeneity of clouds (22). Cloud conditions (cover, type, spatial, and temporal) play an important role and influence on the UV irradiance measured either by surface or by satellite-based instruments (23).

The research reported here extends previous research by considering the influence of cloud on a long-term record of solar noon broadband UVA irradiances evaluated with a model from OMI satellite spectral measurements. Specifically, recent studies have compared the OMI broadband UVA irradiances evaluated with a model and the discrete satellite spectral irradiances for

solar noon on cloud-free days to the corresponding values measured with a ground-based UVA radiometer and a spectroradiometer over a 12-month period (24). However, no such evaluation and validation have been undertaken for broadband UVA irradiances derived from discrete OMI spectral irradiances at a subtropical Southern Hemisphere site to the ground-based data recorded from an independent radiometer over a long-term (decadal) period. Subsequently, there remains limited information in the literature to develop an understanding of the direct seasonal influence of cloud. This is an important consideration, given the prevalence of cloud cover in the day-to-day environment. In this study, comparison of the OMI reconstructed solar noon UVA broadband irradiances with ground-based measurements obtained from 2004 to 2016 are reported for all sky coverage conditions at an elevated regional subtropical Southern Hemisphere site free from major sources of anthropogenic pollution.

MATERIALS AND METHODS

Ground-based data. The sources of the ground-based measurements of this study are three instruments located at a subtropical Australian site, at the University of Southern Queensland Toowoomba (27°36' S 151°55' E, 692 m asl). The first instrument is a UVA biometer (model 501A, Solar Light Inc, PA), which provides broadband UVA irradiance data every 5 min. The UVA biometer is periodically calibrated to a second instrument, a scanning spectroradiometer (Bentham Instruments, model DTM300, Reading, UK) which records the global ultraviolet in 10-min intervals daily. The DTM300 (25) is traceable to the UK National Physical Laboratory standard and records the spectral UV radiation from 280 nm to 400 nm at a resolution of 0.5 nm. The average calibration factor of the UVA biometer to the UVA irradiance derived from the scanning spectroradiometer was 1.007 for the 12-year period of this study. The third instrument installed at the University of Southern Queensland measurement site is a Total Sky Imager (TSI) (model TSI 440, Yankee Environmental Systems, PA). This imager is designed to determine the total sky cloud conditions or cloud fraction (the fraction of the hemispherical sky that has clouds (26)) every 5 min (27). Image analysis of the sky images recorded by this instrument provides the amount of the sky covered by cloud (reported here in octa) and information on whether the sun is obscured by optically thick cloud. The location, structure, technique, and calibration of all three instruments have recently been described (24). In this current research, 1920 days of data were used in the comparison between the biometer UVA irradiances measured at solar noon and the OMI evaluated UVA data at solar noon. The data spans the period from 1 October 2004 to 31 December 2016. The total number of days depends on when both the Total Sky Imager and the UVA Biometer were concurrently collecting data at solar noon together with the OMI satellite. A total of 115 days (5.9%) were excluded from the analysis due to surface instrument malfunction. The available data set was split into four cloud categories at solar noon of 0-2, >2-4, >4-6 and >6-8 octa based on the TSI image data record at solar noon. These four cloud cover categories were each further subdivided into the days when the sun's disk at solar noon was and was not obscured by optically thick cloud.

OMI data. The OMI spectral UV data at solar noon for the three wavelengths of 310, 324, 380 nm were collected from the Giovanni website (<http://giovanni.gsfc.nasa.gov/giovanni/>) for the period 1 October 2004 to 31 December 2016. To calculate the satellite broadband UVA irradiance [$W m^{-2}$] over the waveband of 320-400 nm from the OMI measurements, this study has applied a broadband UVA evaluation model (24),

$$UVA_{\text{irrad}} = 0.57I_{r310} + 31.429I_{r324} + 48I_{r380} \quad (2)$$

UVA_{irrad} is the trapezoidal rule approximation of the irradiance integral where I_r is the satellite spectral UV irradiance for the specified wavelengths of 310, 324 and 380 nm. The evaluated satellite broadband UVA irradiance data were compared with the Biometer broadband solar noon

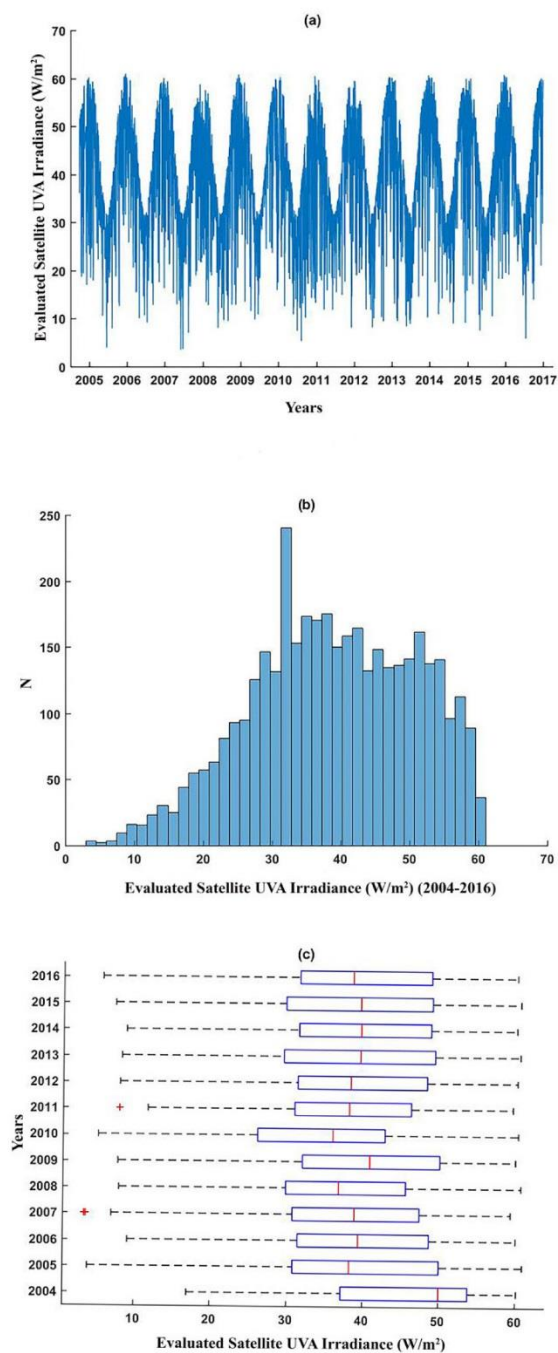


Figure 1. (a) Time series of solar noon time UVA irradiances, (b) solar noon UV irradiance distribution, and (c) box and whisker plots of the broad-band UVA irradiances evaluated from the OMI spectral data from October 2004 to 31 December 2016 for all sky conditions. The line within each box is the median and the box is the data within quartiles one and three. The dashed line of the whiskers represents the range of the data up to ± 5 standard deviations, with two outliers. The dataset for 2004 is shifted to higher irradiances due to only the last three months of the year being available.

UVA irradiance for the four cloud categories and the cases of sun obscured and sun not obscured.

RESULTS AND DISCUSSION

All sky conditions

Figure 1(a) shows the time series of the evaluated satellite UVA irradiances at solar noon for the Toowoomba study site from October 2004 to December 2016 for all sky conditions. This included 3861 values over 3861 days from satellite-based data representing 88% of the available days. The number of values available as recorded by the TSI, for the cloud-free days in the period was 1082 ($n = 1082$). For cloudy days (>2 octa), the number of values when there was available TSI data was 733 ($n = 733$). The annual cyclical pattern of high and low irradiances with the changing seasons is seen in Fig. 1(a) with the variation in the solar noon UVA irradiances changing annually between approximately 30 W m^{-2} and 60 W m^{-2} . The influence of absorption due to ozone is minimal in the UVA waveband. Additionally, the aerosol index over the measurement site is generally low due to unpolluted skies, apart from a small number of days that reported significant dust levels (28). There is no snow at the subtropical site of the research, with no resulting large variation in the ground surface albedo. Consequently, measured reduction in the UVA irradiance below the cloud-free envelope is predominantly due to clouds.

A histogram of the complete set of UVA irradiances is provided in Fig. 1b. The maximum solar noon UVA irradiance over this period is greater than 60 W m^{-2} with the median solar noon UVA irradiance being 38.8 W m^{-2} . The first and third quartile values are 30.8 and 48.4 W m^{-2} respectively. The predominance of low amounts of cloud cover at the subtropical measurement site is evident in the positively skewed distribution of the 12 years data set toward higher noon time UVA irradiance measurements.

The total dataset, split by calendar year is presented as box and whisker plots in Fig. 1c. The box and whisker plot of 2004 is shifted to higher irradiances due to only the last 3 months of the year being available (Fig. 1c). As this is the last 2 months of the austral spring and the first month of summer, the median is higher than that for the other years. For all but 2 years in the twelve-year study period, the distribution of noon time annual solar UVA irradiance appears consistent. Red outliers in Fig. 1c represent 26th of June 2007 and 7th of December 2011, which were completely overcast days.

The solar UVA irradiances for the years of 2009 and 2010 are noteworthy due to the change in the climatic conditions between these two consecutive years. The year 2009 was a particularly dry year characterized by a severe dust storm in September 2009 (28). Annual rainfall for 2009 totalled only 433 mm, a difference of 38.4% from the decadal mean for Toowoomba reported by the Australian Bureau of Meteorology of 703.1 mm. For 2009, the mean UVA irradiance was 40.4 W m^{-2} and the median was 40.9 W m^{-2} compared to the mean and median of the total remaining years of 38.9 W m^{-2} and median 38.8 W m^{-2} respectively. Mann–Whitney U tests show that there was a statistically significant difference in the 2009 irradiance measurements compared to the total remaining years ($P < 0.0264$). Previous research, reporting comparative OMI to ground-based UVA irradiance (24) was evaluated from

Table 1. Distribution statistics for the 2004 to 2016 dataset according to the full range solar noon (between 0 to 8). Q1 is the first quartile of the range, Q3 is the third quartile of the range and N is a number of days with data in the respective category

Octas	Q1	Median	Q3	N	N (plotted data)	N (observed)
0–2	0.032	0.1728	0.7608	1082	1262	0
>2–4	2.456	2.8672	3.4328	203	150	115
>4–6	4.4448	4.9008	5.352	138	116	102
>6–8	7.212	7.9936	8	392	352	368
0–8	0.1024	1.132	5.0256	1815	1880	585
2–8	3.7336	6.2624	8	733	618	585

the 2009 data. Given this year was drier than other years, the current research reports on satellite to ground-based measurements more typical of the subtropical climate experienced at the Toowoomba measurement site taken over a longer decadal time period.

Cloud data

Table 1 shows the number of occurrences of days with the different amounts of solar noon cloud cover from October 2004 to December 2016. At this subtropical site, the majority of the data (62.4%) is in the category of 0–2 octa, with a median of 0.1728 octa. The number of days in the two cloud categories of 0–2 and >2–4 octa of cloud at solar noon was 1285, representing 70.7% of the total number of study days. This means that the broadband UVA evaluation model from the OMI spectral data is applicable for approximately 70% of the days at the Toowoomba subtropical site. The number of the plotted cloud-free days (0–2 octa) is 1262 as this takes into account the days when the Biometer data was employed to confirm a cloud-free day (29). The number of the plotted data from >2–8 octa was less than the total TSI data available due to missing Giovanni satellite data and Biometer data not available on some days.

Sun not obscured sky conditions

The evaluated broadband UVA satellite irradiance at solar noon for the cases of when the solar disk was not obscured by cloud has been compared with the corresponding broadband ground-based UVA irradiances recorded by the ground-based radiometer at the research site over the 1 October 2004 to 31 December 2016 period. This data set of sun not obscured sky conditions is provided in Fig. 2 for the four cloud cover categories of 0–2, >2–4, >4–6 and >6–8 octa.

According to Fig. 2a, which shows data for sun not obscured sky conditions on days with ≤ 2 octa (65.7% of the available data), there is a correlation between the solar noon evaluated UVA satellite and the ground-based irradiances with an R^2 (coefficient of determination) of 0.77, and an rRMSE (relative root mean square error) of 18% and MAE (mean absolute error) of $3.58 \text{ (W m}^{-2}\text{)}$. Figure 2b shows the broadband UVA comparison between the satellite and the ground-based data when the quantity of cloud was from >2–4 octa (7.8% of the available data). As expected, this figure shows lower correlation between the satellite and ground-based data than the correlation for the 0–2 octa data in Fig. 2a. However, despite the low number of data values there is comparable correlation between the data sets (R^2

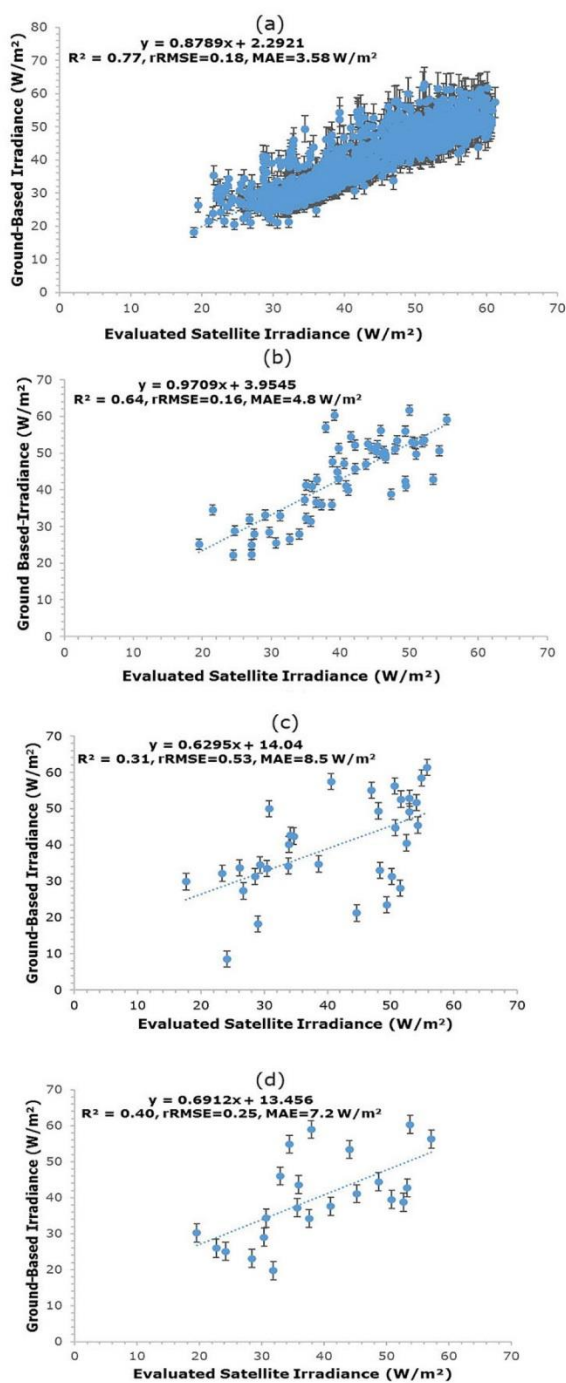


Figure 2. Comparison of the evaluated OMI satellite solar noon UVA irradiances with ground-based UVA data for the four categories of cloud cover of (a) 0 to 2, (b) >2 to 4, (c) >4 to 6 and (d) >6 to 8 octa for sun not obscured sky conditions. The error bars are the $\pm 10\%$ error associated with the ground-based data. The dashed line is the fitted trend line.

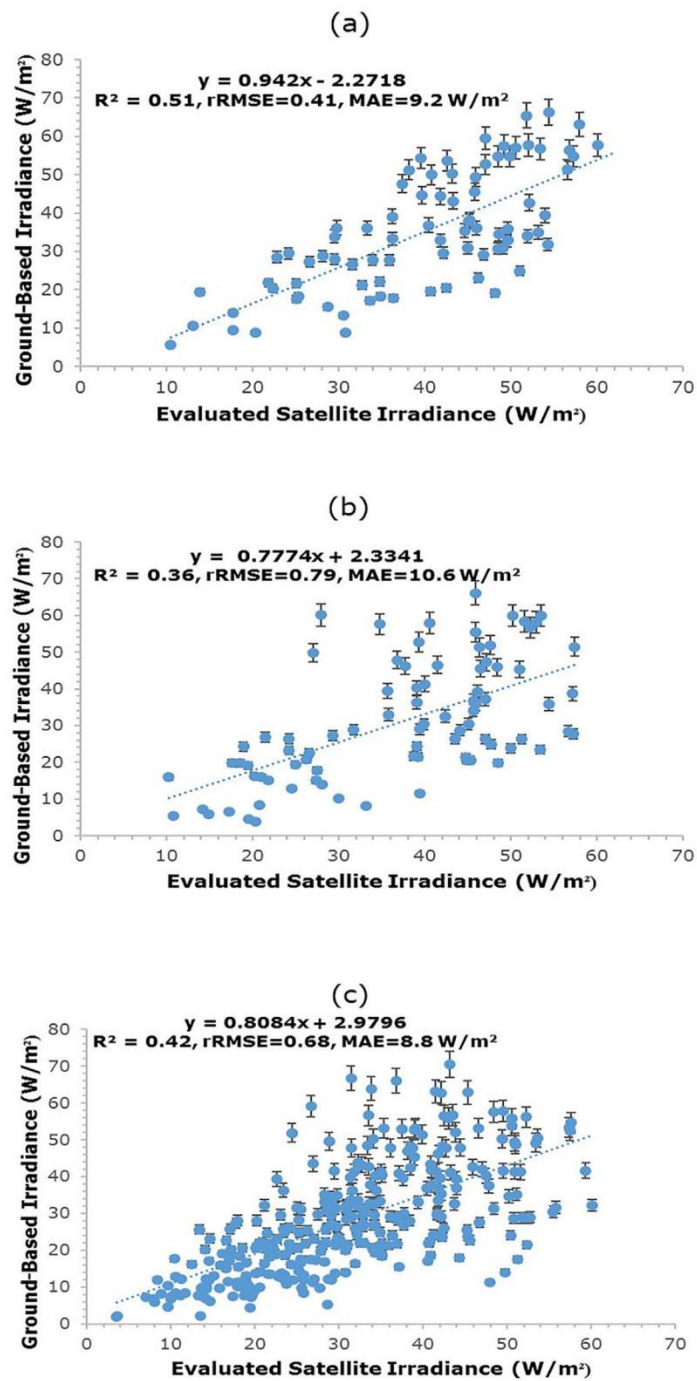


Figure 3. Comparison of the evaluated OMI satellite solar noon UVA irradiances with ground-based UVA data. The data are plotted for the three categories of the amount of cloud cover of (a) >2 to 4, (b) >4 to 6 and (c) >6 to 8 octa for sun obscured sky conditions. The error bars are the $\pm 10\%$ error associated with the ground-based data. The dashed line is the fitted trend line.

is 0.64, rRMSE is 16% and MAE is 4.8 (W m^{-2}). Fig. 2c and d for the cases of >4–6 octa and >6–8 octa show a poor correlation between the satellite and the ground-based measurements due to the (50–100% cloud coverage) with an R^2 of 0.31 and 0.4, an rRMSE of 53% and 25.5% and a MAE of 8.5 and 7.2 (W m^{-2}) respectively. Temporal differences between the cloud observation by satellite at about 1 pm and the actual cloud cover at solar noon for the ground-based measurements are likely to be a significant contributor to the poor correlation in these cloudy condition cases (30). In this case, the satellite over-prediction is greatest. A possible explanation could be due to differences in local cloud cover measured at noon and the sampled satellite data measured at a different time during satellite overpass time. This is evident as a trend to a lower gradient with increasing cloud cover at noon. Additionally, there are likely variations in the local site cloud cover and satellite samples measured over the pixel size of 40×80 km.

Sun obscured sky conditions

Figure 3 shows the data for sun obscured sky conditions in the three categories of cloud cover of >2–4, >4–6 and >6–8 octas. Figure 3a represents a comparison for >2–4 octa. For this range of sky coverage, there is a weaker correlation compared to that with the sun not obscured data with an R^2 of 0.51, an rRMSE of 41% and a MAE of 9.2 (W m^{-2}). Figures 3b (>4–6 octa) and 3c (>6–8 octa) show there is a similarity in the correlation of the comparisons for the sun obscured and sun not obscured sky conditions for the >4 octa cloud cases with a R^2 of 0.36 and 0.42, an rRMSE of 79% and 68% respectively and a MAE of 10.6 and 8.8 (W m^{-2}). For all three categories of sun obscured cloud conditions, the spread of the data about the fitted trend line increases with increasing solar noon irradiance. A possible explanation for this is due to the more noticeable relative amplification and attenuation by cloud with increasing irradiance. For cloud cover greater than 4 octa, the gradient of the graphs presented in Fig. 3b and c is closer to unity than the sun not obscured graphs of Fig. 2c and d. When the sun is obscured, the attenuating cloud reduces the typical overestimation of the satellite UVA.

CONCLUSION

The broadband UVA solar noon irradiances derived from the OMI satellite spectral UV irradiances at the three wavelengths 310 nm, 324 nm, and 380 nm have been provided for the long-term data series of over 12 years at a subtropical Southern Hemisphere site. This study has applied this model for the sky conditions of sun not obscured and sun obscured conditions. For sun not obscured sky conditions, four categories of the amount of cloud cover of 0–2, >2–4, >4–6 and >6–8 octa have been used to investigate the comparisons between remote estimates of the broadband surface UVA evaluated from the satellite UVA spectral irradiances and local ground-based measurements. These categories show an inverse relationship between the amount of cloud and the correlation for the satellite and ground-based data. In this case, the evaluated broadband UVA satellite irradiance model is likely to be less suitable for cloudy sky conditions of more than four octa. For sun obscured sky conditions, an increasing of the cloud amount led to poorer correlation of the satellite-derived UVA irradiance model than for sun not obscured

sky conditions. There was also an observed increase in the spread of the data with increasing UVA irradiance. Investigation on the effect of cloud on the satellite-derived UVA irradiances has shown that the model is valid for sun not obscured conditions with cloud of up to four octa (with an R^2 of 0.77, and an rRMSE of 18% for 0–2 octa and R^2 is 0.64 and rRMSE is 16% for >2–4 octa). At the subtropical site of this research, the satellite-derived UVA irradiances can be calibrated to surface measurements for most conditions, accounting for approximately 71% of the days in the 12-year study period.

Acknowledgements—The authors acknowledge the OMI mission scientists and associated NASA personnel for the production of the data used in this research effort.

REFERENCES

- Frederick, J. E., H. E. Snell and E. K. Haywood (1989) Solar ultraviolet radiation at the earth's surface. *Photochem. Photobiol.* **50**(4), 443–450.
- Hollósy, F. (2002) Effects of ultraviolet radiation on plant cells. *Micron* **33**(2), 179–197.
- Rass, K. and J. Reichrath (2008) UV damage and DNA repair in malignant melanoma and nonmelanoma skin cancer. In *Sunlight, Vitamin D and Skin Cancer* (Edited by J. Reichrath), pp. 162–178. Springer, New York.
- Grant, W. B. (2007) Roles of solar UV radiation and vitamin D in human health and how to obtain vitamin D. *Expert Rev. Dermatol.* **2** (5), 563–577.
- Häder, D. P., H. D. Kumar, R. C. Smith and R. C. Worrest (2007) Effects of solar UV radiation on aquatic ecosystems and interactions with climate change. *Photochem. Photobiol. Sci.* **6**(3), 267–285.
- Caldwell, M. M., L. O. Björn, J. F. Bornman, S. D. Flint, G. Kulandaivelu, A. H. Teramura and M. Tevini (1998) Effects of increased solar ultraviolet radiation on terrestrial ecosystems. *J. Photochem. Photobiol., B* **46**(1), 40–52.
- Calbó, J. and J. A. González (2005) Empirical studies of cloud effects on UV radiation: A review. *Rev. Geophys.* **43**(2). <https://doi.org/10.1029/2004RG000155>
- Andrady, A. L., S. H. Hamid, X. Hu and A. Torikai (1998) Effects of increased solar ultraviolet radiation on materials. *J. Photochem. Photobiol., B* **46**(1), 96–103.
- Parisi, A. V., N. Downs, J. Turner and R. King (2017) Comparison of GOME-2 UVA satellite data to ground-based spectroradiometer measurements at a subtropical site. *IEEE Trans. Geosci. Remote Sens.* **55**(6), 3145–3149.
- Kazantzidis, A., A. F. Bais, J. Gröbner, J. R. Herman, S. Kazadzis, N. Krotkov, E. Kyrö, P. N. Den Outer, K. Garane, P. Görts and K. Lakkala (2006) Comparison of satellite-derived UV irradiances with ground-based measurements at four European stations. *J. Geophys. Res.: Atmospheres* **111**(D13). <https://doi.org/10.1029/2005JD006672>
- Giovanni Website (2018). Giovanni Parameters Definitions, viewed May 2018. https://disc.gsfc.nasa.gov/information/glossary/58ac98c7cac5244b115f80e7/giovanni-parameter-definitions#MOD08_M3_6_Cloud_Optical_Thickness_Liquid_Mean_Mean
- Blanchard, Y., A. Royer, N. O'Neill, D. D. Turner and E. W. Eloranta (2017) Thin ice clouds in the Arctic: Cloud optical depth and particle size retrieved from ground-based thermal infrared radiometry. *Atmospheric Measurement Techniques* **10**(6), 2129.
- Antón, M., D. Loyola, C. Clerbaux, M. López, J. M. Vilaplana, M. Banón, J. Hadji-Lazarou, P. Valks, N. Hao, W. Zimmer and P. F. Coheur (2011) Validation of the Metop-A total ozone data from GOME-2 and IASI using reference ground-based measurements at the Iberian Peninsula. *Remote Sens. Environ.* **115**(6), 1380–1386.
- Cachorro, V. E., C. Toledano, M. Antón, A. Berjón, A. D. Frutos, J. M. Vilaplana, A. Arola and N. A. Krotkov (2010) Comparison of UV irradiances from Aura/Ozone Monitoring Instrument (OMI) with Brewer measurements at El Arenosillo (Spain)—Part 2: Analysis of site aerosol influence. *Atmos. Chem. Phys.* **10**(23), 11867–11880.

15. Kazadzis, S., A. Bais, A. Arola, N. Krotkov, N. Kouremeti and C. Meleti (2009) Ozone Monitoring Instrument spectral UV irradiance products: Comparison with ground based measurements at an urban environment. *Atmos. Chem. Phys.* **9**(2), 585–594.
16. Kerr, J. B. (2005) Understanding the factors that affect surface ultraviolet radiation. *Opt. Eng.* **44**(4), 041002.
17. McKenzie, R. L., G. Seckmeyer, A. F. Bais, J. B. Kerr and S. Madronich (2001) Satellite retrievals of erythemal UV dose compared with ground-based measurements at northern and southern. *J. Geophys. Res.* **106**(D20), 24–051.
18. Antón, M. and D. Loyola (2011) Influence of cloud properties on satellite total ozone observations. *J. Geophys. Res.: Atmospheres* **116** (D3208).
19. Kazantzidis, A., K. Eleftheratos and C. S. Zerefos (2011) Effects of cirrus cloudiness on solar irradiance in four spectral bands. *Atmos. Res.* **102**(4), 452–459.
20. Herman, J., M. T. DeLand, L. K. Huang, G. Labow, D. Larko, S. A. Lloyd, J. Mao, W. Qin and C. Weaver (2013) A net decrease in the Earth's cloud, aerosol, and surface 340 nm reflectivity during the past 33 yr (1979–2011). *Atmos. Chem. Phys.* **13**(16), 8505–8524.
21. Simic, S., M. Fitzka, A. Schmalwieser, P. Weihs and J. Hadz-
imustafic (2011) Factors affecting UV irradiance at selected wave-
lengths at Hoher Sonnblick. *Atmos. Res.* **101**(4), 869–878.
22. Bais, A. F., R. L. McKenzie, G. Bernhard, P. J. Aucamp, M. Ilyas,
S. Madronich and K. Tourpali (2015) Ozone depletion and climate
change: Impacts on UV radiation. *Photochem. Photobiol. Sci.* **14**(1),
19–52.
23. Udelhofen, P. M., P. Gies, C. Roy and W. J. Randel (1999) Surface
UV radiation over Australia, 1979–1992: Effects of ozone and cloud
cover changes on variations of UV radiation. *J. Geophys. Res.:
Atmospheres* **104**(D16), 19135–19159.
24. A Jebar, M.A., A.V. Parisi, N.J. Downs and J. Turner (2017) Validation of OMI UV satellite data using spectral and broadband surface based measurements at a Queensland site. *Photochem. Photobiol.*, **93** (5), 1289–1293.
25. Parisi, A. V. and N. Downs (2004) Cloud cover and horizontal plane eye damaging solar UV exposures. *Int. J. Biometeorol.* **49**(2), 130–136.
26. Kassianov, E., C. N. Long and M. Ovtchinnikov (2005) Cloud sky cover versus cloud fraction: Whole-sky simulations and observations. *J. Appl. Meteorol.* **44**(1), 86–98.
27. Sabburg, J. M. and C. N. Long (2004) Improved sky imaging for studies of enhanced UV irradiance. *Atmos. Chem. Phys.* **4**(11/12), 2543–2552.
28. Downs, N., H. Butler and A. V. Parisi (2016) Solar ultraviolet attenuation during the Australian (Red Dawn) dust event of 23 September 2009. *Bull. Am. Meteorol. Soc.* **98**, 2039–2050.
29. Long, C. N. and T. P. Ackerman (2000) Identification of clear skies from broadband pyranometer measurements and calculation of downwelling shortwave cloud effects. *J. Geophys. Res.: Atmospheres* **105**, 15609–15626.
30. Tanskanen, A., A. Lindfors, A. Määttä, N. Krotkov, J. Herman, J. Kaurola, T. Koskela, K. Lakkala, V. Fioletov, G. Bernhard and R. McKenzie (2007) Validation of daily erythemal doses from Ozone Monitoring Instrument with ground-based UV measurement data. *J. Geophys. Res.: Atmospheres* **112**(D24). <https://doi.org/10.1029/2007JD008830>

**Influence of Cloud on OMI Satellite Total Daily UVA Exposures over a 12-year Period
at a Southern Hemisphere Site**

A Jebar, Mustapha A.,¹ Parisi, Alfio V.,^{1,*} Downs, Nathan J.¹ and Turner, Joanna¹

¹Faculty of Health, Engineering and Sciences, University of Southern Queensland,
Toowoomba, Queensland

*Corresponding author: Email: parisi@usq.edu.au

Word count: 4,722

ABSTRACT

This research investigated and evaluated the influence of cloud on the total daily UVA (320-400 nm) exposures calculated from the three OMI UV spectral irradiances at solar noon. These evaluated satellite total daily UVA exposure data were compared to the total daily UVA exposures of a ground-based instrument over the period of October 2004 to December 2014 at a sub-tropical Australian site (27.5°S, 151.9°E) under all cloud cover conditions including sun obscured and not obscured sunshine states. The method was employed to evaluate the influence of cloud on the total daily UVA. When the sun was not obscured by cloud, there was good agreement between satellite and ground-based daily UVA exposure measurements with R^2 between 0.8 and 0.84 for the cloud conditions 0 to 2, > 2 to 4, > 4 to 6 and > 6 to 8 okta. For sun obscured by cloud, the R^2 was 0.71, 0.64 and 0.75 respectively for > 2 to 4, > 4 to 6 and > 6 to 8 okta. The method was validated using total daily UVA exposures from ground measurements taken in 2015 and 2016 giving a mean absolute error of 84.2 kJ/m² (10%) and 138.8 kJ/m² (30%) respectively for the cases of sun not obscured cloudy days and sun obscured by cloud cover. Total daily UVA exposures were able to be calculated from the OMI satellite spectral irradiance for all cloud conditions, including cases where the sun was obscured, demonstrating the potential of the technique to be applied in locations that do not record surface UVA measurements directly.

INTRODUCTION

Scientifically and socially, high levels of exposure to UV radiation in both the UVA (320 – 400 nm) and the UVB (280 – 320 nm) are of significant interest. Exposure to UV radiation is an important factor in the damage done to several biological systems on the earth (Hollosy, 2002; Caldwell 1998). Solar UVB radiation has significant effects on human health such as skin, eye and eyelid diseases (Armstrong et al., 2001). Although UVA radiation has a longer wavelength (less energy) in comparison to UVB radiation, it can penetrate deeper into biological systems, including human skin tissue, potentially contributing to biological damage at a greater depth (Lavker et al., 1995).

Historically, it is difficult to achieve accurate and widespread spectral UV and broadband UV measurements using ground-based instruments (Kalliskota 2000). These difficulties are a result of UV radiation being subjected to a series of absorption and scattering processes because of aerosols, clouds and ozone during its path through the atmosphere to the receiving object, making the UV distribution complex. Furthermore, there are real difficulties in maintaining the instruments in accordance with long-term stability and calibration standards (Sharma et al., 2011; Kerr, 2002). Prior to discovery of the Ozone hole (late 1980s); accurate measurement of UV radiation was not available (McKenzie et al., 2011). By the mid-1990s, there was a noticeable development in the accuracy of UV radiation measurements, especially with spectroradiometers and radiometers (Bais, 2015). These instruments are located at a limited number of sites globally, therefore there is a need for satellite-based instrumentation to provide coverage in sites not covered by surface instrumentation (Paulescu 2012).

There have been a number of comparative studies between ground-based and satellite based UV irradiance measurements. Kerr et al, (2002) conducted a validation of UV Brewer instruments, located in some areas of Canada to UV data from TOMS (Total Ozone Mapping

Spectrometer). This comparison showed a correspondence between the two sets of results with differences ranging from 3-11%. There are many expected factors that could change the results of such comparisons, including differences between surface and satellite instrumentation in solar zenith angle (SZA), clouds, calibration errors, and aerosols. McKenzie et al, (2001) have addressed the variation of UV exposure data between satellite and ground-based measurements in the Southern and Northern Hemisphere. This study found that the data of ground-based instruments were less than the satellite data in most of the study areas while in some unpolluted areas there was a good agreement between the satellite and ground-based measurements. Arola et al, (2002) have assessed the UV measurements of GOME (Global Ozone Monitoring Experiment) satellite and Brewer ground-based instruments. The results showed significant differences between the values of UV daily exposure of satellite and ground-based data. The differences could reach up to 30-60%. Deviation of the results have been attributed to many factors such as snow and spatial effects. The study of Arola et al (2002) found that there is still a requirement for regular comparisons of satellites to ground-based instruments, as the uncertainties in satellite-based instrumentation can be significantly reduced by careful calibration to surface measurements.

In the UVA waveband, the GOME-2 satellite data provides the UVA daily maximum irradiance and the total daily UVA exposure. A comparison has been provided between this data and that from a ground-based spectroradiometer at a Southern Hemisphere site (Parisi et al., 2017). However, the earlier launched OMI (Ozone Monitoring Instrument) does not provide the total daily UVA exposure integral and it is important to have information on UV exposures, as the risk of some sun related disorders is related to cumulative exposure. Solar UV radiation is subject to many factors, which determine and influence the irradiance that reaches the earth's surface (Madronich et al. 1998). Surface solar radiation is particularly

sensitive to cloud (An and Wang 2015) which can be measured by both ground-based and satellite based instruments (Fontana et al., 2013).

Previous research has addressed the influence of cloud to make comparisons between ground-based and OMI satellite based solar noon UVA irradiance for different amounts of cloud cover at a Southern Hemisphere site (A Jebar et al., 2018). No previous research has considered the influence of cloud on the total daily UVA exposures evaluated from OMI satellite spectral irradiance data. The research in this paper reports on the influence of cloud on the OMI satellite total daily UVA exposures evaluated from the OMI solar noon spectral irradiances for a Southern Hemisphere sub-tropical site.

Materials and Methods

Measurement site

This research is located at the Southern Hemisphere sub-tropical site of Toowoomba (27°36' S 151°55' E), Australia. Toowoomba is a rural site and inland city, which is located about 120 km west of Brisbane (Queensland's capital city) and 691 m above sea level with a population of approximately 135,000. It has a relatively unpolluted atmosphere with low aerosols. The instruments used in this study are a UVA Biometer (model 501A, Solar Light Inc, PA, USA) and a Total Sky Imager (TSI) (model TSI 440, Yankee Environmental Systems, PA, USA) which are installed on an unshaded roof top site at the University of Southern Queensland in Toowoomba.

Total daily UVA

The OMI satellite total daily UVA exposures (UVA_{Day}) have been calculated from the daily solar noon broadband UVA irradiance evaluated from the three OMI spectral irradiance measurements at 310 nm, 324 nm and 380 nm (A Jebar et al., 2017) with the following equation:

$$UVA_{Day}[kJm^{-2}] = \frac{E_{UVA} \times 3600 \times H \times F}{1000}. \quad (1)$$

where the daily UVA integral expressed in kJ/m^2 is modeled as the fraction (F) of maximum daily broadband UVA irradiance determined from the OMI satellite (E_{UVA} [$W m^{-2}$]), the constant 3600 is the number of seconds in an hour and H is the number of hours (expressed as a decimal) from sunrise to sunset. F represents the normalized fraction of the day occupied by a bell-shaped UVA cloud-free distribution rising at sunrise, peaking at solar noon and falling at sunset. Ground-based UVA exposures were recorded from the UVA Biometer measuring the UVA exposures in J/cm^2 for every five minutes of the day. These total daily UVA exposures have been evaluated for all sky conditions over 1 October 2004 to 31 December 2014. These data were further categorised into the cases of the solar disc not obscured by cloud and the solar disc obscured by cloud and for each of these two cases, the data were separated into the four cloud categories of 0 to 2, > 2 to 4, > 4 to 6 and > 6 to 8 okta based on available sky image data recorded by the ground based Total Sky Imager (TSI).

The OMI satellite total daily UVA exposures for the ten-year period were derived with the model in equation (1) from the solar noon UVA irradiances calculated from the OMI spectral irradiances at 310, 324 and 380 nm for the different cloud categories, then compared to the ground based total daily UVA exposures measured with the calibrated UVA Biometer at the measurement site. The UVA Biometer provides the five-minute exposures in units of J/cm^2 and these were summed over the day to provide the total daily UVA exposures in kJ/m^2 .

Validation

The technique for the satellite daily UVA exposure estimates developed using remotely sensed data to December 2014 was also applied to remotely sensed data collected in 2015 and 2016 using the respective relationships between the ground-based and satellite total daily UVA exposure for each cloud category. This was compared to integrated surface measurements to

test the validity of the method. For this purpose, surface measurement data from the broadband UVA meter and remote sensed satellite data from 2015 and 2016 was categorized into the cases of days with the solar disc not obscured and the solar disc obscured.

RESULTS

All sky conditions

Figure 1 shows the time series of the satellite total daily UVA exposures evaluated from the three OMI solar noon spectral irradiances for the study site from October 2004 to the end of 2016 for all sky conditions. This includes the 10 year data set and 2 year validation set. This figure has 3,511 daily UVA exposures based on when there was OMI satellite data available. The pattern of peaks and troughs in the exposures due to the seasons is shown in this figure, with a variation between approximately 840 kJ/m² and 1600 kJ/m². Superimposed on the seasonal pattern is the influence due to cloud. The time series is then sub-divided according to cloud cover categories as box and whiskers plots in Figure 2. Figure 2(a) shows the total daily satellite UVA exposure at all sky conditions. Figure 2(b) represents total daily satellite UVA exposure of the time series for the four cloud amount categories (0-2, > 2-4, > 4-6 and > 6-8 okta) for sun not obscured sky conditions. Figure 2(c) represents total daily satellite UVA exposure at the three cloud amount categories (> 2-4, > 4-6, and > 6-8 okta) for sun obscured sky conditions.

<insert Figure 1>

<insert Figure 2>

Figure 3 presents the total daily satellite UVA dataset as box and whisker plots for each of the years (from 2004 to 2016). For each year, the horizontal line is the median for each year, the box represents the 1st and 3rd quartile and the dashed line represents the range of the satellite

data. Except for 2004 where there are only three months of satellite based data available (to compare to the ground-based data), the distribution of the annual medians of the total daily UVA exposures appears consistent. In this figure, 2010 has a lower median, and 1st and 3rd quartiles due to the above average annual rainfall of 1161 mm compared to the average annual Toowoomba rainfall of 679.75 mm, resulting in higher amounts of cloud.

<insert Figure 3>

Cloud and fractions of maximum daily exposure data

Table 1 shows the number of days in the different cloud categories for the cases of solar disc obscured and solar disc not obscured. The number of days in each category represent the days when there was available sky camera data at solar noon. This table presents the average over the ten years of the fraction, F of maximum daily exposure used in equation (1) for all categories.

<insert Table 1>

Sun not obscured sky conditions

The total daily UVA satellite exposures calculated from the satellite solar noon UVA irradiances for the cases of when the sun was not obscured by cloud have been compared with total daily ground-based UVA exposure at the measurement site over the period of 1 October 2004 to the end of December 2014 (Figure 4). The comparisons between the two data sets for the sun not obscured sky conditions are shown in Figure 4 for the cloudy days for the four cloud cover categories of 0 to 2, > 2 to 4, > 4 to 6 and > 6 to 8 okta. The dashed lines are the regression lines fitted to the data and the error bars represent the $\pm 10\%$ uncertainty associated with the measured ground-based data.

<insert Figure 4>

Sun obscured sky conditions

Figure 5 shows the comparison of the satellite total daily UVA exposure evaluated from the OMI spectral irradiances and the ground-based total daily UVA exposure for sun obscured sky conditions. These are separated into the three cloud cover categories of > 2 to 4, > 4 to 6 and > 6 to 8 okta with the dashed line in each figure representing the fitted regression line.

<insert Figure 5>

Model Validation

The model was developed using the OMI satellite based solar noon UVA irradiances data set from 2004 to 2014. The dataset from 2015 to 2016 was used to test the developed model. Figure 6 shows the comparison of the satellite total daily UVA exposure and the ground-based total daily UVA exposure for sun not obscured and for sun obscured sky conditions for the 2015 and 2016 data set.

<insert Figure 6>

DISCUSSION

The median of the total daily satellite UVA exposure is reduced from about 1100 kJ/m² to less than 600 (54.5%) kJ/m² with the amount of cloud (Figure 2(a)). Figures 2(b) and Figure 2(c), show, as expected, that the increase of the amount of cloud reduces the total daily satellite UVA exposure. In figures 2(b), the median for > 4 to 6 okta is higher than that for > 2 to 4 okta possibly due to the sample set, but in general the trend is decreasing UVA exposure with

increasing cloud cover which is as expected. Additionally, the medians are generally lower for the sun obscured cases compared to the sun not obscured cases.

According to the table 1, there is an inverse relationship between the fraction of the maximum daily exposure and the amount of cloud cover. In addition, the values of the fraction of maximum daily exposure for the sun not obscured sky conditions are bigger than the values of the fraction of maximum daily exposure for the sun obscured sky conditions. For the sun not obscured cases when the amount of cloud was 0-2 and > 2 to 4 okta as shown in Figure 4 (a) and (b), there is a reasonable correlation between the total daily UVA satellite exposures evaluated from the OMI spectral irradiance measurements at solar noon and total daily ground-based UVA exposures with an R^2 of 0.81 and 0.84, relative root mean square error (rRMSE) of 0.13 and 0.10, mean absolute error (MAE) of 97.3 and 75.2 kJ/m^2 respectively. For the cloudy days of more than 4 okta, Figure 4 (c) shows a good agreement between the satellite and ground based total daily UVA exposure with R^2 of 0.80, rRMSE of 0.17 and MAE of 98.7 kJ/m^2 when the amount of cloud was > 4 to 6 okta. The use of the respective values of F for each category of cloud cover is likely contributing to this agreement. Similarly, for the days with > 6 to 8 okta, Figure 4 (d) shows a reasonable correlation between the satellite and ground based total daily UVA exposures with R^2 of 0.84, rRMSE of 0.10 and MAE of 87.8 kJ/m^2 .

For the sun obscured cases in figure 5 (a), there is a good correlation between the satellite and ground based total daily UVA exposure with an R^2 of 0.71, rRMSE of 0.36 and MAE of 124.9 kJ/m^2 . This figure shows a smaller R^2 compared to the sun not obscured cases due to the influence of cloud over the sun. In Figure 5 (b), even though, the cloud cover is > 4 to 6 okta, the correlation is still reasonable with R^2 of 0.64, an rRMSE of 0.36 and MAE of 124.9 kJ/m^2 . For the categories of > 6 to 8 okta cloud coverage shown by Figure 5 (c), the correlation is slightly weaker compared with the sun not obscured cases with the same cloud coverage with

an R^2 of 0.75, an rRMSE of 0.29 and MAE of 133.3 kJ/m². The larger rRMSE for the three cases of cloud cover > 2 to 4, > 4 to 6 and > 6 to 8 okta is expected as the cloud conditions used to determine the cloud categories are at solar noon and this amount of cloud cover, whether the sun is obscured or not obscured, is often variable during the day.

In figure 6 (a), the validation comparison has a good correlation with a MAE of 84.2 kJ/m² (10%) for the sun not obscured cases. Figure 6 (b) shows the validation of the sun obscured cloudy days which has a reasonable agreement with a MAE of 138.4 kJ/m² (30%). This larger MAE compared to the sun not obscured cases is due to the variability of the sun obscured cloud influence on the solar UVA.

CONCLUSION

This research has employed a technique to calculate the total daily UVA exposures from the broadband UVA irradiances derived from the three OMI satellite spectral irradiances at solar noon to provide a comparison between total daily UVA satellite exposure data and total daily UVA ground-based exposure data over a 10 year time period. This has enabled the influence of cloud on the total daily UVA satellite exposures to be considered. This has been for all cloud conditions for different cloud cover for the solar disc not obscured and solar disc obscured cases. For the sun not obscured sky conditions, the cloud cover categories of 0 to 2, > 2 to 4, > 4 to 6 and > 6 to 8 okta have been considered. In addition, for the case of the solar disc obscured sky conditions, the cloud categories of > 2 to 4, > 4 to 6 and > 6 to 8 okta have been considered. For all four cloud cover categories of sun not obscured cloud coverage, there is a good correlation in the development of the model between the total daily UVA satellite exposure data and the total daily UVA ground-based exposure data, with R^2 values of better than 0.8 and rRMSE values of 0.17 or less. The > 2 to 4 okta cases with the sun obscured days for the model development provided an R^2 value of 0.71 and rRMSE value of 0.36, with R^2

values of 0.64 and 0.75 for the cases of > 4 to 6 and > 6 to 8 okta cloud. The model validation provided a MAE of 84.2 kJ/m² (10%) and 138.8 kJ/m² (30%) respectively for the cases of sun not obscured and sun obscured sky conditions. At the Southern Hemisphere site of this research, the total daily UVA exposures can be calculated from the OMI satellite spectral irradiance for sun not obscured cloudy days and sun obscured cloudy days, with further research required to compare the OMI satellite derived total daily UVA exposures to ground based data at other sites.

Acknowledgements – The authors acknowledge the OMI mission scientists and associated NASA personnel for the production of the data used in this research effort.

Disclosure Statement – There is no benefit to the authors that will arise from the direct applications of this research.

REFERENCES

A Jebar, M.A., A.V. Parisi, N.J. Downs, and J.F. Turner. 2017. "Validation of OMI UV satellite data using spectral and broadband surface based measurements at a Queensland site." *Photochemistry and Photobiology* 93(5): 1289-1293. doi: 10.1111/php.12784.

A Jebar, M.A., A.V. Parisi, N.J. Downs, and J.F. Turner. 2018. "Evaluated UVA irradiances over a twelve year period at a sub-tropical site from Ozone Monitoring Instrument data including the influence of cloud." *Photochemistry and Photobiology*. doi: [10.1111/php.12948](https://doi.org/10.1111/php.12948).

An, N., and K. Wang. 2015. "A comparison of MODIS-derived cloud fraction with surface observations at five SURFRAD sites." *Journal of Applied Meteorology and Climatology* 54(5): 1009-1020. doi: 10.1175/JAMC-D-14-0206.1.

Armstrong, B.K., and A. Krickler. 2001. "The epidemiology of UV induced skin cancer." *Journal of Photochemistry and Photobiology B: Biology* 63(1-3): 8-18. [doi.org/10.1016/S1011-1344\(01\)00198-1](https://doi.org/10.1016/S1011-1344(01)00198-1).

Arola, A., S. Kalliskota, P.N. Den Outer, K. Edvardsen, G. Hansen, T. Koskela, T.J. Martin, J. Matthijsen, R. Meerkotter, P. Peeters, and G. Seckmeyer. 2002. "Assessment of four methods to estimate surface UV radiation using satellite data, by comparison with ground measurements from four stations in Europe." *Journal of Geophysical Research: Atmospheres* 107 (D16): ACL-11. doi.org/10.1029/2001JD000462.

Bais, A.F., R.L. McKenzie, G. Bernhard, P.J. Aucamp, M. Ilyas, S. Madronich, and K. Tourpali. 2015. "Ozone depletion and climate change: Impacts on UV

radiation.” *Photochemical & Photobiological Sciences* 14 (1): 19-52. doi: 10.1039/c4pp90032d

Caldwell, M., L. Bjorn, J. Bornman, S. Flint, G. Kulandaivelu, A. Teramura, and M. Tevini. 1998. “Effects of increased solar ultraviolet radiation on terrestrial ecosystems.” *Journal of Photochemistry and Photobiology B: Biology* 46: 40-52. [doi.org/10.1016/S1011-1344\(98\)00184-5](https://doi.org/10.1016/S1011-1344(98)00184-5).

Frey, R.A., S.A. Ackerman, Y. Liu, K.I. Strabala, H. Zhang, J.R. Key, and X. Wang. 2008. “Cloud detection with MODIS. Part I: Improvements in the MODIS cloud mask for collection 5.” *Journal of Atmospheric and Oceanic Technology* 25(7): 1057-1072. doi: 10.1175/2008JTECHA1052.1.

Fontana, F., D. Lugrin, G. Seiz, M. Meier, and N. Foppa. 2013. “Intercomparison of satellite- and ground-based cloud fraction over Switzerland (2000–2012).” *Atmospheric research* 128: 1-12. doi.org/10.1016/j.atmosres.2013.01.013.

Hollósy, F. 2002. “Effects of ultraviolet radiation on plant cells”. *Micron* 33(2): 179-197. [doi.org/10.1016/S0968-4328\(01\)00011-7](https://doi.org/10.1016/S0968-4328(01)00011-7).

Kalliskota, S., J. Kaurola, P. Taalas, J.R. Herman, E.A. Celarier, and N.A. Krotkov. 2000. “Comparison of daily UV doses estimated from Nimbus 7/TOMS measurements and ground-based spectroradiometric data.” *Journal of Geophysical Research: Atmospheres* 105(D4): 5059-5067. doi.org/10.1029/1999JD900926.

Kerr, J.B., G. Seckmeyer, A. Bais, M. Blumthaler, S.B. Diaz, N. Krotkov, D. Lubin, S. Madronich, R.L. McKenzie, A.A. Sabzipavar, and J. Verdebout. 2003. Surface ultraviolet radiation: past and future, Chapter 5 in: *Scientific Assessment of Ozone Depletion: 2002 Global Ozone Research and Monitoring Project*. World Meteorological Organization, Geneva, Switzerland.

Lavker, R.M., G.F. Gerberick, D. Veres, C.J. Irwin, and K.H. Kaidbey. 1995. "Cumulative effects from repeated exposures to suberythemal doses of UVB and UVA in human skin." *Journal of the American Academy of Dermatology* 32(1): 53-62. [doi.org/10.1016/0190-9622\(95\)90184-1](https://doi.org/10.1016/0190-9622(95)90184-1).

Madronich, S., R.L. McKenzie, L.O. Björn, and M.M. Caldwell. 1998. "Changes in biologically active ultraviolet radiation reaching the Earth's surface." *Journal of Photochemistry and Photobiology B: Biology* 46(1-3): 5-19. [doi.org/10.1016/S1011-1344\(98\)00182-1](https://doi.org/10.1016/S1011-1344(98)00182-1).

McKenzie, R.L., G. Seckmeyer, A.F. Bais, J.B. Kerr, and S. Madronich. 2001. "Satellite retrievals of erythemal UV dose compared with ground-based measurements at northern and southern midlatitudes." *Journal of Geophysical Research* 106(D20): 24-051. doi.org/10.1029/2001JD000545.

Parisi, A.V., N.J. Downs, and J.F. Turner, and R. King. 2017. "Comparison of GOME-2 UVA satellite data to ground-based spectroradiometer measurements at a subtropical site." *IEEE Transactions on Geoscience and Remote Sensing* 55(6): 3145-3149. doi: 10.1109/TGRS.2017.2662714.

Paulescu, M., E. Paulescu, P. Gravila, and V. Badescu. 2012. *Weather modeling and forecasting of PV systems operation*. Springer Science & Business Media.

Sharma, N.P., B.K. Bhattarai, B. Sapkota, and B. Kjeldstad. 2011. "Comparison of ground based measurements of solar UV index with satellite estimation at four sites of Nepal." *Journal of the Institute of Engineering*, 8(3): 58-71. doi.org/10.3126/jie.v8i3.5932.

Table 1. Number of days in each category of cloud cover between zero and eight okta and the average over ten years of the fraction (F) of the maximum daily exposure for all categories.

Categories of the cloud amount (okta) for sun not obscured sky conditions	Number of days	Fractions of maximum daily exposure (F)	Categories of the cloud amount (okta) for sun obscured sky conditions	Number of days	Fractions of maximum daily exposure (F)
0-2	712	0.50			
>2-4	38	0.45	>2-4	62	0.41
>4-6	29	0.42	>4-6	64	0.39
>6-8	19	0.42	>6-8	299	0.37

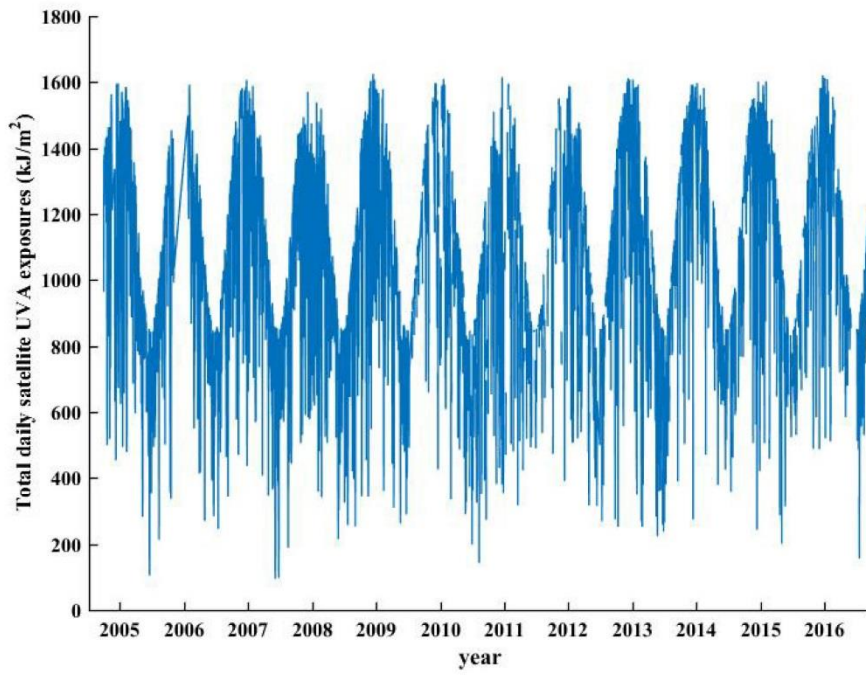
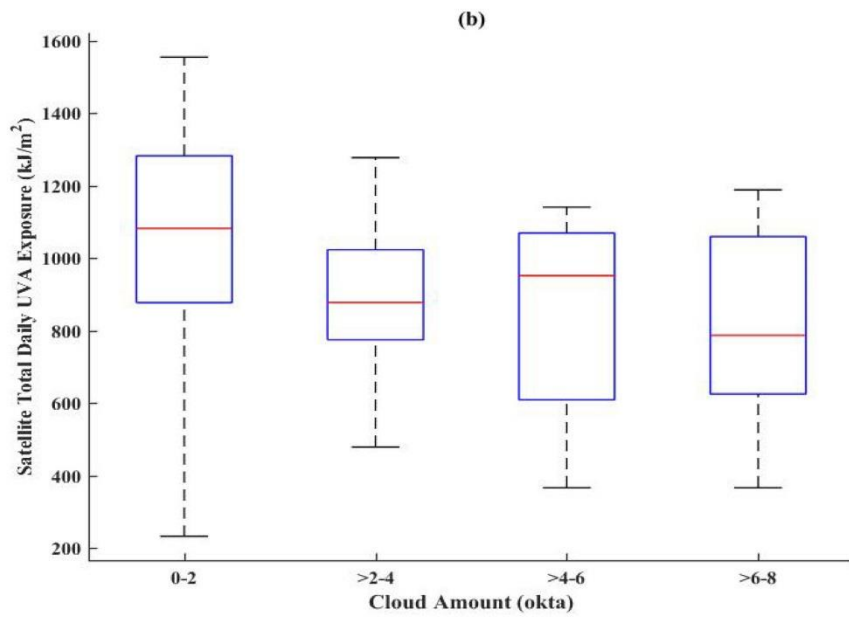
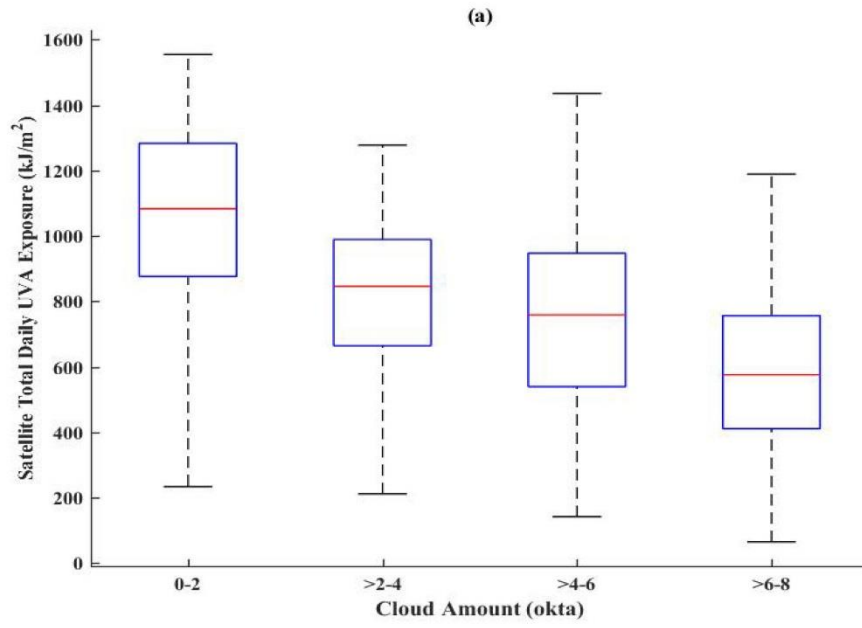


Figure 1: Time series of satellite total daily UVA exposures evaluated from the OMI solar noon spectral irradiances.



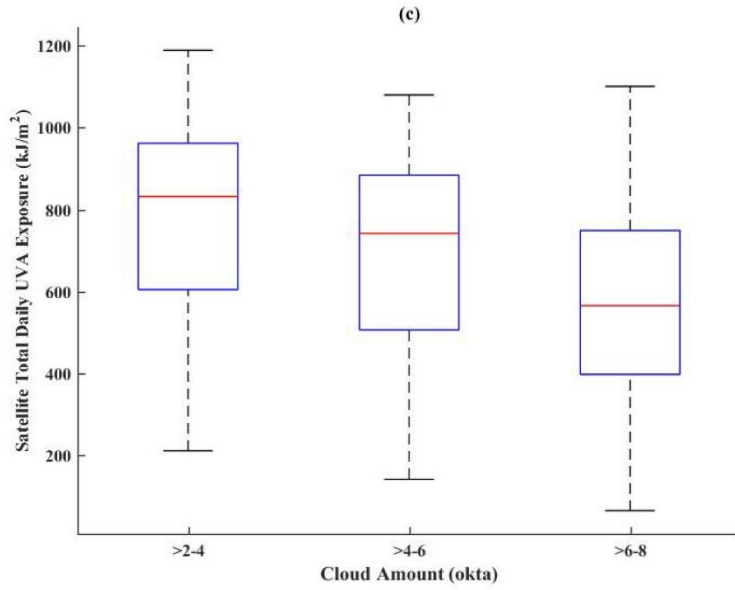


Figure 2: (a) The total daily satellite UVA exposure for all sky conditions. (b) The total daily satellite UVA exposure at the four cloud amount categories (0-2, > 2-4, > 4-6 and > 6-8 okta) for sun not obscured sky conditions. (c) Total daily satellite UVA exposure at the three cloud amount categories (> 2-4, > 4-6, and > 6-8 okta) for sun obscured sky conditions. The horizontal line in each box and whisker is the median, the box is the Q1 and Q3 range and the dashed vertical line is the range of values.

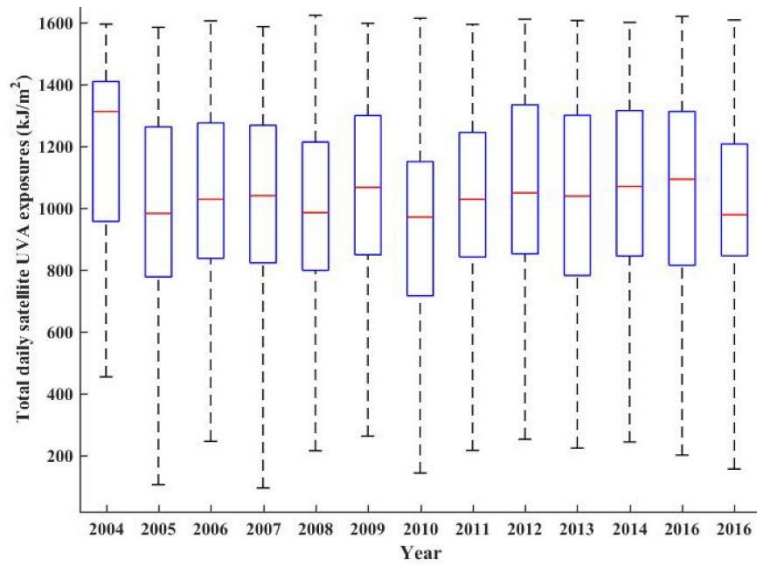
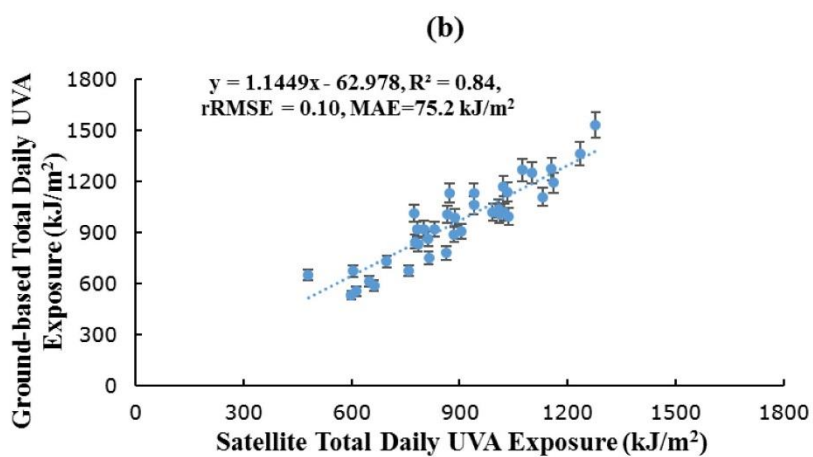
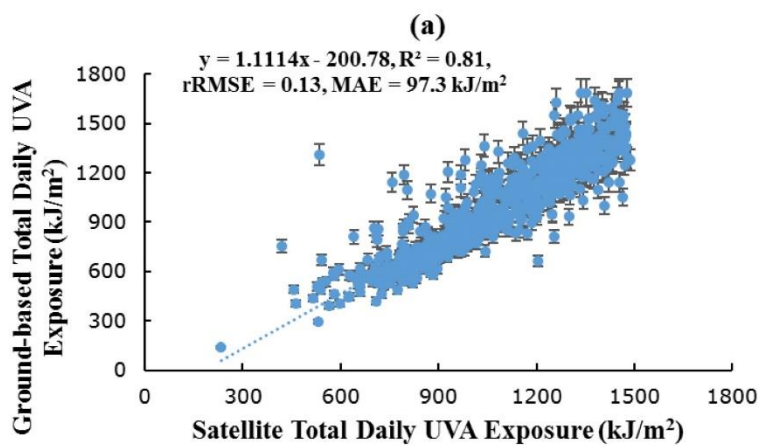


Figure 3: Box and whisker plots for each year of satellite total daily UVA exposures data October 2004 to December 2016.



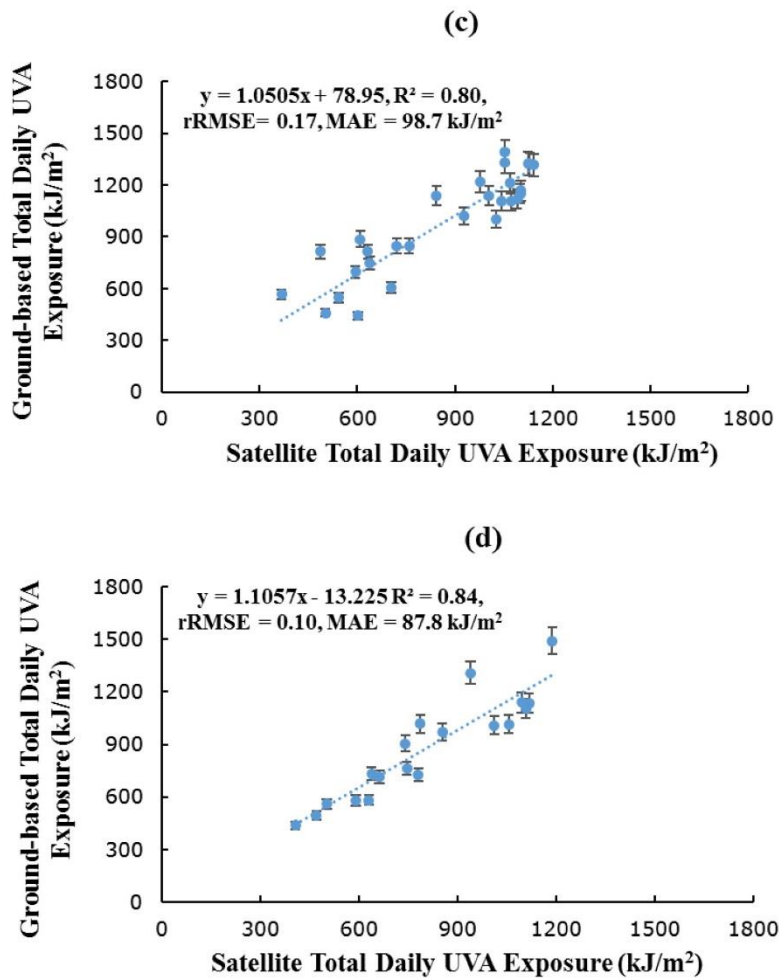


Figure 4: Comparison of the 2004 to 2014 satellite total daily UVA exposure evaluated from the OMI spectral irradiances at solar noon with the ground-based total daily UVA exposure for the four categories of cloud cover of (a) 0 to 2, (b) > 2 to 4, (c) > 4 to 6 and (d) > 6 to 8 okta for solar disc non-obscured sky conditions. The dashed lines are the regression lines fitted to the data and the error bars correspond to the $\pm 10\%$ error associated with the ground-based data.

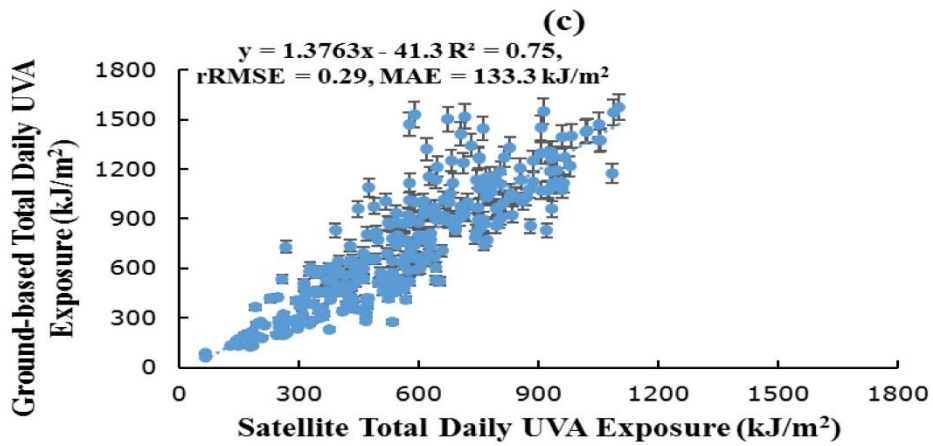
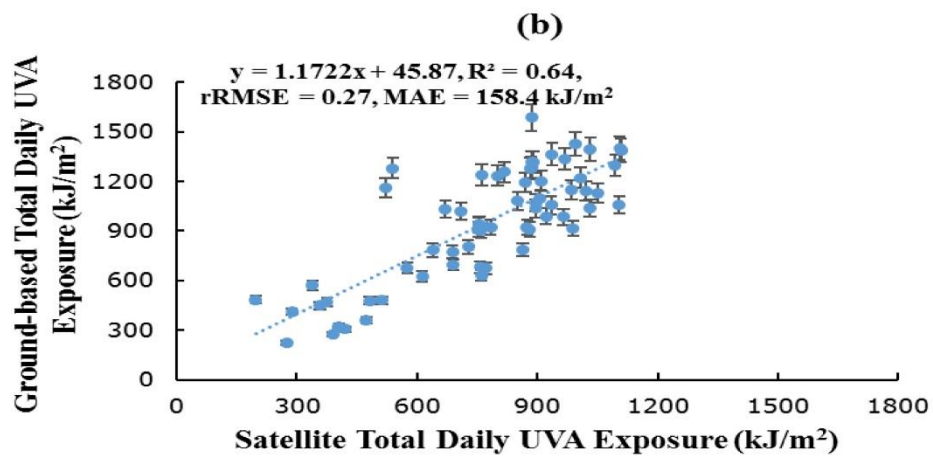
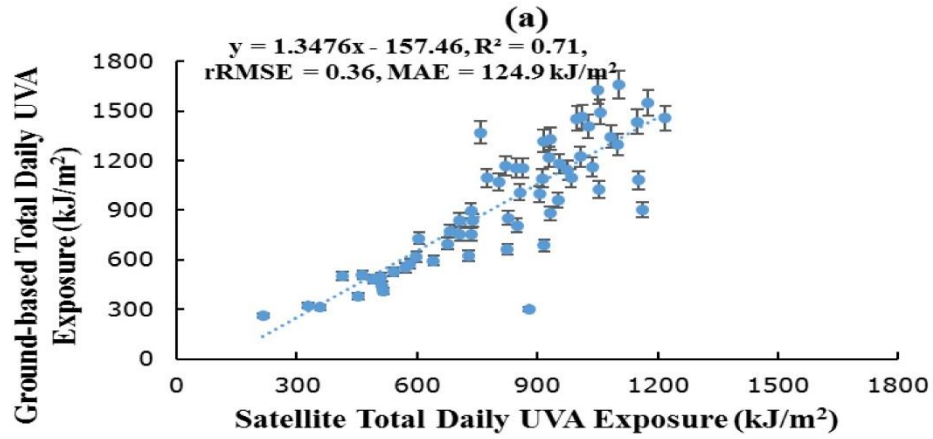


Figure 5: Comparison of the satellite total daily UVA exposure for 2004 to 2014 evaluated from the three OMI spectral irradiances with the ground-based total daily UVA exposure for the three categories of cloud cover of (a) > 2 to 4, (b) > 4 to 6 and > 6 to 8 okta for sun obscured sky conditions. The dashed lines are the regression lines fitted to the data and the error bars represent the $\pm 10\%$ errors with the measured ground-based data.

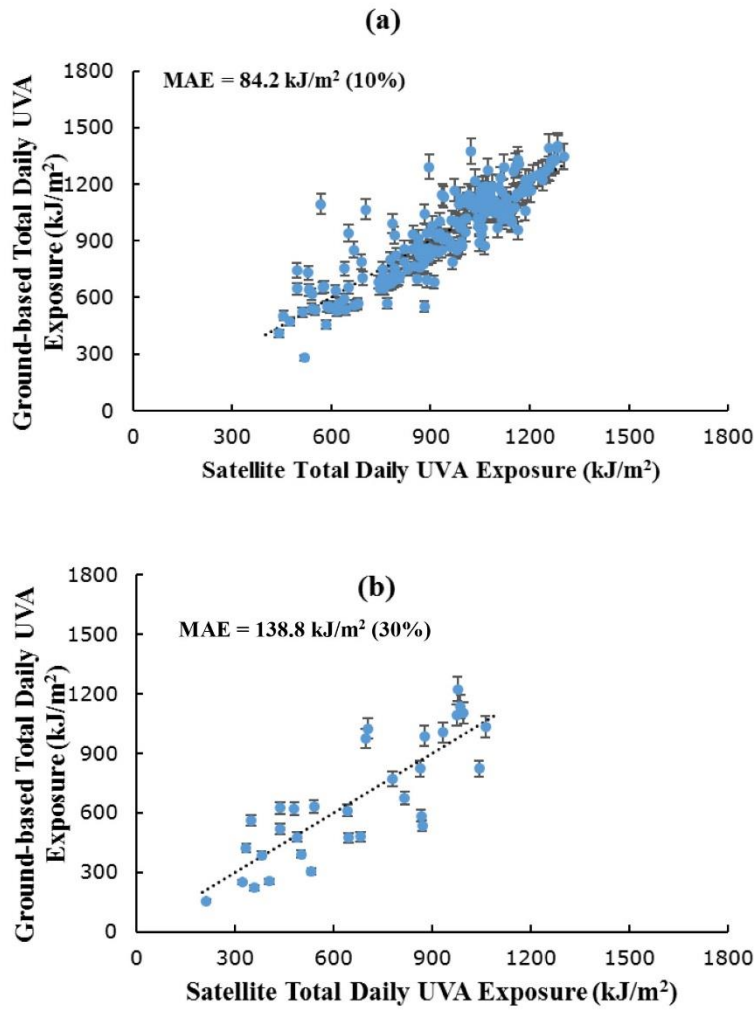


Figure 6: Validation of the satellite total daily UVA exposure evaluated from the three OMI spectral irradiances with the ground-based total daily UVA exposure for the three sky conditions of (a) sun not obscured cloudy days and (b) sun obscured cloudy days for the 2015 and 2016 data set. The dashed line in each graph is the 1:1 line.

Figure Captions

Figure 1: Time series of satellite total daily UVA exposures evaluated from the OMI solar noon spectral irradiances.

Figure 2: (a) The total daily satellite UVA exposure for all sky conditions. (b) The total daily satellite UVA exposure at the four cloud amount categories (0-2, > 2-4, > 4-6 and > 6-8 okta) for sun not obscured sky conditions. (c) Total daily satellite UVA exposure at the three cloud amount categories (> 2-4, > 4-6, and > 6-8 okta) for sun obscured sky conditions. The horizontal line in each box and whisker is the median, the box is the Q1 and Q3 range and the dashed vertical line is the range of values.

Figure 3: Box and whisker plots for each year of satellite total daily UVA exposures data October 2004 to December 2016.

Figure 4: Comparison of the 2004 to 2014 satellite total daily UVA exposure evaluated from the OMI spectral irradiances at solar noon with the ground-based total daily UVA exposure for the four categories of cloud cover of (a) 0 to 2, (b) > 2 to 4, (c) > 4 to 6 and (d) > 6 to 8 okta for solar disc non-obscured sky conditions. The dashed lines are the regression lines fitted to the data and the error bars correspond to the $\pm 10\%$ error associated with the ground-based data.

Figure 5: Comparison of the satellite total daily UVA exposure for 2004 to 2014 evaluated from the three OMI spectral irradiances with the ground-based total daily UVA exposure for the three categories of cloud cover of (a) > 2 to 4, (b) > 4 to 6 and > 6 to 8 okta for sun obscured sky conditions. The dashed lines are the regression lines fitted to the data and the error bars represent the $\pm 10\%$ errors with the measured ground-based data.

Figure 6: Validation of the satellite total daily UVA exposure evaluated from the three OMI spectral irradiances with the ground-based total daily UVA exposure for the three sky conditions of (a) sun not obscured cloudy days and (b) sun obscured cloudy days for the 2015 and 2016 data set. The dashed line in each graph is the 1:1 line.